UNIVERSIDADE
BEIRA INTERIOR

Development of dermic application systems made from micro/nano cellulose biopolymeric materials with 3D porosity simulation to optimize the retention and release of essential oils biomolecules

Joana Maria Honorato Pina Moreira

Dissertação para obtenção do Grau de Mestre em
Biotecnologia
(2º ciclo de estudos)

Orientadora: Professora Doutora Joana Maria Rodrigues Curto

janeiro de 2023

Declaração de Integridade

Eu, Joana Maria Honorato Pina Moreira, que abaixo assino, estudante com o número de inscrição M10165 de Biotecnologia da Faculdade de Ciências, declaro ter desenvolvido o presente trabalho e elaborado o presente texto em total consonância com o **Código de Integridades da Universidade da Beira Interior**.

Mais concretamente afirmo não ter incorrido em qualquer das variedades de Fraude Académica, e que aqui declaro conhecer, que em particular atendi à exigida referenciação de frases, extratos, imagens e outras formas de trabalho intelectual, e assumindo assim na íntegra as responsabilidades da autoria.

Universidade da Beira Interior, Covilhã 20/ 01 /2023

Joana Maria Honorato Pina Moreira

Joana Maria Honorato Pina Moreira

Dedication

Dedicated to my parents Maria José and João and beloved husband Tiago.
I dedicate it, especially to the woman who cared for me, taught me many things, and helped me grow, making me the woman I am today. For my grandmother Maria. I hope you're proud. I'm sure you'll be seeing this wherever you are. You will always be my little star.

Acknowledgments

In the course of this work, a year of hard work and dedication has made me grow personally and professionally.

To my supervisor, Professor Doctor Joana Maria Rodrigues Curto, for her knowledge and all the advice she made available, for her availability, tireless support, dedication, and tireless motivation during this year of work, and for encouraging every idea that came to me, advising me and making me believe in my value, has always believed in my value, motivating me throughout the experimental activity and development of the work, having grown immensely at a personal and professional level.

To the FibEnTech Research Unit, to its Coordinator Professor Doctor Paulo Fiadeiro, to Professor Doctor Rogério Simões responsible for the Research Group, and the Researchers and Professors of the Chemistry Department of the University of Beira Interior, without whom it would not be possible to have access to the laboratories and equipment for carrying out the experimental work.

To the laboratory technician, César Marques, to the researchers, MSc João Coelho, and PhD Vera Costa, and especially to PhD Flávia Morais, for their availability and help in the preparation and visualization of the samples in SEM, contribution to the revision of the document, and above all for always provide me with a good working environment, reveal companionship and team spirit, as well as all available, in clarifying the various doubts that have arisen throughout the work. A special thanks to people who were not only an excellent team, providing a good environment in the laboratory, but also people I also take for life. I could not fail to mention this team constituted by Flávia Morais, Paulo Saraiva, Catarina Lopes, and José Mendes.

To Professor Doctor Lúcia Silva for all her availability, help, and clarifications regarding the use of Gas Chromatography with Mass Spectrum combined with essential oils. I'm grateful for your experience in this field, it was crucial for this work.

To Professor Manuel Lis Árias, from the POLQUITEX department, Chemical Engineering Dep., Polytechnic University of Catalunya, Terrassa, Spain, for the availability and supply of chitosan, allowing us to add another aspect to this work.

To Dr. Ana Paula Gomes for the availability and acquisition of the different images from the Scanning Electron Microscope.

I want to thank people who belong to my life outside the University, whom I could not fail to mention because they helped me during this process. To Lara Alves, Rita Sedas Nunes and Vanda Godinho for helping me, believing in me, and for all the words of support.

A special thanks to the best friend I could have and whom I have the privilege to call husband, Tiago Alves, who was a crucial support throughout this journey, who always had the right word in the most challenging moments, and who believed in me when I doubted my worth. Thank you for believing in me, and for your encouragement, sincerity, compassion, and understanding in times of distress. Regardless of the distance, he was always there, even in the most difficult moments.

To Eugénia and Artur, my in-laws, and Lurdes, my grandmother from the heart, that is the family that I chose, for their constant support.

And finally, I want to thank my parents, Maria José and João, for their support and understanding, for their unconditional love, and for helping me to be the person I have become today. Without your support, this long stage of my life would not have been possible.

Resumo

Num mundo em mudança, onde a preocupação com o meio ambiente está cada vez mais forte, a procura por produtos biodegradáveis e biocompatíveis aumenta. Destes produtos com estas características destacam-se as fibras de celulose, bem como os óleos essenciais que também apresentam efeito terapêutico.

Devido à elevada volatilidade dos óleos essenciais, a aplicação cutânea na forma de máscaras com capacidade de reter estas moléculas terapêuticas prolonga seu período de ação, sendo uma vantagem. Neste sentido, o objetivo deste trabalho é criar uma máscara de micro/nanocelulose que seja refinada mecanicamente e enzimaticamente para atingir as qualidades necessárias. As fibras são avaliadas em termos de morfologia e biometria, e o tratamento enzimático é ajustado de forma a produzir fibras mais flexíveis com estruturas porosas e resistentes ao mesmo tempo.

A estrutura da máscara facial resulta numa matriz 3D porosa que é uma mistura otimizada de fibras de celulose na escala micro e nano. As fibras de celulose em microescala nesta rede conferem resistência e estabilidade, enquanto as fibras de celulose em nanoescala contribuem para a criação de uma estrutura com elevado grau de retenção e estabilidade de moléculas terapêuticas.

Os óleos essenciais de *Mentha piperita* (Hortelã-pimenta), *Lavandula angustiolia* (Lavanda) e *Citrus limon* (Limão) foram incorporados na estrutura porosa produzida, conferindo assim propriedades terapêuticas à rede de fibras micro/nanofibriladas.

As molécula ativas encontram-se protegidas numa emulsão de Água em Óleo, que permite reter as moléculas dos óleos essenciais e evitar a sua degradação/oxidação e mantê-las “aprisionadas” na rede de fibras, para retardar ainda mais a libertação das moléculas, garantindo que a mesma seja controlada. Estes óleos essenciais possuem propriedades antibacterianas e antifúngicas, que podem ser um recurso útil para o tratamento da pele. Como estas biomoléculas são tão voláteis, a otimização da rede 3D das estruturas torna-se essencial, pois permite que os óleos essenciais sejam preservados e libertados gradualmente.

As estruturas foram produzidas em laboratório utilizando as normas ISO e posteriormente impregnadas com moléculas medicinais de óleos essenciais, em bulk, resultando numa estrutura para aplicações cutâneas com boa resistência, suavidade e estabilidade a longo prazo.

As moléculas primárias dos princípios ativos encontrados nos óleos essenciais foram identificadas por CG-MS, e sua estrutura e grupos funcionais foram modelados em 3D. A Simulação Computacional 3D foi utilizada para representar as unidades estruturais porosas formadas pelas fibras de celulose em micro e nanoescala, e os resultados foram

comparados com as imagens de MEV obtidas para as estruturas de laboratório, confirmando que a espessura da estrutura e dimensão dos poros são comparáveis. Além disso, o uso de um simulador computacional validado permite otimizar a porosidade, tamanho e distribuição dos poros e, assim, atingir a cinética de liberação desejada.

Palavras-chave

Aplicações dérmicas e cosméticas, Celulose Micro/Nanofibrilada (M/NFC), Sistemas de Entrega de fármacos (DDS), Materiais celulósicos, Materiais fibrosos, Óleos essenciais, Simulação computacional, Otimização

Abstract

In a changing world, where the preoccupation with the environment is going stronger each year, the search for biodegradable and biocompatible products increases. Some of those products with these characteristics, cellulose fibers stand out, as well as essential oils that also present therapeutic effects. Due to the high volatility of essential oils, cutaneous application in the form of masks with the ability to store therapeutic molecules prolongs their action period, which is an advantage. In this regard, the goal of this project is to create a mask made of micro/nano cellulose that is refined mechanically and enzymatically to achieve the needed qualities. The fibers are assessed in terms of shape and biometry, and the enzymatic treatment is adjusted in order to produce more flexible fibers with porous and resistant structures at the same time.

The structure of the face mask results from a porous 3D matrix that is an optimized mixture of cellulose fibers on a micro and nano scale. The micro-scale cellulose fibers in this network give strength and stability, while the nano-scale cellulose fibers contribute to the creation of a structure with a high degree of therapeutic molecule retention and stability.

The therapeutic properties of the cellulose micro/nano fibrillated fiber network are obtained by adding *Mentha piperita* (Peppermint), *Lavandula angustifolia* (Lavender), and *Citrus limon* (Lemon) essential oils to the porous structure.

This was obtained by a process of a Water in Oil emulsion, to protect the essential oils molecules from degradation or oxidation and to keep them imprisoned or retained in the fiber network, to retard even more the release of the molecules, ensuring that the release is controlled. These essential oils have antibacterial and antifungal properties, which can be a useful resource for skin treatment. Because these biomolecules are so volatile, cellulose's network structure becomes critical, as it allows the essential oils to be preserved and released gradually.

The structures were created in the lab utilizing ISO standards and then impregnated with medicinal molecules of essential oils, in bulk, resulting in a structure for cutaneous applications with good resistance, softness, and long-term stability.

The primary molecules of the active principles found in essential oils have been discovered by GC-MS, and their structure and functional groups have been shown in 3D. The 3D Computational Simulation was used to represent the porous structural units formed by cellulose fibers in the micro and nanoscale, and the results were compared to the SEM images obtained for the laboratory structures, confirming that the structure thickness and dimension of the pores are comparable. Also, the use of a validated

computer simulator allows for optimizing the porosity, size, and distribution of pores, thus achieving the desired release kinetics.

Keywords

Cellulose-based materials, Drug Delivery Systems, Essential oils, Computational simulation, Fibrous materials, Dermic and cosmetic applications, Micro/nanofibrillated cellulose, Optimization

Index

Figure Index

Table Index

Acronym Index

2D	Two Dimension
3D	Three Dimensions
CMC	Carboxymethylcellulose
DDS	Drug Delivery Systems
DMC	Dry Mass Content
EO	Essential Oil
FTIR-ATR	Fourier Transform Infrared Spectroscopy with Attenuated Total Reflection
CG-MS	Gas chromatography–mass spectrometry
HW	Hardwood Fiber
ISO	International Organization for Standardization
MFC	Microfibrillated Cellulose
NSW	Non-Bleached Softwood Fiber
SEM	Scanning Electron Microscopy
SR	Schopper Riegler
SW	Softwood Fiber

Chapter I
Introduction

1. Introduction

In a changing world where environmental concerns are growing by the year, the search for biodegradable and biocompatible products is intensifying. Cellulose fibers and essential oils are two examples of items that exhibit these qualities. Cellulose fibers and essential oils are both biocompatible and biodegradable, while essential oils are known for their therapeutic properties.

As a result of the high volatility of essential oils, topical use in the form of masks that have the capacity to retain therapeutic molecules allows for a prolongation of the action period of the essential oils, which is an advantage. In light of this, the objective of this project is to develop a mask that is composed of micro/nano cellulose and is improved using both mechanical and enzymatic processes in order to attain the desired attributes. The enzymatic treatment is changed after the fibers' form and biometry are evaluated in order to produce more flexible fibers that also have porous and resistant structures.

The construction of the face mask is formed from an ideal blend of cellulose fibers at the micro size and cellulose at the nanoscale, which, when combined, provide a porous three-dimensional matrix. The nano-scale cellulose fibers in this network help to create a structure with a high level of medicinal molecule retention and stability while also adding strength and stability.

1.1 Motivation

In light of this, the goal is to develop a face mask that is made up of a porous three-dimensional matrix that is produced by the ideal combination of cellulose fibers in the micro and nano dimensions. The mask will be created using this as its foundation. Non-woven cosmetic masks that are made from non-biodegradable raw materials obtained from fossil fuels, which are a problem for the environment, making one of the main motivations of this work to replace with more environmentally friendly alternatives such as those made from materials based on cellulose that are derived from naturally renewable sources.

The network of cellulose fibers at the nanoscale helps to create a structure that provides strength and stability while also retaining a lot of medicinal compounds and maintaining their stability.

1.2 Objectives

The overall objective of this work is to develop cellulosic fiber-based delivery systems, or DDS containing essential oils for dermal application, from mechanically treated cellulose and enzymatically treated cellulose. The objective is to use a combination of experimental methods and computational tools to optimize the structures in order to achieve a controlled release of essential oils over an extended period of time. To reach this final objective, the specific objectives of this work are:

1. Manufacture in the laboratory structures made from cellulose fibers using Kraft pulps from *Pinus Pinaster* and *Eucalyptus globulus*.
2. Characterize the fibers biometry and morphology.
3. Characterize the porosity of the structure using ISO standards and SEM.
4. Laboratory production of cellulosic structures containing additives such as chitosan
5. Produce a water-in-oil emulsion containing essential oils and incorporate it into a cellulosic matrix
6. Study the composition of essential oils using gas chromatography
7. Determine the kinetics of essential oil release from the structures produced,
8. Make a benchmark marketing with products that already exist in the market to compare to our DDS prototype
9. Computationally simulate porous polymeric structures using a previously validated Matlab ® simulator, The Voxelfiber, to optimize the DDS structure.

Chapter II
Bibliographic Revision

2. Bibliographic revision

Since there are a variety of considerations that go into the manufacturing of drug delivery systems for cutaneous applications, these will be discussed at length throughout this chapter. Although the structure is predominately made up of a cellulose three-dimensional matrix, the other constituents that contribute to the prototypes generated as a result of this work will also be discussed.

2.1. Drug delivery systems

A formulation or device is referred to as a "Drug Delivery System" (DDS) if it enables the entrance of a medicinal material into the body while enhancing its efficacy and safety by managing the rate, timing, and site of drug release. This procedure involves administering the therapeutic product, having the product release active chemicals, and then moving those compounds through biological membranes to the site of action (Mura et al., 2013). The specificity of the drug target, the reduction of toxicity while maintaining the same therapeutic effects, the improvement of biocompatibility/biodegradability and safety, the speedier development of novel safe pharmaceuticals, among other factors, should all be considered when building DDS (Owen et al., 2016). Therefore, the primary goal of employing a DDS is to maintain the drug level in the body within the therapeutic window while also supplying a biologically active molecule in a regulated manner for a period of time and with a certain release rate, thereby lowering the drug's blood concentration peaks (pulse release). The most recent delivery methods are constructed of polymer-based components. These materials are among the most researched classes in DDS development because of their variety, adaptability, and characteristics (Arafa & Ayoub, 2017). In fact, new polymers with increasingly specialized features are being developed at the same time as new, more advanced, and efficient DDS (Kim et al., 2009; Villanova et al., 2010). Since they offer good specificity/release and low toxicity, biocompatible, biodegradable, non-toxic, non-immunogenic, natural, semi-synthetic, and synthetic polymers have become the most popular choice for DDS during the past ten years (Mogoşanu et al., 2016; Safari & Zarnegar, 2014; Sun et al., 2017). When it comes to the transport of other molecules, as it does in the case of cosmetics, transport and controlled release systems are comparable to drug delivery systems (Moulton & Wallace, 2014). Due to their enormous interior surface areas, porous materials are employed in the creation of transport and controlled release systems to hold and convey a variety of molecules (Ulker & Erkey, 2014).

2.1.2. Dermic delivery systems

The skin serves as a barrier that guards against external contaminants and infections A straightforward illustration of the variations between transdermal and cutaneous drug delivery mechanisms is shown in Figure. 2.1 (Sabbagh & Kim, 2022).
Since the skin is an organ that is easily accessible and may be used to provide medications that don't cause discomfort, dermal and transdermal administration have emerged as an appealing alternative to conventional routes like oral and parenteral.
Drug administration differs between these two routes in the following ways, though:

- dermal administration—requires the crossing of the drug through the stratum corneum, revealing its location in the underlying layers of the skin.
- transdermal delivery—the medication is transferred to the skin dermis before being able to enter the systemic circulation(Ciolacu et al., 2020).

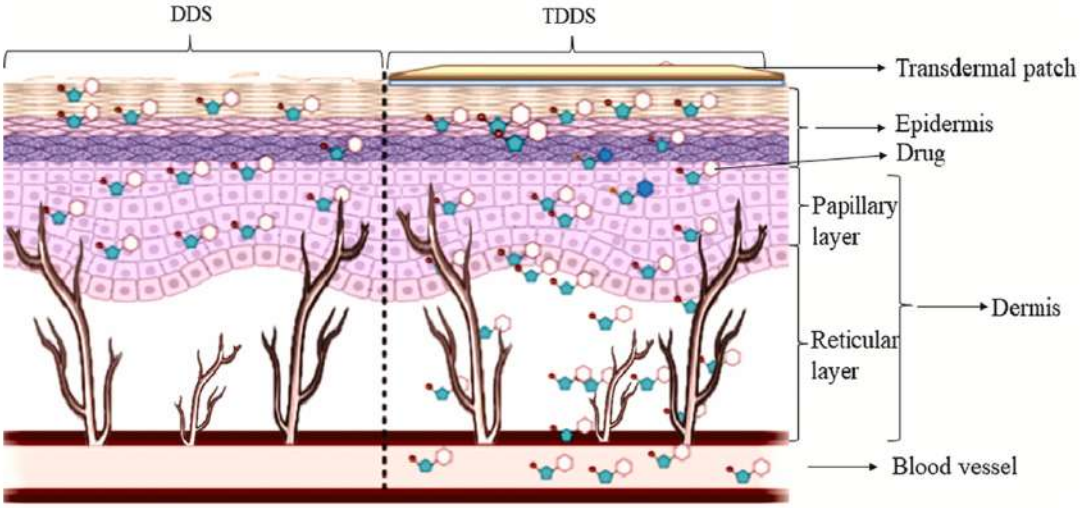

Figure 2. 1 - Comparison of Dermic Drug Delivery Systems (left) and Transdermic Drug Delivery Systems (adapted from (Sabbagh & Kim, 2022)).

Transdermal drug delivery has some advantages, including the ability to deliver drugs for a longer period of time at a constant rate, the ability to quickly stop drug administration by simply taking out the device, suitability for self-administration, and—most importantly—the ability to prevent hepatic first-pass metabolism and gastro-intestinal incompatibility (Ciolacu et al., 2020; Simões et al., 2012; Vlaia et al., 2016).
Drug administration through the skin is not an easy process, however. The epidermis, which is the top layer of the skin, the dermis, and the hypodermis are the three functional layers that make up the stratified tissue that is human skin. The stratum corneum (SC), the epidermis' outermost structure, is an area rich in proteins and lipids that reduces the inflow and outflow of chemicals, water, and oxygen. Active substances cannot enter the deeper skin layers through this protective barrier structure. It serves as the primary part

of the alleged skin barrier. Skin penetration is influenced by the active molecules's physicochemical characteristics and is encouraged if it satisfies the following requirements: low molecular weight (500 Da), satisfactory polarity (log Po/w = 1-3), and low melting point (Bos & Meinardi, 2000; Hadgraft, 2004; van Gheluwe et al., 2021). The amount of drug absorbed will also vary depending on a number of physio-pathological factors, including the patient's age, skin type, temperature, and circulation, as well as the presence of lesions on the skin. The makeup and structure of the skin impose penetration constraints that restrict cutaneous medication administration due to the variety of active molecules and their physicochemical properties. An active ingredient is never used directly in its pure form; alternatively, it is incorporated into a suitable dosage form, which is mostly made up of excipients. This facilitates the active component's conductivity on the skin and speeds up its diffusion in the epidermis. A number of formulation-related variables influence how thoroughly and deeply an AI penetrates the skin (Ahmad et al., 2018; van Gheluwe et al., 2021).

2.2. Bionatural materials

2.2.1 Cellulose Fibers

Cellulose is one of the most prevalent polymers on the planet and may be extracted from trees and annual plants by an alkaline method, such as the Kraft process (Chakar & Ragauskas, 2004; Demuner et al., 2021; Fearon et al., 2020). Cellulose is a polymer that is constituted of glucose units that are joined to one another through β-1,4 glycosidic linkages (Rajnish et al., 2021). Cellulose is a polymer, consisting of long chains of glucose anhydride, also known as anhydridoglucose (AGU), which has three hydroxyl groups. These groups give polymer cellulose the ability to make hydrogen bonds, which allows for great stability and strength (resistance) (Jorfi & Foster, 2015; Lavoine et al., 2012). Cellulose is produced by biosynthesis in plants, animals, and bacteria, in the Eubacteria domain, which leads to many variations of this polymer (Abeer et al., 2014). Cellulose has a hierarchy structure, as it has crystalline and amorphous areas, as illustrated in figure 2.2.

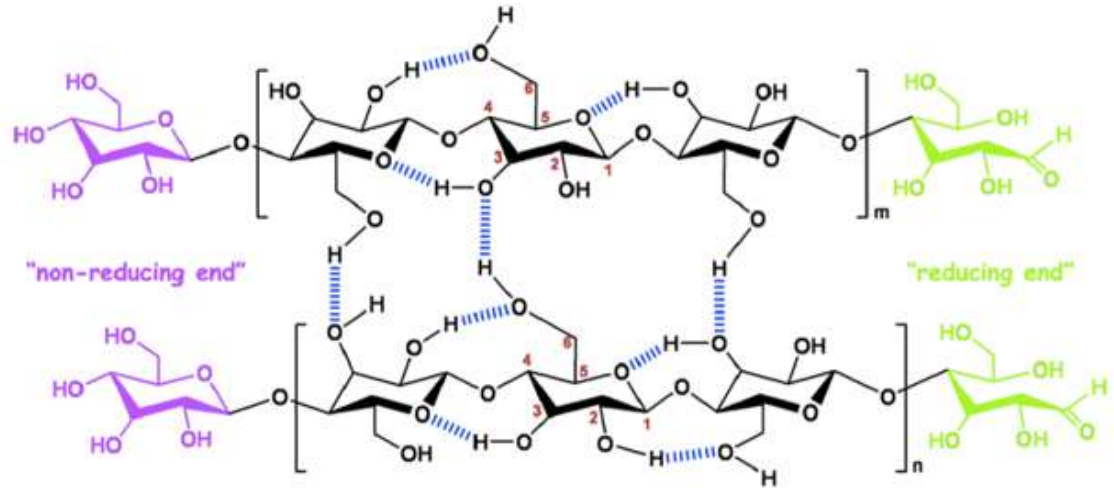

Figure 2. 2 – Schematic representation of the chemical structure and intra- and inter-molecular hydrogen bonds in crystalline cellulose (Adapted from (Lin & Dufresne, 2014)).

Cellulose is structured in the form of elementary fibrils, which range in size from 3-5 nanometers and are connected to one another via hydrogen bonds formed between the hydroxyl group and the oxygen of the neighboring rings of the cellulose molecules. These elementary fibrils then aggregate to create bigger structures known as microfibrils, which range in size from 10-20 nanometers (figure2.3). Given the huge number of microfibrils it contains, cellulose is an exceptionally stable polymer, and it also gives the fibers their stiffness (Moon et al., 2011; Rajnish et al., 2021; Zhang et al., 2021).

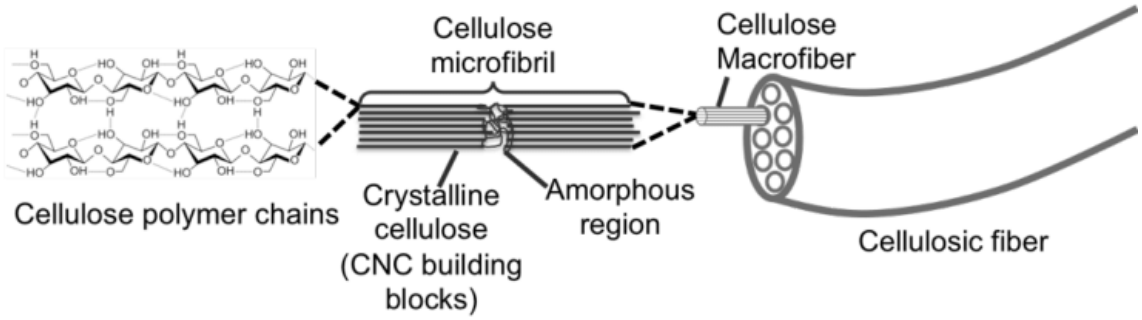

Figure 2.3 - Hierarchical structure of cellulose fibers (Adapted from (Parry, 2016))

Cellulose from plants requires processes to remove lignin and hemicelluloses, which can be tricky to solve experimentally (Abitbol et al., 2016). Cellulose is a renewable source of biopolymers, being produced by several species, such as plants, animals, and bacteria. Cellulose is the structural unit of plants and is therefore one of the most abundant natural materials (Abitbol et al., 2016). In addition, cellulose can be subjected to a variety of different treatments, including mechanical, enzymatic, and chemical processes, in order

to produce a wide variety of derivatives, such as CMC and NFC. These compounds represent a great importance in the development of DDS due to the many different qualities they possess, since they are applied for regulated and delayed release of active chemicals (Kamel et al., 2008; Sindhu et al., 2014).
One of the most significant elements in the process of developing cellulosic-based DDS is the development and optimization of a porous three-dimensional matrix in which the active molecules will be kept and released in a regulated manner. This is one of the most crucial steps in the process (Nicu et al., 2021).

2.2.2 Micro/Nano Fibrillated Cellulose (M/NFC)

Cellulosic material known as micro/ nanofibrillated cellulose (MFC/NFC) is made of moderately deteriorated, highly expanded, and expanded high-volume cellulose and is produced using homogenization methods. The cellulose microfibril aggregates that make up MFC/NFC have lengths of several micrometers and diameters between 20 and 60 nm (Klemm et al., 2018).
Amorphous and crystalline components can be seen in the MFC/NFC, which also exhibits a web-like structure. Furthermore, the length to breadth ratio is extremely high, giving it a very low percolation threshold (Mishra et al., 2018). The ability of MFC/NFC to create a rigid network is thus quite good. Depending on the intended type of MFC/NFC, several mechanical and enzymatic processes have been used more and more frequently (Lavoine et al., 2012).
MFC/NFC has been used as an additive in paper-based goods to enhance various papermaking capabilities because of its high specific surface area, rheological properties, specific orientation, chemical surface reactivity, biocompatibility, biodegradability, absence of toxicity, and other qualities (Ferrer et al., 2017).
Since they improve hydrogen bonding, which in turn increase inter-fiber connections and structural strength, micro/nanofibers are regarded as a very suitable material for tissue products (Beuther et al., 2009). The possibility to combine the various micro- and nanofiber properties with the features of tissue paper materials could improve the manufacturing of tissue products with value-added.

To form the DDS the two main components are the cellulose-based matrix and the therapeutic molecules. The molecules with activity were chosen from medicinal plants in form of essential oils.

2.2.3. Carboxylmethylcellulose

CMC is a polycarboxylic ether of cellulose that is generated through the Williamson reaction. This reaction is initiated by the treatment of cellulose with monochloroacetic acid in the presence of sodium hydroxide in an excessive amount (Caraschi & Campana Filho, 1999). Its empirical formula is written as [C6H10-xO5(CH2CO2)x]n, where "x" represents the degree of substitution and "n" represents the degree of polymerization (Nóbrega & Amorim, 2015; Varshney & Naithani, 2011).The degree of polymerization is the factor that determines the viscosity of the substance. Once it has been modified to facilitate interactions with metal particles, this polymer possesses a high level of chemical stability, is safe, non-toxic, biocompatible, biodegradable, and soluble in water with carboxylate and hydroxyl groups (Butun et al., 2011).

CMC has seen widespread application in DDS as a direct result of the properties that it possesses. In 1997, Efentakis and colleagues investigated the impact that non-swelling excipients had on the rate at which pharmaceuticals are released from matrix systems. The results of this investigation led us to the conclusion that the "swelling" and the release of medications both exhibit behaviors that are, respectively, proportionate in a direct sense and proportional in an inverse sense to the levels of CMC that are present (Efentakis et al., 1997) On the other hand, a different study that was conducted by Rao and colleagues in the year 2001 was able to verify that the release of drugs from CMC matrix systems is slower when compared to the release of drugs from systems that contain another polymer ((Rao et al., 2001).This study was carried out so that Rao and colleagues could verify this. When this is factored into the design of DDS, it becomes a major consideration. In more recent research, CMC was employed as a hydrogel for the integration of amoxicillin, and the researchers came to the conclusion that this particular DDS is effective as an antibacterial agent (Sood et al., 2017).

2.2.4. Essential oils

Essential oils are multifaceted as they are used in various industries, such as the cosmetic, pharmaceutical, and food industries (Klimek-Szczykutowicz et al., 2020). These are produced by plants and extracted from them, in which many extracts have been recognized as GRAS (Generally Recognized As Safe) (Morais et al., 2020; Pavoni et al., 2020). These by-products have anti-inflammatory, antimicrobial, and even antiviral properties (Bedoya-Serna et al., 2018; Hajhashemi et al., 2003; Klimek-szczykutowicz et al., 2020; Mutlu-Ingok et al., 2020; Orchard & van Vuuren, 2017).

Essential oils can be extracted from various parts of the plant such as flowers, fruits, seeds, and leaves. Such extraction can be done in a variety of ways, such as solvent

extraction, steam distillation, and cold pressing. The extraction product's consistency, quantity, and composition can differ depending on the environment, soil composition, plant organ, age, and vegetative cycle stage (Angioni et al., 2006). To obtain the same composition of EOs, they must be harvested under the same conditions, i.e., from the same organ of the plant, which must be growing in the same soil, atmosphere, and season. (Baptista-Silva et al., 2020).

Each essential oil is a complex sample, composed by many volatile compounds, mostly terpenes (Shaaban et al., 2012). Monoterpenes can be present in small amounts in almost all essential oils. They are made up of 10 carbon atoms that are derived from two isoprene units. Monoterpenes may have a straight chain or a single-ring backbone. Because of their smaller size, they respond easily to air and heat, and they degrade faster than their more complex molecules (Pavoni et al., 2020).

2.2.4.1. Types of essential oils

In this particular instance, the various kinds of essential oils that were selected ought to be since they are a part of an experimental set. This particular research looked at the effects of three different essential oils: peppermint, lavender, and lemon. Every one of them is unique in terms of its characteristics and applications.

2.2.4.1.1. Peppermint Essential Oil

The Peppermint Essential Oil that was used is from *Mentha piperita*. The main components are Menthol, menthone, and 1,8-cineole (eucalyptol) (Table2.1). This essential oil is mainly found on leaves (Alankar, 2009; Kalemba & Synowiec, 2020)

Some of the properties of peppermint essential oil include a decrease of appetite and hunger cravings, reduce daytime sleepiness, ease the sting of sunburn, reducing the redness in inflamed skin by cooling it down due to its vasoconstrictor properties (Alankar, 2009).

It has antibacterial activity against *Escherichia coli*, and *Pseudomonas aeruginosa* among others, and antifungal activity against *Candida albicans*, *Aspergillus niger*, *Saccharomyces cerevisiae*, among others (Alankar, 2009; Mutlu-Ingok et al., 2020; Tsai et al., 2013).

Table 2. 1 - Main components of *Mentha piperita* essential oil, with their respective molecular classification and visual representation. Molecules made using ChemDraw ® Professional 16.0 by Joana Moreira.

Principal Components	*Classification*	*Visual Representation 3D*	*Linear Representation*
Menthol	Monoterpene	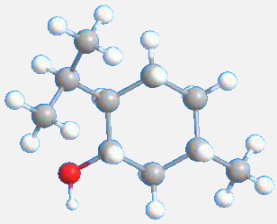	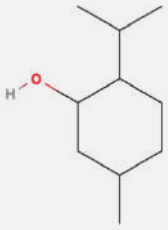
Menthone	Monoterpene	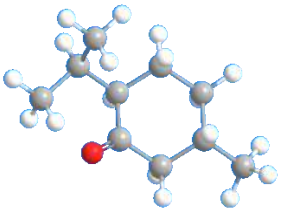	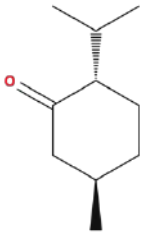
1,8-cineole (eucalyptol)	Monoterpene	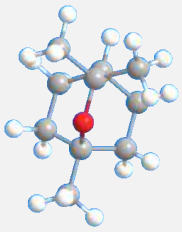	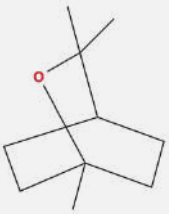

2.2.4.1.2 Lavender Essential Oil

The lavender Essential Oil that was used is from Lavandula angustiolia. The main components are Linalool, linalyl acetate and ocimene (Table 2.2).

The extraction method normally used for lavender can be cold pressing or steam distillation, but steam distillation can lead to the formation in hydrolates, which lack in linalyl acetate, and that's the major component of lavender essential oil.

It's normally used in cosmetics, perfumes, food and aromatherapeutic industry. Studies proved that it has antioxidant activity, reduces anxiety, and helps improve sleep, showing an increase of beta-waves (Hajhashemi et al., 2003; Koulivand et al., 2013; Prusinowska & Śmigielski, 2014).

It has antibacterial activity against *Escherichia coli*, *Pseudomonas aeruginosa*, *Staphylococcus aureus* and antifungal activity against *Candida albicans*, *Aspergillus niger*, *Penicillium expansum* and others (Prusinowska & Śmigielski, 2014).

Table 2.2 - Main components of *Lavandula angustiolia* essential oil, with their respective molecular classification and visual representation. Molecules made using ChemDraw ® Professional 16.0 by Joana Moreira.

Principal Components	*Classification*	*Visual Representation 3D*	*Linear Representation*
Linalool	Monoterpene	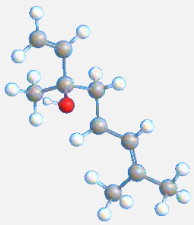	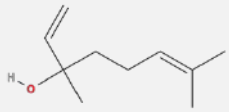
Linalyl acetate	Monoterpene	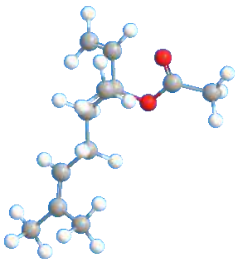	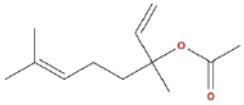
Ocimene	Monoterpene	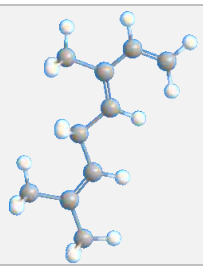	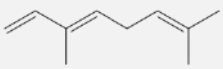

2.2.4.1.3 Lemon Essential Oil

The lemon Essential Oil that was used is from *Citrus limon*. The main components are D-Limonene, Beta- pinene and gamma-terpinene (Table 2.3). It's usually extracted by cold pressing since the majority of the components of lemon essential oil are found on the lemon's outer skin.

According to some studies, it has anti-inflammatory activity, compared to ibuprofen. It also shows cosmetology applications, such as positive effects on acne, and can be used as a promoter to aid the penetration of active substances through the skin (Klimek-szczykutowicz et al., 2020; Orchard & van Vuuren, 2017).

It has antibacterial activity against *Bacillus subtilis*, *Escherichia coli*, *Micrococcus luteus*, and others and antifungal activity against *Candida albicans*, *Aspergillus parasiticus*, *Penicillium digitatum*, and others (AL-Jabri & Hossain, 2018; ben Hsouna et al., 2017; Klimek-szczykutowicz et al., 2020; Mutlu-Ingok et al., 2020; Orchard & van Vuuren, 2017).

Table 2. 3 - Main components of *Citrus limon* essential oil, with their respective molecular classification and visual representation. Molecules made using ChemDraw ® Professional 16.0 by Joana Moreira-

Principal Components	***Classification***	***Visual representation 3D***	***Linear representation***
Limonene	Monoterpene	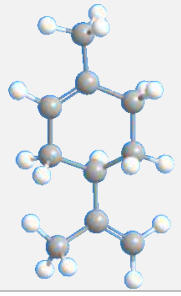	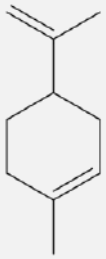
Beta-pinene	Monoterpene	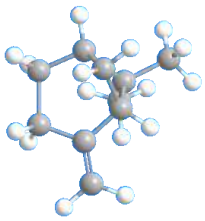	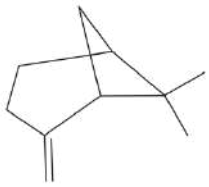
Gamma- terpinene	Monoterpene	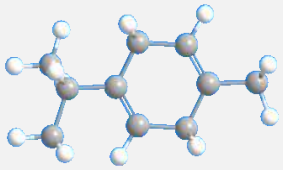	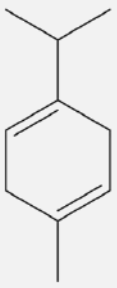

2.2.4.2. Examples of Extraction Processes

There are a number of methods available for the extraction of essential oils from plants, including cold pressing, which is also known as expression, steam distillation, and solvent extraction. In this subchapter, they are discussed in this order owing to the contribution that they make to the environment. This is done while keeping in mind that certain more conventional procedures produce chemical compounds that are not favorable to the environment, which does not match with the purpose of this project.

2.2.4.2.2. Expression

Essential oils from citrus fruits such as oranges, bergamot, grapefruits, lemons, and limes are most widely extracted using expression (Kalemba & Synowiec, 2020). The rind of the fruit, or the outermost waxy layer of the fruit's peel, is used in this process. Since this process, unlike steam distillation, does not require a heat source, it is commonly referred to as “cold pressing.” This method allows for the mechanical extraction of EO, which is widely utilized and suitable for direct consumption without heat treatment. In order to generate the essential oil, the oil is expeller-pressed at low pressure and temperatures to produce EO using the cold press technique(Rassem et al., 2016). The material must first undergo pre-treatment, which influences oil yield and can include peeling, drying, solvent, or enzymatic treatment. One inlet on a cold press machine is used for seed material, while the other two are outputs for collecting a cake that hasn't been oiled and oil (Çakaloğlu et al., 2018). This cold pressing method is employed as a result of the drawbacks of various solvent-using procedures. The benefits of cold pressing include being straightforward, safe, eco-friendly, traditional, and less expensive. After extraction, there is little fat left in the cake, and there is no need for any chemical or heat treatment at all during the extraction process. Because of this, EO has a high quality, doesn't need to be processed, and is safe for consumption right away. Other benefits of this method include the preservation of a variety of temperature-sensitive phenolic compounds, lipophilic phytochemicals like antioxidants, which protect us from illnesses and keep us healthy, and the extension of oil's shelf life. However, the cleansing procedure also includes centrifugation, filtration, and washing with water. Low yield and variable product standards are the main drawbacks, making it challenging to seize(Çakaloğlu et al., 2018). It is difficult to preserve for a long time, which is another issue that has been noted. It only lasts for fewer than six months.

2.2.4.2.2 Steam distillation

The most popular method for collecting essential oils is steam distillation. It is a delicate and time-consuming method that necessitates close attention to detail. This method is widely used not only because it produces extremely pure and clean products, but also because it allows for the collection of temperature-sensitive aromatic compounds. Steam distillation, as opposed to simple distillation, uses a pressurized device. Critical oils can be distilled at temperatures well below their natural boiling point when the device is pressurized, preserving the quality of their fragile and complex chemical profiles.(Hajhashemi et al., 2003)

This technique is frequently used for the mass manufacture of EOs, and the processing duration is between 8 and 9 hours. In this procedure, a steam boiler produces steam that is blown into the steel's bottom via a pipe. About 70–75 psi of pressure was needed in the boiler to produce steam. Steam-containing volatile oil components flow through the condenser, which transforms vapor into a liquid that contains a combination of water and oil. Crude oil can be stored in appropriate containers after distillation. Equipment, ingredients, temperature, and steam pressure are just a few of the variables that might affect this technique's yield and EO quality. As opposed to the hydrodiffusion approach, this method does not necessitate high temperatures or vacuum conditions. (K. Bhardwaj et al., 2020).

Compared to water distillation, this procedure is easier, more pleasant, repeatable, and less expensive. Additionally, the apparatus related to the apparatus for water distillation This distillation produces oil with a higher yield that is more repeatable. It is well known that steam distillation uses less energy and is faster than water distillation. The sample substance, however, cannot come into direct contact with the fire resource underneath the still. The main disadvantage of this form of distillation is that because the steam must evaporate the water in order for it to condense farther up the still, it makes the plant material wet during the process, which slows down distillation (Asbahani et al., 2015; Bhardwaj et al., 2020).

2.2.4.2.3 Solvent Extraction

Solvent extraction can be used on any plant material, but it is most widely used on flowers that are extremely fragile or cannot withstand the conditions needed for steam distillation. Absolutes are distinguished from essential oils in that they can contain both aromatic and non-aromatic chemical constituents. Choosing a good solvent is an essential first step. Solvents are usually less polar compounds (such as pentane or hexane) or alcohols (such as methanol or ethanol). Since the form of solvent used will

change the absolute, it is critical to choose a solvent that will cause minimal changes to the specific fragrance (Řebíčková et al., 2020).

This method involves gently heating the sample while utilizing organic solvents such petroleum ether, hexane, acetone, ethanol, or methanol to extract the essential oils (EOs) from delicate or fragile flower materials that cannot be removed using heat or steam(Tongnuanchan & Benjakul, 2014). Filtration and solvent evaporation come next in the procedure. As the filtrate comprises a mixture of wax, resinoid, fragrance, and EOs, this process is more difficult. The EOs must therefore be dissolved into the filtrate by mixing alcohol with it before being distilled at a low temperature.

This approach, however, is a bit more time- and money-consuming(Li et al., 2009). Although this method is quite straightforward, less expensive, and effective, it has drawbacks such as the use of a volatile solvent in a high amount that requires time to remove from EO, as well as the process taking more time and temperature to extract EO relative to other methods and frequently having poor reproducibility(Dawidowicz et al., 2008). Environmental contamination caused by these organic solvents has the potential to be highly harmful to the environment. It is required to separate the solvent from the EO. If not, the solvent odor will contaminate the EO, and any solvent residue that is left behind might trigger allergies and have an adverse impact on the immune system(Yen & Lin, 2017).

2.2.5 Emulsions

The cosmetic and pharmaceutical industries are especially interested with emulsification procedures. Emulsions can be designed to emphasize a variety of properties, according to the purposes for which they are intended. Emulsions can be described by a variety of factors, including the nature of the dispersed and continuous phases, the volume content of the dispersed phase, the particle size distribution of droplets, and the stability (Nehme et al., 2021).

Among the most popular types of cosmetic and medicinal preparations are emulsions. A heterogeneous dispersion system with two immiscible liquids or liquids with restricted miscibility, one of which is the dispersion portion in the form of particles in the liquid environment of the other provided liquid, is referred to as an emulsion. Emulsifiers are necessary to make emulsions that are suitable for actual application. Based on the polarity of the dispersion surroundings and the dispersed substance, there are two different forms of emulsions: water in oil (w/o) and oil in water (o/w) (Pavlačková et al., 2018).

Figure 2. 4 - Cellulosic structure in the former containing the emulsion

2.2.6 Chitosan

Chitosan is a linear polysaccharide that, like cellulose, is abundant and affordable. Chitosan is a linear polymer generated from the partial deacetylation of natural chitin. Chitosan is formed from creatures such as crustaceans and fungi, and because it occurs naturally, it has the advantages of being biodegradable, biocompatible, and harmless (Moreira et al., 2022). Chitosan is a deacetylated form of chitin generated from animals like fungi, crabs, and wasps (Black Soldier Fly- *Hermetia illucens*) (Valle et al., 2021). Chitosan has various benefits, including being nontoxic, having a rich and wide diversity of sources, being affordable, having facile film production, having good biocompatibility, and being enzymatically biodegradable. Furthermore, much research is being conducted to maintain its original biodegradability and biosafety while improving its solubility and antimicrobial capacity (quaternization and carboxylation) through structural modifications and chemical additions, which is why there is an ever-increasing amount of research. Chitosan is biocompatible, biodegradable, harmless to mammalian cells, antibacterial, and possesses varied chemical and physical properties that make it a good candidate for textile functionalization. Furthermore, the US Federal Drug Administration (FDA) has approved chitosan as GRAS (Generally Recognized as Safe) for tissue engineering, drug delivery, wound dressing, nutritional use, and plant protection applications. (Arias et al., 2021).

2.3 Computer Simulation

The porosity of the 3D network is crucial to optimize the function of transport and controlled release of molecules (Curto et al., 2016; Ferreira et al., 2016; Morais & Curto, 2018).

The investigation of many physical properties using traditional experimental techniques is challenging or even impossible. It became possible to model some of these aspects using computational codes as processing power developed. It is possible to alter the "input," or input variables, and watch how the "output," or output variables, of the process are impacted, just like in an experimental process. These studies are known as computational experiments, and experimental techniques are increasingly supplemented and replaced by them (Santner et al., 2003).

The tuning of structural characteristics to accomplish intended functions is essential in the development of DDS in the field of medicinal chemistry. As a result, the utilization of 3D computational models was found to be a highly successful approach for enhancing DDS. A polymeric DDS's 3D structure and porosity play a key role in determining how well it will perform in terms of drug release and transport (Y. R. Bhardwaj et al., 2014).

In 1994, Niskanen and Alava proposed the first 3D model (Figure 2.22), which they called the KCL-PAKKA model. This model replicates the 3D geometry of structures with a random arrangement of fibers in the xy plane. Niskanen and Alava's model was the first to accomplish so. In addition to this element, the pliability of the fibers is what causes them to equally occupy the z dimension. This means that they conform to each other according to the input value for their flexibility, which ultimately results in the formation of three-dimensional structures (Alava & Niskanen, 2006; Niskanen & Alava, 1994). A three-dimensional model of fibrous "fluff" materials was proposed by Heyden and Gustafsson in the year 1998. In this model, each fiber is represented by an arc of a single circle and placed in a "box" to form a periodic network; however, the bending of the fibers that takes place when they adjust to the already formed structure is not described. This is because the bending of the fibers takes place when they adjust to the already formed structure (Heyden, 2000). The KCL-PAKKA model has undergone various advancements during the course of its existence, and it wasn't until 2003 when Provatas and Uesaka revealed fiber deposition rules (Provatas & Uesaka, 2003).

Curto et al. presented and validated in 2011 a 3D modelling model of fibrous materials that they had developed and implemented in MATLAB®, which was based on the KCL-PAKKA model. This model was based on a cellular automaton, in which there is a Cartesian cell division, which causes each fiber to be represented as a sequence of voxels,

each occupying a pre-established volume that can be defined by the user Curto et al., 2011a, Curto et al., 2011b), as shown in Figure 2.1.

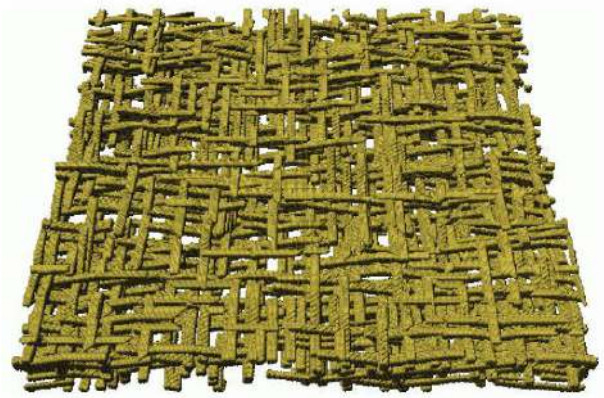

Figure 2.5 - Cellulosic structure in 3Dobtained using the KCL-PAKKA model (adapted from (Alava & Niskanen, 2006).

The phases that determine the process must be carefully chosen in order to understand the mechanism at the atomic level and to get 3D data for the polymer coating and molecules that will be taken into account for transport. Thus, the size, flexibility, and collapse of the structural units are modeled (Martins et al., 2018). To achieve certain goals, one must choose the inputs to calculate the outcomes of a computational experience. The "experimental design" consists of these chosen inputs. The "Latin Hypercube Sampling" is the basis for the simulation method used for the model validated by (Curto et al., 2011). This technique, which can also be used in three dimensions (Santner et al., 2003) involves subdividing the space created by two variables into n x n squares and choosing n points from each subsquare to include in the sample so that no two points occupy the same row or column. This technique is illustrated in Figure 2.4.

The model's input variables include the length/width ratio, wall thickness, lumen thickness, structural unit flexibility, and resolution (number of layers in the direction of thickness). The space is specified as a Cartesian uniform grid of cells, with each structural unit in the model represented by a set of cells (Curto et al., 2011). Additionally, the fibers are placed one at a time, each fiber taking up a separate space. The deposition procedure is repeated if any of these are rejected. The fiber complies with the underlying structure depending on its location, size, and flexibility (Curto et al., 2015; Ferreira et al. 2016). In order to obtain a model close to reality, it is important to choose the determining parameters, in this case, the dimensions of the fibers and pores. The fibers are generated computationally using the combination of voxels that allows to obtain their dimensions of length, width and thickness, flexibility, and collapsibility. The most important input

parameters are the length, width, the thickness of the fiber, as well as the number of voxels needed in order to obtain the desired resolution. The 3D structures are formed by the random deposition of the fibers, one at a time, and oriented in an x-y plane as in the formation of the experimental transport and delivery systems and which were used to validate the model (Figure2.5) (Curto et al., 2011).

The three-dimensional simulation can be performed using a simulator developed in Matlab® previously validated (Curto et al., 2011). 3D simulations of porous materials can describe the release behavior of a drug and, therefore, can provide a useful tool in the development and optimization of transport systems and controlled release of molecules (Curto et al., 2016; Ferreira et al., 2016; Morais & Curto, 2018; Yu et al., 2008).

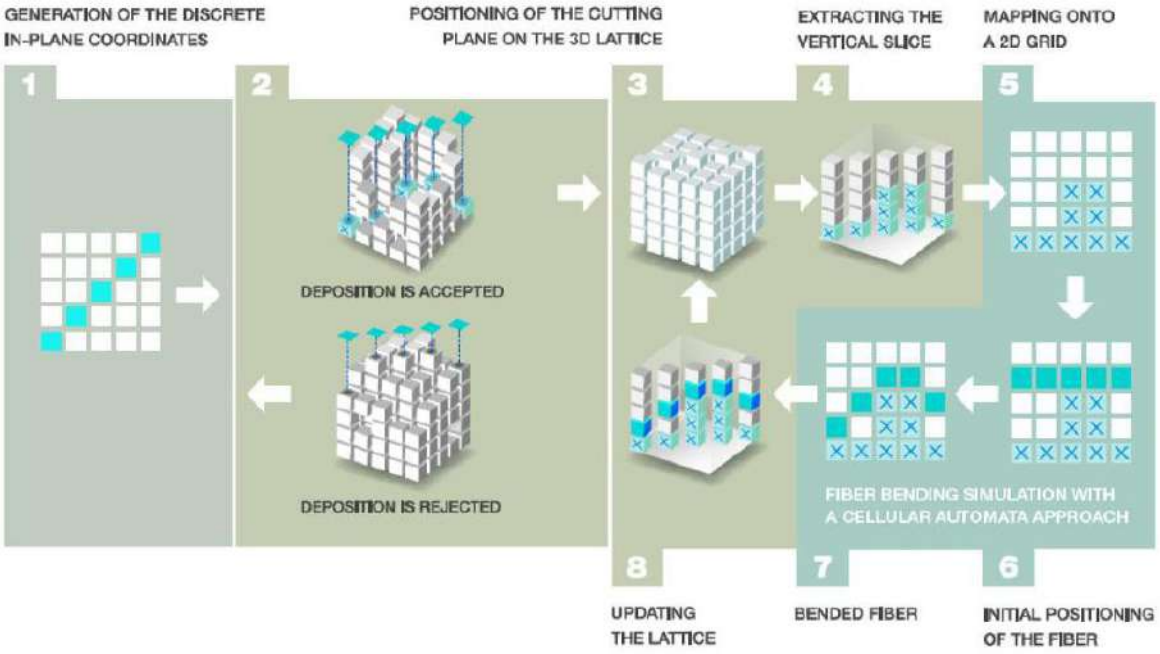

Figure 2.6 - Scheme representation of the 3D computational model validated by Curto (adapted from (Conceição, Curto, Simões, & Portugal, 2010; J.M.R. Curto, Conceição, Portugal, & Simões, 2011; J.M.R. Curto, 2012).

Chapter III
Materials and Methods

3. Materials and Methods

This chapter describes the numerous materials and reagents utilized throughout the study. There will be a description of the many methods employed, including cellulose fibers and essential oils, the creation of entirely new structures, FTIR-ATR, computational simulation using a validated model, and a comparison of the structures produced with existing products sold already on the market.

3.1 Materials

The materials are divided into three categories: the cellulosic fibers used, the active molecules that were added to the system fabricated and the additive.

3.1.1. Cellulose fiber materials

The cellulosic materials used for the production of the structures were Pinus Pinaster, denominated throughout this work as Softwood and Eucalyptus globulus, denominated Hardwood. MFC was produced in the laboratory by our FibEnTech research unit, as they were used for previous studies.

3.1.2 Essential Oils

The essential oils used were peppermint (*Mentha piperita*), lavender (*Lavandula angustifolia*) and Lemon (*Citrus Limon*).

3.1.3 Additives

Chitosan (Low molecular weight) from Sigma Aldrich, Chitosan of different chemical characteristics (Viscosities between 65 - 173 cP), provided by Professor Manuel Lis Arias, from POLQUITEX, Chemical Engineering Department, Polytechnic University from Catalunya, Terrassa, Spain

Cellulose microcrystalline for thin layer chromatography from Merck

Additionally, Carboxymethylcellulose, which Sigma-Aldrich acquired and had a high viscosity (1500-3000) <3cP at 1% H2O (250C) and analytical purity.

3.2 Equipment

Weighings were carried out on a Mettler analytical balance, model Toledo AG104. DMC was determined using a Mettler infrared scale, model LJ16 Moisture Analyzer.

For characterization of the fibers determined automatically by image analysis of a diluted suspension (20 mg/L and 30 mg/L 145 to hardwood and softwood samples, respectively) in a flow chamber in MORFi Fiber Analyzer (TECHPAP, Grenoble, France).

All pulp studied in this work were disintegrated using a laboratory disintegrator (Karl Frank GMBH, Germany).

The fibers' morphological properties were determined automatically by image analysis of a diluted suspension (20 mg/L and 30 mg/L to hardwood and softwood samples, respectively) in a flow chamber in MorFi Fiber Analyzer (TECHPAP, Grenoble, France).

The Gas Chromatography was performed using an Agilent technologies 7890A GC A.01.13 with Agilent Technologies 5975 inert XL MSD with Triple-Axis Detector.

SEM images were performed using Hitachi S-2700 (Tokyo, Japan). The structures were cross-sectioned were covered with gold using a Sputter Quorum Q 15 OR ES (Laughton, East Sussex, UK) and analyzed at different magnifications.

FTIR-ATR was used to analyze the face mask prototypes without and essential oil active molecules. The equipment used was a FTIR-ATR Thermo-Nicolet IS10,(Waltham, MA, USA).

Programs were also used for designing the structures of the materials used in the studies, for image treatment and analysis, for computational simulations and for statistical analysis, ChemDraw Ultra 16.0, MATLAB® version 9.9.0 (R 2020b) and Microsoft Office Excel 2022, respectively.

3.3 Methods

3.3.1 Dry mass content

To determine the dry matter content of the fiber pulp, it was necessary to proceed to the exact determination of the amount of mass that was necessary to weigh. Thus, the procedure used consisted of using a Infra-Red (IR) scale balance that heated the samples to a temperature above 100ºC, to evaporate the water. At the end of the chosen time interval, 30-60 minutes, it is possible to obtain the dry matter content of the sample.

The quantity of dry material contained in wet samples heated under controlled laboratory settings, removing as much water as feasible, is referred to as the dry matter content of a sample.
As a result, in accordance with ISO 5263/1, a sample was put on a Mettler infrared balance, model LJ16 Moisture Analyzer, to measure the TMS of the various materials utilized during the investigation.

3.3.2 Disintegration Process

The disintegration operation has the goal to separate the fibers and for this ISO 5263/1was used using a laboratory disintegrator. The procedure consists of using 2 liters of suspension containing 30 grams of dry pulp, that was previously soaked for at least 24h. The suspension is disintegrated at 30000 revolutions or 10000 depending on the pulp consistency, and this information is included in the ISO.

3.3.3 Fiber Modification Processes

3.3.3.1 Mechanical Treatment

This unitary operation consists of carrying out a mechanical treatment on the cellulosic fibers in an aqueous medium in order to increase their flexibility and enhance their paper properties. The pulps were refined in the PFI mill, using 30 grams of dry pulp with 10% consistency, according to ISO 5264/2. The main can be described as following:

- Make sure that the PFI equipment pressure is 2.3 / 2.4 bar, which corresponded to the value indicated in the ISO, by turning the frontal knob to the desired pressure.

- Preparation of the pulp
- Disintegrate the soaked pulp at 30000 revolutions, as described in 3.2.2.
- Pour the pulp into the leaf former and take the largest portion out of the water to form a pulp disk.
- Place this pulp disk in a goblet and weigh, adding water until it reaches 300g (to make 10% consistency).
- Stir well to dismantle the pulp a little and make the mixture more homogeneous.
- Switch on the equipment that regulates the pressure on the black side switch.
- Make sure that the equipment pressure is 2.3 / 2.4 bar. If not, turn the frontal knob to the desired pressure.
- Select the desired revolutions and press "ok".
- Place the pulp on the walls of the container that is placed on the bottom. Be careful as it needs to be homogeneous on the wall (without holes).
- Wipe the rubber with a cloth dampened with a little soap to prevent it from drying out.
- Press the two side "start" buttons at the same time.
- Place the cover on the blades, turning slightly.
- Beat with a rubber mallet with some vigor while turning the reservoir to ensure that it is tightly closed.
- Press the two start buttons again, for the equipment to begin the refinement process.
- Quickly, turn the side screw, so that the end of it is no longer visible.

- When the refining process is finished, press the side "stop" button and place the side screw as it was initially.

- Take the pulp out of the container into a goblet.

- Lift the cover of the blades, placing it in the initial position.

- With a recipient containing water, wash the blades and place the water with fiber next to the fiber that is already in the goblet.

- Turn off equipment on the side black button. Then disintegrate the pulp at 10000 revolutions and make a 6 L bucket.

Figure 3. 1 - Representation of the PFI mill equipment, that was used to refine fiber, in which (a) overall representation of the equipment and (b) visualization of cellulosic fibers on the walls of the container that is placed on the bottom

3.3.3.2 Enzymatic treatment

Biotechnology can improve pulp and paper raw material quality and productivity, cut production costs, and produce high-value new products. New enzymatic methods can lessen environmental problems and modify fiber qualities (Kenealy & Jeffries, 2003).
The enzymatic treatment reduces refining time and energy to achieve specified fiber qualities (Bajpai, 1999; Jeffries, 1992). Enzyme use facilitates retting, selectively eliminates fiber components, altering their characteristics and increases their flexibility, and covalently connects side chains or functional groups (Kenealy & Jeffries, 2003).
Enzymes are biocatalysts made of linked amino acids. Types of amino acid bonds affect enzyme action. Enzymatic activity is assessed by converting substrates into products over time in established conditions of substrate concentration, pH, and temperature (Yang et al., 2019).
Enzymes act on pulp fiber surface to fibrillate, as in refining. This fibrillation improves all attributes that depend on it, like strength. So, mechanical refining's energy savings are justified by biorefining (de Assis et al., 2018; Singh et al., 2016).
Enzymatic methods make refining more efficient, requiring less energy to obtain the same fibrillation and end sheet strength. This decrease in refiner energy enhances tissue architecture. In recent years, techniques to optimize enzyme performance in tissue have been identified (Morais et al., 2020b).

- Use 30 grams of soaked pulp. Disintegrate it at 30000 revolutions in 2L.
- After disintegrating, place it in the leaf former and drain the water to form a disc.
- Remove the pulp disc to a goblet and weigh and adjust up to 750g (4% consistency).
- Set the pH to 7.
- Place the "thermopar system" properly assembled to control the temperature to desired value or set-up. The control of temperature must be effective because the enzymes will be inactive for inadequate ranges of temperature.
- Add the enzyme when the temperature reaches 40°C.

- Let it act for 2 hours, stirring continuously to ensure that the pulp is mixed evenly, and has a uniform

- Denature the enzyme using sodium hypochlorite, allowing it to act for 5 minutes.

- At the end of the procedure, the pulp is ready for other processes, be it mechanical refining or structure formation.

Figure 3. 2 - Representation of the reactor where it was made the enzymatical treatment of the cellulosic fibers

3.3.4. Fiber mixtures formulations

In order to investigate a wider variety of possible cellulosic matrix configurations, the assortment of fibers was regarded to be a component of the experimental set. Due to this, is it possible to reach a proportion that is appropriate, having better capacity for retaining the active molecule as well as greater porosity and smoothness, given that the application on the skin is the goal. In light of this, the following sets of cellulosic mixes were taken into consideration.

Table 3. 1 - Assay description of fiber mixtures

Assay number	*Assay Description*
1	75% Hardwood fiber Slush + 25% Softwood fiber Refined at 4000 rev + Enzyme + Biopolymer (2%) + MFC (2%)
2	75% Hardwood fiber Slush + 25% Softwood fiber at 4000 rev + Enzyme + Biopolymer (2%)
3	75% Hardwood fiber Slush + 25% Softwood fiber Refined at 4000 rev + Enzyme + MFC (2%)
4	75% Hardwood fiber Slush + 25% Softwood fiber Refined at 4000 rev + Enzyme
5	90% Hardwood fiber Slush + 10% Softwood fiber Refined at 4000 rev + Enzyme + Biopolymer (2%) + MFC (2%)
6	90% Hardwood fiber Slush + 10% Softwood fiber Refined at 4000 rev + Enzyme + Biopolymer (2%)
7	90% Hardwood fiber Slush + 10 %Softwood fiber Refined at 4000 rev + Enzyme + MFC (2%)
8	90% Hardwood fiber Slush + 10% Softwood fiber Refined at 4000 rev + Enzyme
9	Softwood fiber Refined at 4000 rev + Enzyme
10	Softwood fiber + Enzyme

After preparing the mixes for each set, run everything through a disintegrator at 10000 revolutions per minute and proceed with the construction of the structures in accordance with ISO 5269/1.

3.3.5. Fiber suspension characterization

3.3.5.1. Fiber morphology and biometry using a Fiber Analyzer, the MorFi

The morphological properties of the fibers have a direct influence on the structural and mechanical properties of laboratory paper structures. In this way, the morphology of the fibers was characterized, namely, the average length weighed in length, the width, and the coarseness, among others, using the MORFi® device, which consists of a system based on image analysis.

This test consists of adding about 0.3 g of dry pulp (o.d.) to a dilution tank, and this suspension is diluted and analyzed by the image analysis system. This image capture

system is connected to a computer, which has a specific program for the required determinations.

- Open the faucet that contains compressed air and the faucet that contains demineralized water.
- Turn on the green button that is below the computer and turn on the computer.
- Open the MorFi program.
- Select the Fiber "family" that we are going to use, in this case, Softwood. The program will say how many grams of o.d. fiber is necessary. For the Softwood fiber "family", it needed 0.3 grams.
- In the program, Zone 1 stands for sample name and Zone 2 stands for replication number.
- Always do triplicate tests for each experiment.
- After every sample, save the file and/or print.
- When the experiment is done, turn off the computer and turn the faucets into the initial position (first the water faucet and then the air-compressed faucet).

3.3.5.2. Fiber morphology using an optical microscope

For this method, it was used a Nikon Labophot-2 optical microscope with a Leica MC190HD camera attached.

The microscope is first connected in the button found on the base and then the Leica camera connected to the microscope is turned on.
Then start the computer, opening the LAS X software.
The previously prepared sample is placed under the microscope, focusing the image as desired. In this case, the goal was to obtain exemplary images of the various fibers, showing how the refining process can affect them.
After that, the binocular part is turned to the left, thus passing the image to be transmitted on the computer screen.

Within the LAS X software, access the Acquire menu and select the objective (magnification) on the microscope. After that, click on *Acquire Image → Ok*.
After the image is obtained, in the Analysis menu, the image can be modified, such as numbering fibers or even measuring the distance between their walls, allowing the calculation of the lumen size. Then click on *Merge all → Create Duplicate → Ok*. This allows you to save a copy of the image obtained with the changes made, while also preserving the original.

3.3.5.3. Drainability using ºSR method

According to ISO 5267/1, the pulp suspension drainability was assessed in triplicate using the Schopper-Riegler degree method.

- For the portion of the equipment's top to rise, turn on the faucet. Since the reservoir is a net, it must be washed in water before being placed on top because it can include the residues of previous experiments.

- Put the reservoir in the equipment's base and handle it there (upper part will go down)

- Calculate how much pulp equals 2g of fiber, then measure that amount out and put it in the graduated cylinder. Put one liter or more in the same graduated cylinder. It should be mentioned that the temperature must be at 20±0,5°C for the test to be as accurate as possible.

- Pour the amount that was in the sample, over the apparatus

- To pour the suspension into the graduated cylinder, rotate the knob at the equipment's base once more.

- The Schopper Riegler degree (ºSR) is calculated considering the volume that emerges from the graduated cylinder at the front.

- To determine the mass of the same, a structure made in accordance with ISO 5269/1.

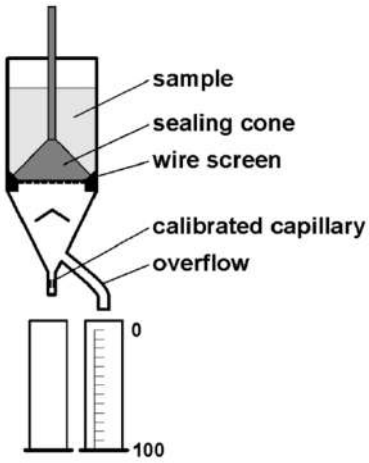

Figure 3. 3 - Schopper-Riegler freeness tester (Adapted from (Przybysz et al., 2014))

3.3.6. Essential oils characterization using GC-MS

The Gas Chromatography was performed using an Agilent technologies 7890A GC A.01.13 with Agilent Technologies 5975 inert XL MSD with Triple-Axis Detector (figure 3.4).

Figure 3. 4 – Agilent technologies 7890A GC A.01.13 with Agilent Technologies 5975 inert XL MSD with Triple-Axis Detector representation

After obtaining and separating the oil, 0.1 mL of it is dissolved in 1 mL of dichloromethane for analysis of its compounds.

A mobile phase composed of helium was used that will drag each component present in our oil.

The polar stationary phase used is composed of DB-5 (Dimethyl polysiloxane) having 5% phenyl groups. Its characteristics are represented in figure 3 .4.

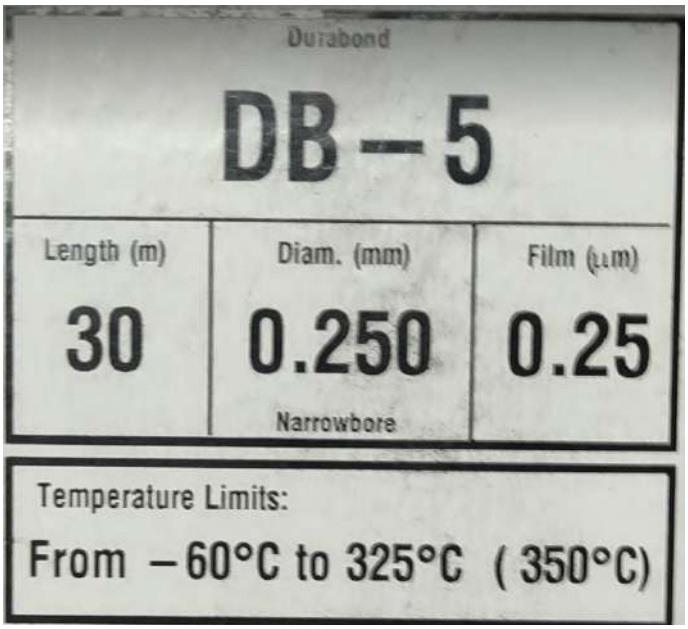

Figure 3. 5 - Dimensions and limits of the stationary phase used in the analysis

It is necessary to identify the position where the sample is introduced in order to program the system. In this analysis, the essential oils method (*Method: Oleos_essencial*) was used to evaluate the compounds present in the oil.

The temperatures of the different components of the equipment are mentioned in table 3.1.

Table 3. 2 - CG-MS initial conditions

Equipment	Division	Temperature ºC
GC	Injector	250
	Initial Oven Temperature	40
MS	Interphase	280
	Source	230
	Quadrupole	180

In this analysis, a flow rate of 1 ml/min was used, the initial oven temperature was 40 ºC and an increase of 5ºC per minute was performed until reaching 250ºC, thus reaching a total of 52 minutes of analysis. During this time, the compounds were eluted with their respective retention times depending on their affinity with the stationary phase.
Using the Gerstel maestro 1 – sequences program, it was possible to analyze the peaks obtained and compare them with the existing database, thus determining the compounds present in the oil.

3.3.7. Production of Dermic Delivery Systems

3.3.7.2.1 Peppermint essential oil emulsion (*Mentha x piperita L.*)

The infusion consists of 1 g of Tetley peppermint tea in 50 g of water at 100°C for 5 min. An emulsion is a mixture of liquids that are normally immiscible. In this case, 200 g of sunflower oil and 50 g of peppermint infusion from Tetley were used to make the emulsion, this one containing 5 drops of the essential oil of peppermint.
An important aspect is to add drops of essential oil to the infusion only when it is already cold, considering that the essential oil volatilizes very easily. There were also added 2 g of NaCl to facilitate the formation of the emulsion.

The infusion containing the infusion with the essential oil tastes and NaCl is placed on a Thermomix, that it is turned on at a medium speed (3700rpm) and the vegetable oil is added slowly and in a thread.
The agitator will continue to operate until the two phases are well mixed.
After this is done, it is stored at 0-4ºC.
The emulsion was added to the pulps' bulk, and then disintegrated according to the relevant standard. The structures were produced using the same methodology described above.

Figure 3.6 – Emulsion containing sunflower oil and *Mentha piperita* essential oil

3.3.7.2.2. Preparation of functionalized structures

- For structure formation, ISO 5269/1 was used to produce structures with a high level of reproducibility. The procedure is summarized in the following steps:

- Place the net in the equipment and close it.

- Open the faucet that contains demineralized water and let it rise to the first indication (marked inside the equipment).

- Place the sample, that is going to produce the structure and it was previously calculated from the oven-dried (o.d.) mass.

- Let the water rise to the second mark.

- Use a homogenizer, stir 6 times, according to ISO, to assure the perfect homogenization.
- Open the drainage valve, so all the water goes through the net, and wait about 10 sec, to assure there's no more water left.

- Close the drainage valve and open the equipment.

- Place a round blotter above the fiber that is on the net and, above that place 3 square blotters and press slightly. That would allow to remove all the excess water;

- Remove the square blotters and put them aside;

- Remove the round blotter containing the fiber and place it on a drying disc, containing the fiber upwards, and leave them to dry in a constant environment, with temperature 22±1ºC, with a relative humidity of 50±2%, according to ISO 187.

3.3.8. Dermic delivery systems characterization

3.3.8.1 Structural properties

The basis weight (ISO 12625- 6), thickness, and volume of the produced structures were used to characterize them (ISO 12525-3). The base weight was calculated by dividing the average mass of each building by its respective surface area (0.02138 m2). Using a Frank-PTI micrometer, the thickness was measured. The volume of the structures was determined by dividing the thickness by their basis weight. In addition, the apparent theoretical porosity (porosity) of the structure was determined using the following formula:

$$Porosity\ (\%) = 100 \times \left(1 - \frac{\rho_{structures}}{\rho_{cellulose}}\right) \quad (1)$$

where $\rho_{cellulose}$ was the density of the cellulose (1.5 g/ cm3) and $\rho_{structure}$ was the apparent density of the structures (g/ cm^3).

3.3.8.2. Morphological characterization using image analysis by SEM

The SEM (Scanning Electron Microscopy) procedure was performed to perform the respective structural analysis and morphological characterization. Since the analysis is done on structures in that were dried in a controlled temperature and humidity laboratory, it is only necessary to make cuts for the sections to be visualize them. The samples are fixed to the disk with a little double-sided glue. If we are going to visualize the structure on the Z axis, the sample must be a little larger, and we must bend it so that it remains at an angle of 90 degrees. The sample must be covered with a conductive substance, in this case gold (a gold powder, more specifically), by sputtering, in order to

be able to reflect the electrons, and consequently obtain an image. SEM images were performed using Hitachi S-2700 (Tokyo, Japan). The structures were cross-sectioned were covered with gold using a Sputter Quorum Q 15 OR ES (Laughton, East Sussex, UK) and analyzed at different magnifications.

3.3.8.3. Chemical characterization and kinetics using FTIR-ATR

FTIR-ATR was used to analyze the face mask prototypes without and essential oil active molecules. The equipment used was a FTIR-ATR Thermo-Nicolet IS10, (Waltham, MA, USA)

Open the OMNIC Software, as it can be seen in figure 3.7.

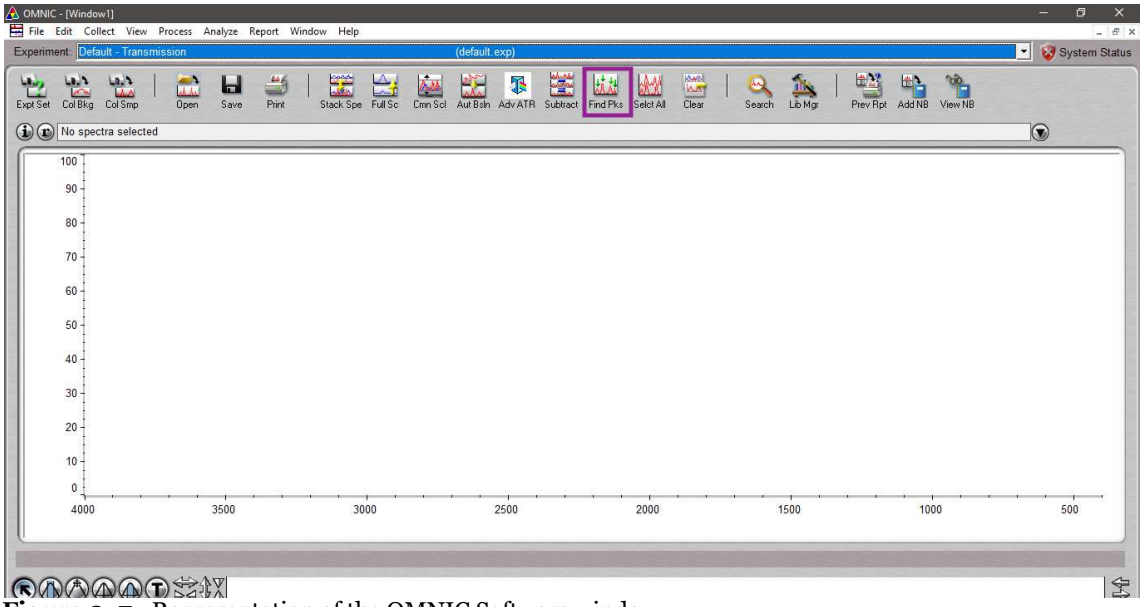

Figure 3. 7 - Representation of the OMNIC Software window

In the “Smart Accessory Change” window, select “Smart itr diamond ATR” (last option in the list)

To collect the background, select the button “Col Bkg”. After collection, the save to a folder of your choice.

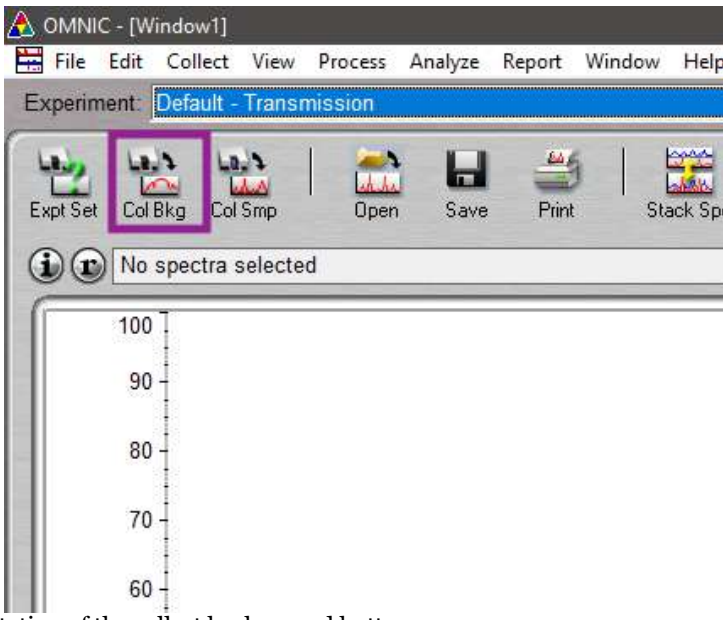

Figure 3. 8 - Representation of the collect background button

In "Expt set" (that means Experimental set) (figure 3.9), it is going to open a secondary window, and it is important to put the select settings bellow. These settings already are represented in figure 3.7.

- Collect No. Scans 32
- Resolution: 4cm^{-1}

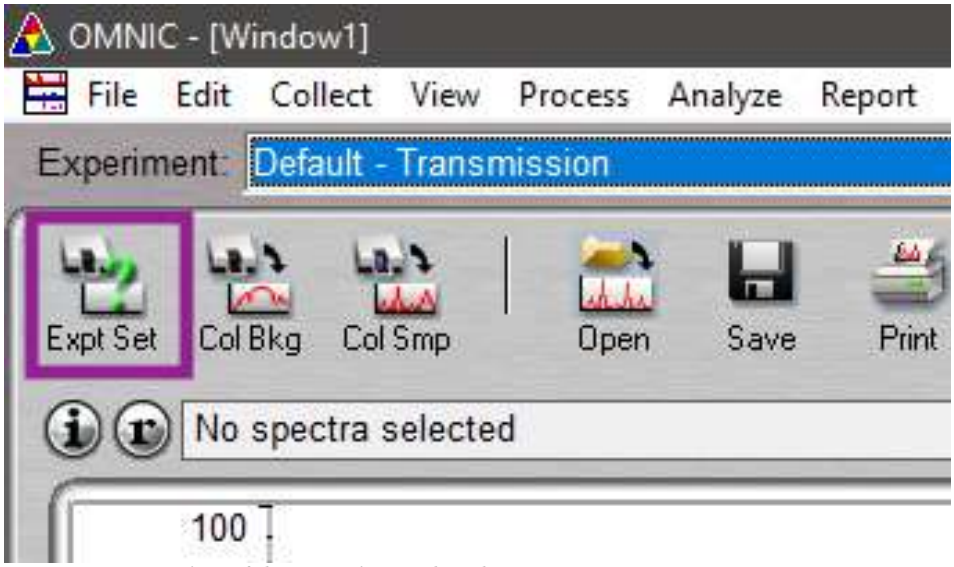

Figure 3. 9 - Representation of the Experimental set button

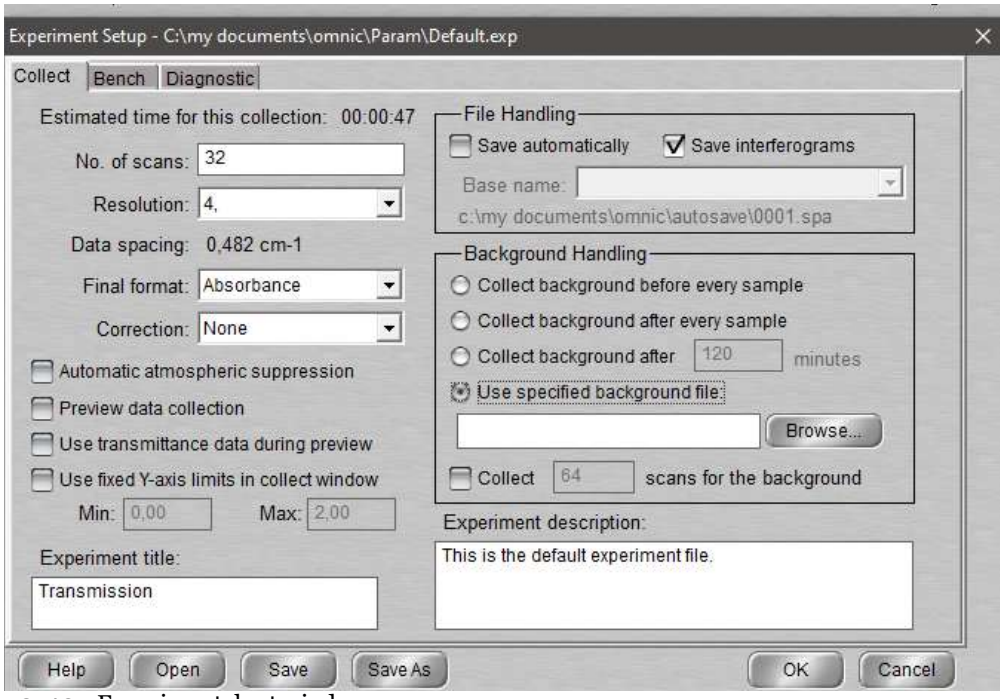

Figure 3. 10 - Experimental set window

Under "Background handling" select there are various ways that can be used, as seen in figure3.10

Collect background can be done before every sample, after every sample or after a defined amount of time. The other option is to "use specified background file", but first is needed:

- 1st collect background
- 2nd browse (to search and select the previously saved background file after its collection)

Given that we will be using this procedure with volatile essential oils, it would be most appropriate to gather the background file, save it to a properly labeled folder, and then open the file. This provides for greater precision, as collecting each sample before each sample could detect essential oil molecules in the air would not generate the most accurate kinetics or experimental procedure.

Select "col smp" (collect sample), as can be seen in figure 3.11. After insert the name of the sample and press "ok". After spectrum acquisition click "yes".

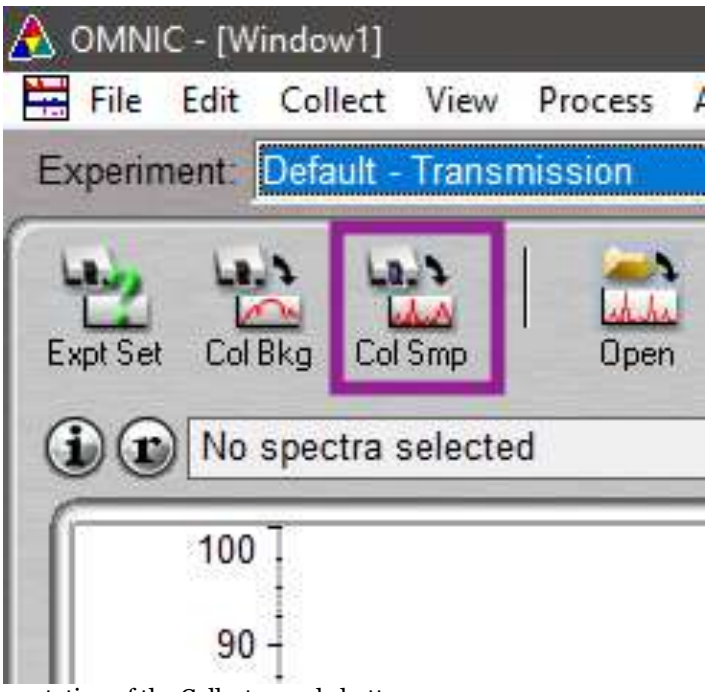

Figure 3. 11 - Representation of the Collect sample button

Once acquired the spectra, click on “find pks” (find peaks), as can be seen in figure 3.12. Place line where you desire, as represented in figures 3.13 and 3.14 and click on replace. If not all peaks appear, press full scale.

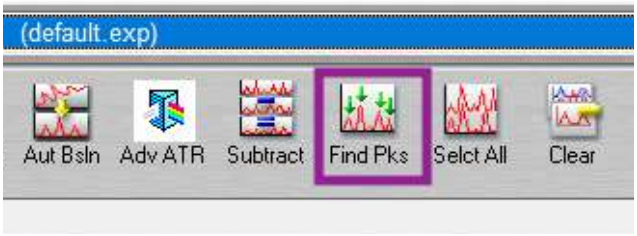

Figure 3. 12 - Representation of the find peaks button

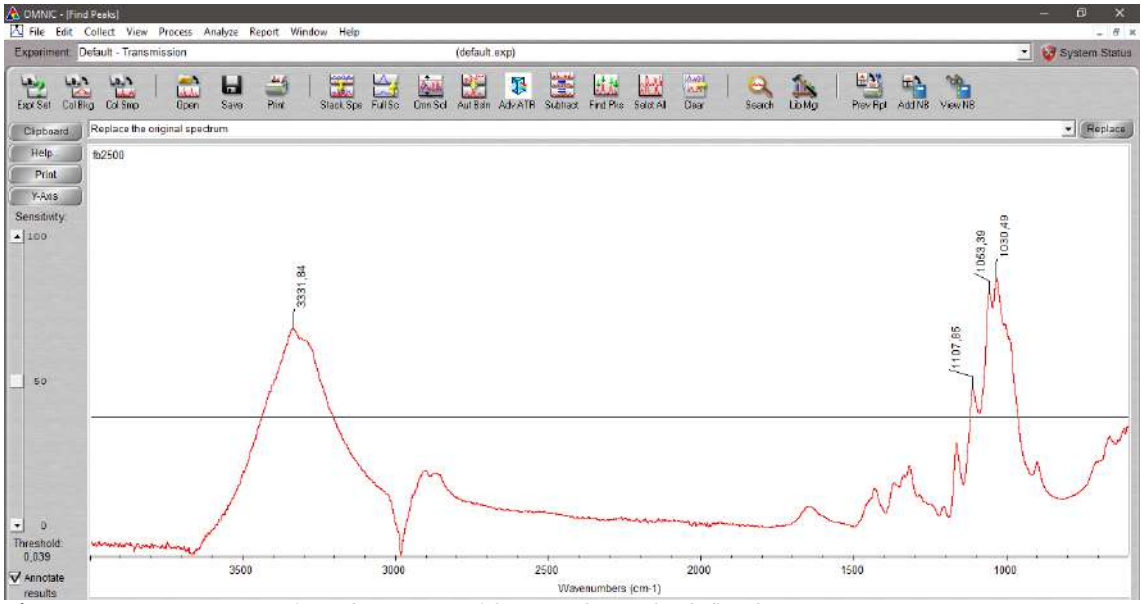

Figure 3. 13 - Representation of a spectra with some the peaks defined

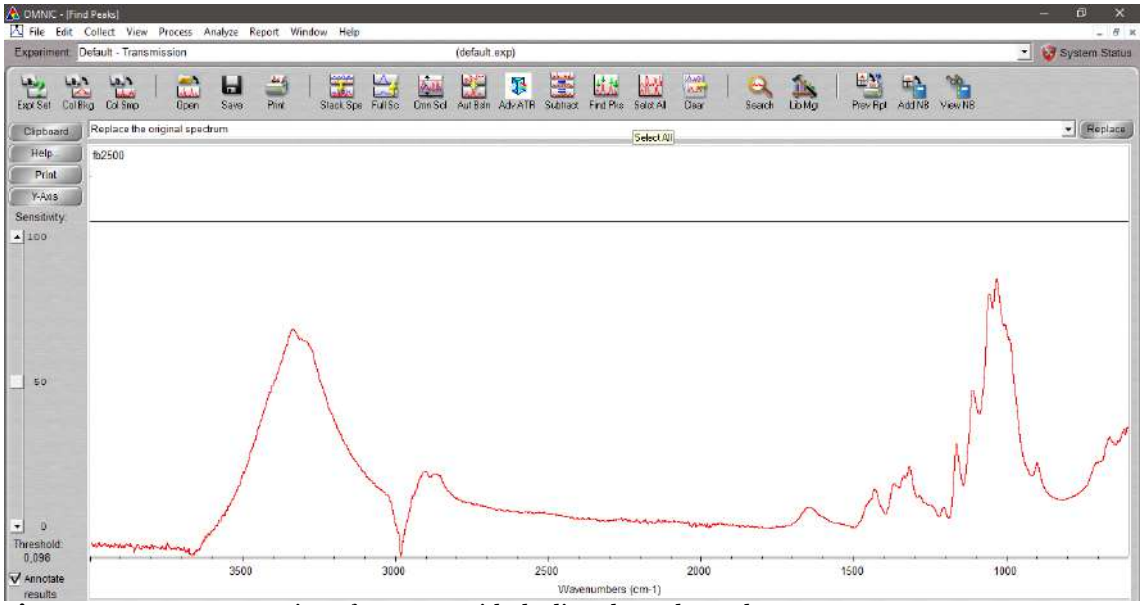

Figure 3. 14 - Representation of a spectra with the line above the peaks

To keep everything organized, create a folder with the name of the sample that was examined.

To save the file, simple go to: File-> Save as. Is important to save the file as a Spectra(.spa), TIFF(.tif) e CV Text(.csv).

3.3.9. Computational Simulation studies for structure optimization

The Voxelfiber simulator, created and validated by Conceição, Curto, Simões, and Portugal (Conceição et al., 2010; Curto et al., 2011) was used in the study to identify and optimize the amount of cellulose fibers to be used in the preparation of the DDS in order to obtain an ideal proportion as well as the analysis of these fibers when combined with other types of fibers, with its programming in MATLAB® version (R 2020b).

The simulator is built on a cellular automata, in which each fiber is represented as a sequence of voxels, each of which fills a predetermined volume (Morais & Curto, 2022). Through this simulator, one can create a 3D model of the fibrous structures made by each individual fiber or conjugated one while manipulating the fibers' various properties, such as their lengths and widths, flexibility, fiber wall thickness, lumen thickness, and resolution (Morais et al., 2020a, 2020b).

In the scope of this work, a handbook for the simulator user/researcher is being developed by the authors Joana Moreira and Joana Curto.

Chapter IV Results and Discussion

4. Results and Discussion

The main goal is to develop systems made to retain and release active molecules using a 3D Cellulose-based polymeric matrix made from a combination of fibers.
To accomplish that the investigation of different fibers from different pulps is essential.
To achieve this main goal, varied outcomes of the many experimental sets conducted are presented in this chapter, including:

The characterization of several kinds of mechanical softwood cellulosic fiber processing, as well as mixes of mechanically and enzymatically processed cellulose matrices
A prototype made of hardwood fiber was also utilized to apply an emulsion containing *Mentha piperita* essential oil.

Both biometric analyses utilizing MorFi and the study of laboratory-built structures, where the thickness variation, which affects porosity variation, can be determined, were used to carry out this evaluation. Appendix B contains all of the characterization tables for cellulose matrix structures.

Images were also gathered from SEM analysis, allowing us to identify the different types of pores and fibrillation in the structures. This allowed us to determine how much mechanical treatment can affect fibrillation, creating more fine elements, which will allow us to better implant active molecules in our structure. A characterization of the fiber morphology was also developed utilizing an optical microscope with a camera as a supplement to this viewing. This assay offers a distinct viewpoint on cellulose matrix fibrillation.

For the accurate analysis of the essential oils in this experimental set, Gas Chromatography with Mass Spectrometry (GC-MS) was performed, allowing for the verification of the major components of each oil.

A characterization by FTIR-ATR was conducted once cellulosic matrices and oils had been properly characterized. This allowed for the development of kinetic tests that demonstrated the release of the active molecules over time, as would be predicted, as well as the ability to confirm the existence of the essential oil in the cellulosic structure.

Also, a benchmark marketing analysis was conducted, which involves comparing our prototype with some existing products. This gives us a better understanding of what is already available as well as what we can add and improve to turn our prototype into an innovation.

Finally, this project's utilization of a previously verified computational simulation, which enables the simulation of various types and quantities of cellulosic matrices, is one of its major innovations. We were also able to determine the length, width, thickness, flexibility, and collapsibility of the 3D network, which is essential for optimizing the function of transport and regulated release of active molecules. This is crucial because it enables the simulation of several alternatives, which improves transportation systems and controlled release while also contributing to resource preservation.

4.1 Fiber suspension characterization

4.1.1 Fiber morphology and biometry using a Fiber Analyzer, the MorFi

A fiber analysis program, MorFi®, created by Techpap, Grenoble, France, was used to determine the morphological characteristics of the fibers. The system combines an image analysis program and a camera for the measurement of suspended fibers. The length, width, coarseness, twist, and curvature of the fiber, among other parameters, were examined.

To modify the pulp fibers to the main operation were done, one consisting of a mechanical treatment, designated by “beating” or “refining”, and the other of an enzymatic process.

The mechanical refinement of the fibers was done using PFI laboratory equipment using distinct beating levels, corresponding to the interval between 500 and 7500.

Assay for Hardwood Fiber (Eucalyptus Fiber)

Table 4. 1 - Biometry results of hardwood fiber, obtained by MorFi.

	Hardwood Fiber
Fibers (million/g)	21,269±0,010
Length arithm. (mm)	0,681±0,0023
Length weighted in length (mm)	0,793±0,002
Width (µm)	19,267±0,115
Coarseness (mg/100 m)	0,0692±1,528E-04
Kink angle (º)	130±0
Kinked fibers (%)	32,733±0,404
Curl (%)	8,233±0,0577
Rate in length of MacroFibrills (%)	0,495±0,011
Broken Ends (%)	20,783±0,211
Fine elements (% in length)	36,8±0,173
Percentage of fine elts (% in area)	12,07±0,139

Values reported are the mean ± standard deviations.

4.1.1.1 Influence of mechanical treatment of SW

In table 4.2 are represented the results of Softwood Fiber Refined Mechanically Assays, obtained by MorFi.

Table 4. 2 - Biometry results for Softwood fiber refined at various revolutions, obtained by MorFi.

	SW	***SW_Ref 500***	***SW_Ref1000***	***SW_Ref 1500***	***SW_Ref 2000***	***SW_Ref 3000***	***SW_Ref 4000***	***SW_Ref 6000***
Fibers (million/g)	4,742 ±0,538	5,930 ±0,276	5,298 ±0,280	4,892 ±0,144	5,186 ±0,446	6,187 ±0,310	6,714 ±0,058	6,687 ±0,128
Length arithm. (mm)	1,059 ±0,042	1,098 ±0,021	1,094 ±0,025	1,083 ±0,007	1,102 ± 0,032	0,989 ±0,020	0,953 ±0,016	0,929 ±0,019
Length weighted in length (mm)	1,858 ±0,047	1,921 ±0,045	1,910 ±0,061	1,866 ±0,040	1,918 ±0,056	1,727 ±0,010	1,693 ±0,026	1,616 ±0,029
Width (µm)	30,1 ±0,2	31,2±0,3	30,5 ±0,2	30,6 ±0,1	30,7 ±0,2	32,4 ±0,3	32,3±0,3	31,8±0,3
Coarseness (mg/100 m)	0,2052 ±0,0323	0,1586± 0,0085	0,1771± 0,0121	0,1934± 0,0067	0,1798± 0,0194	0,1665± 0,0110	0,1581± 0,00216	0,1626± 0,0048
Kink angle (º)	130 ± 1	131 ± 1	131 ± 1	131±0	131±0	130±1	130±1	130±1
Kinked fibers (%)	50,6 ±0,4	43,5 ±0,3	48,3 ±0,8	47,9 ±0,4	46,6 ±0,5	47,2 ±0,8	32,8 ±0,2	43,1 ±0,8
Curl (%)	13,1 ±0,2	12 ±0,3	12,8 ±0,3	12,5 ±0,1	12,5 ±0,2	13,3 ±0,2	10,6 ±0,1	12,2 ±0,2
Rate in length of MacroFibrills (%)	0,618 ±0,023	0,717 ±0,019	0,618 ±0,007	0,597 ±0,007	0,624 ±0,018	1,263 ±0,053	1,486 ±0,009	1,342 ±0,041
Broken Ends (%)	46,32 ±1,22	45,12 ±0,65	44,47 ±0,81	44,37 ±0,47	45,00 ±2,04	49 ±0,76	48,27 ±0,40	47,50 ±1,52
Fine elements (% in length)	24,4 ±21,3	35,2 ±1,4	33,1 ±2,2	33,9 ±0,9	32,7 ±2,5	43,6 ±5,0	42,7 ±2,2	43,2 ±0,2
Percentage of fine elts (% in area)	2,39 ±2,12	3,46 ±0,4	3,31 ±0,71	3,93 ±0,3	3,53 ±0,76	4,08 ±0,53	3,30 ±0,27	3,82 ±0,04

Values reported are the mean ± standard deviations.

During this investigation, several assays of mechanical treatment were carried out, with the number of rotations being gradually raised.
It was concluded that there was a change in the fine elements, which is evidence that the cellulose material fibrillated.
Overall, comparing the SW sample without refining with an intense refining (6000 revolutions), the results indicated that this mechanical treatment decreased the length weighted in length by 13%, the coarseness by 21%, the kinked fibers by 15%, the curl by 7%, and increased the rate of macrofibrils rate by 117%, and the fines content by 77%. The variation of properties throughout the assays depends on the detection limits of the fiber analyzer used. In line with the goal of producing optimized structures, this study allowed selecting a suitable sample with the desired morphological properties to be combined with a hardwood slush pulp and additives. The SW_Ref_4000 sample was selected for the next steps.

Assays that combination of Hardwood fiber and Softwood that was mechanically treated through PFI and enzymatically treated

4.1.1.2. Influence of fiber mixture formulations

The assay description is presented in Table 4.3
The results of the analysis of the biometry of the fiber mixtures are presented in Table 4.4.

Assays that combination of Hardwood fiber and Softwood that was mechanically treated through PFI and enzymatically treated

Table 4. 3 - Description of the assays containing the different fiber mixture

Assay Number	*Assay Description*
1	75%HW+25%SW_Ref4000+Enz+Biopolymer (2%) +MFC (2%)
2	75%HW+25%SW_Ref4000+Enz+Biopolymer (2%)
3	75%HW+25%SW_Ref4000+Enz+MFC (2%)
4	75%HW+25%SW_Ref4000+Enz
5	90%HW+10%SW_Ref4000+Enz+Biopolymer (2%)+MFC (2%)
6	90%HW+10%SW_Ref4000+Enz+Biopolymer (2%)
7	90%HW+10%SW_Ref4000+Enz+MFC (2%)
8	90%HW+10%SW_Ref4000+Enz
9	SW_Ref4000+Enz
10	SW+Enz

Despite the fact that assay 8 (90%HW+10%SW_Ref4000+Enz) is mentioned in all experimental test tables involving fiber mixing, no data will ever be provided. This is because, according to the procedure outlined in section 3.3.4, 270 g of Slush pulp formed from hardwood fibers would be required, however only 2.261 grams were available. This rendered the experiment impractical to conduct, not only because the mixture would not coincide with the remaining of the experiments, but also because it would not correspond with the total fiber content required by ISO standard 5269/1.

Table 4. 4 - Biometry results for the assays containing various fiber mixtures, obtained by MorFi.

	1	***3***	***4***	***5***	***7***	***9***	***10***
Fibers (million/g)	19,994 ±1,530	20,379 ±0,416	20,894 ±0,252	21,771 ±0,745	21,852 ±0,879	6,704 ±0,067	5,542 ±0,264
Length arithm. (mm)	0,608 ±0,004	0,612 ±0,004	0,618 ±0,004	0,614 ±0,004	0,613 ±0,001	1,009 ±0,006	1,100 ±0,023
Length weighted in length (mm)	0,717 ±0,003	0,722 ±0,004	0,729 ±0,003	0,722 ±0,005	0,720 ±0,002	1,745 ±0,009	1,889 ±0,052
Width (µm)	20,0 ±0,2	20,1±0,1	19,4 ±0,6	19,1±0,2	18,9 ±0,0	32,2 ±0,1	30,6 ±0,4
Coarseness (mg/100 m)	0,0827± 0,0068	0,0804± 0,0018	0,0778± 0,0013	0,0749± 0,0031	0,0747± 0,0033	0,1509± 0,0017	0,1692± 0,0065
Kink angle (º)	131±1	131±0	130±1	131±1	131±1	129±0	131±1
Kinked fibers (%)	41,1±0,6	41,2±0,8	42,4 ±0,5	43,3 ±0,7	39,4 ±0,3	32,4 ±0,9	49,9±0, 8
Curl (%)	9,5±0,2	9,6±0,1	10,3±0,1	10,4±0,1	9,5±0,2	10,4±0, 0	13,1±0,1
Rate in length of Microfibrils (%)	0,766 ±0,030	0,763 ±0,008	0,777 ±0,035	0,772 ±0,027	0,755 ±0,059	1,108 ±0,031	0,659 ±0,043
Broken Ends (%)	25,21 ±0,82	23,22 ±0,75	23,88 ±0,83	22,44 ±0,53	22,00 ±0,20	46,95 ±0,71	45,84 ±1,59
Fine elements (% in length)	35,7±0,4	33,4±1,3	29,7±5,5	32,8±1,7	20,3 ±17,6	37,8±1,5	37,9±1,7
Percentage of fine elts (% in area)	8,66 ±0,29	6,55 ±0,85	6,62 ±0,47	6,95 ±0,31	4,94 ±4,28	3,20 ±0,28	3,68 ±0,38

Values reported are the mean ± standard deviations.

During this investigation, several mixtures of fibers were carried out, as is described in table 4.3.

Overall, comparing the SW sample without refining to the SW sample that underwent enzymatic treatment (assay 10), the results indicated that the enzymatic treatment increased the length weighted in length by 2%, decreased the coarseness by 18% and the kinked fibers by 11%, and increased the rate of macrofibrils rate by 7%, as well as the fines content by 56%.

While paralleling a SW sample without refining to one that underwent mechanical refining (4000 rev) and enzymatic treatment (assay 9) revealed that the combination of mechanical and enzymatical treatment decreased the length weighted in length by 6%, the coarseness by 26%, the kinked fibers by 36%, and the curl by 21%, while increasing the rate of macrofibrils by 79% and the fines content by 55%.

Finally, contrasting SW that underwent mechanical treatment (4000 rev) with SW that underwent mechanical refining (4000 rev) and enzymatic treatment (assay 9) revealed that the combination of mechanical and enzymatical treatment increased the length weighted in length by 3% and decreased the coarseness by 5%, the kinked fibers by 1%, the curl by 2%, the rate of macrofibrils rate by 25%, and the fines content by 12%. The fluctuation of characteristics among experiments is contingent on the detection limits of the fiber analyzer employed.

4.1.2. Fiber morphology using an optical microscope

The characterization of the fibers was done using a microscope with a camera attached to visualize the fibers morphology. Figure 4.1 and 4.2 presented the influence of the mechanical treatment in the fibers of bleached and non-bleached softwood pulps, respectively.

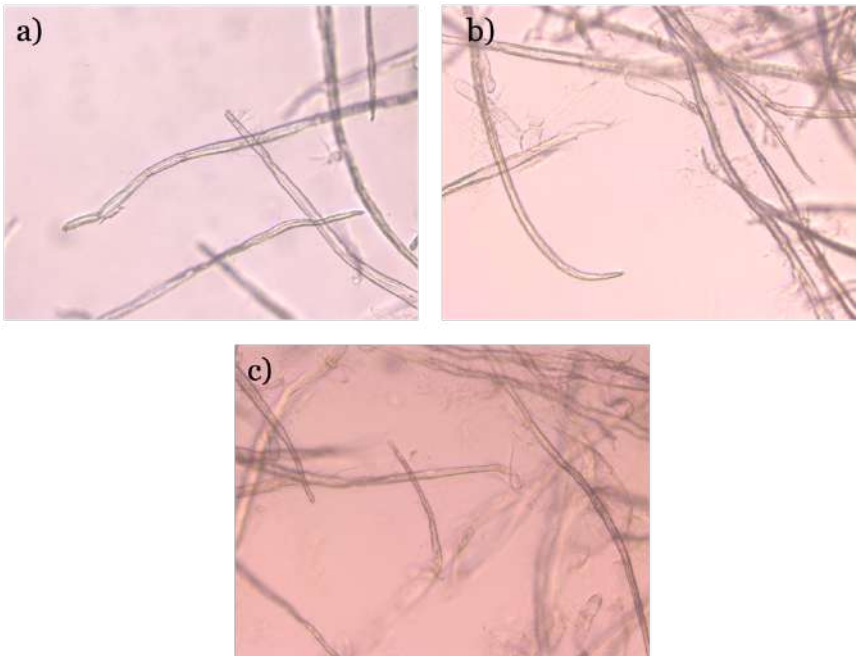

Figure 4.1 - Images obtained with Optical microscope with camera of bleached cellulose refined at various revolutions, in which (a) Bleached Cellulose refined at 2500 rev, (b) Bleached Cellulose refined at 4500 rev and (c) Bleached Cellulose refined at 7500 Rev.

As a result, it is possible to identify fine elements as well as some fibrillation in figure 4.1, in particular in figures 4.1 (b) and (c). This is due to the fact that the higher the level of mechanical treatment, the more prominent the appearance of fine elements.

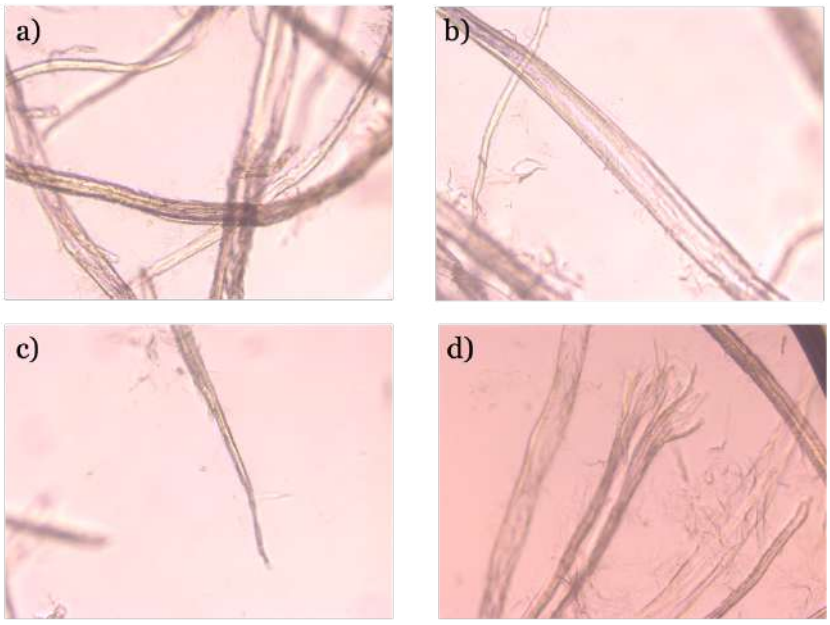

Figure 4.2 - Images obtained with an Optical microscope with camera of softwood non-bleached cellulose refined at various revolutions, in which (a) Non-Bleached Cellulose refined at 2500 Rev, (b) Non-Bleached Cellulose refined at 4500 Rev, (c) Non-Bleached Cellulose refined at 4500 Rev and (d) Non-Bleached Cellulose refined at 7500 Rev

What can be observed in figure 4.2 is what greater mechanical treatment can do to cellulosic fiber if it is exposed to it. The fibrillation of the fibers rises in proportion to the degree to which they have been refined. This can be observed more plainly in figures 4.2 (c) and 4.2 (d), specifically in the later of these two figures, in which the presence of fine materials towards the end of the cellulosic fiber can be plainly seen, and in which one can consider the fiber to have split up into multiple different segments.

4.1.2. Drainability using ºSR method

The refining process was also monitor by the Schopper Riegler Degree (ºSR), which is a drainage test. Table 4.5 presented the ºSR values for the SW sample, treated mechanically. The results indicated that the ºSR increases with refining and is mainly related to the fiber surface area and the fines content. With the mechanical refining, the fibers become more flexible, the outer wall develops fibrillation, and fines form, allowing for enhanced interfiber connections and structure strength.

Table 4. 5 - Schopper Riegler Degree (ºSR) of Softwood Refined Fiber

Softwood Fiber Refined (Rev)	*ºSR*	*Weight (g)*
0	11	1,721
500	14	1,945
1000	14	2,032
1500	14	1,866
2000	14	1,859
3000	46	-
4000	66	1,92
6000	74	-

As is it shown in Table 4.5, it's able to perceive that the mechanical treatment process through the PFI has a direct impact on the Schopper Riegler Degree. For a better visualization of the correlation of this data, it was a made a linear regression represented in figure 4.3.

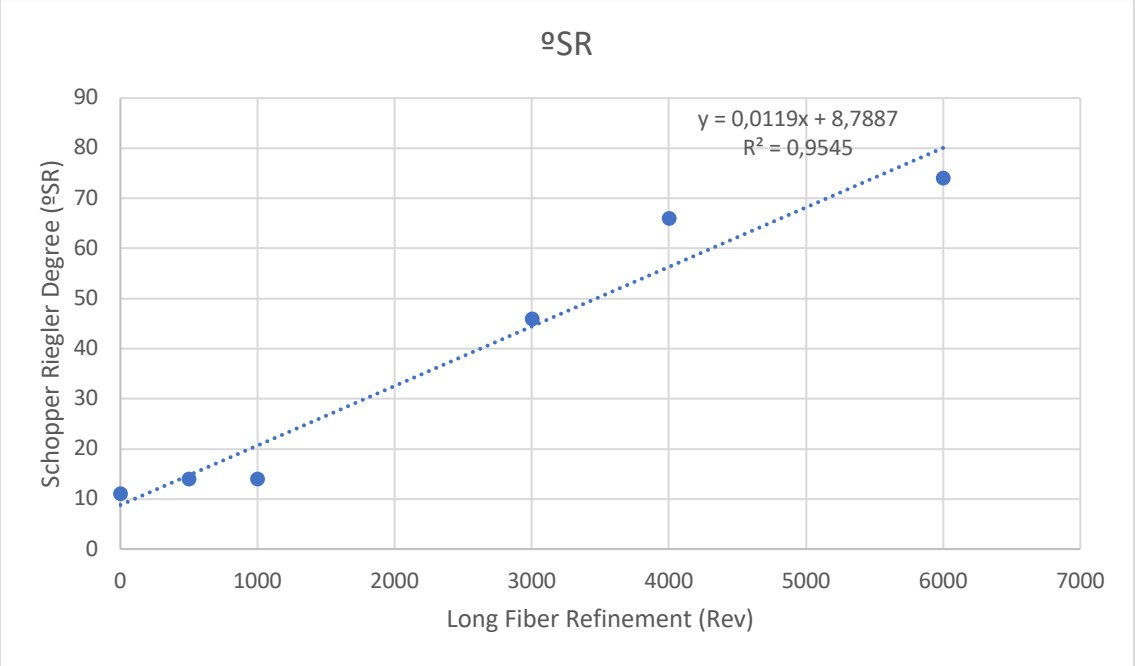

Figure 4.3 - R-squared representation of Shopper Riegler Degree of Softwood Fiber Refined

The Softwood (SW) pulp e Hardwood (HD) SW_ref4000

Table 4.6 - Schopper Riegler Degree (ºSR) of fiber mixtures

Assay Number	*Description*	*ºSR*	*Weight (g)*
1	75%HW+25%SW_Ref4000+Enz+Biopolymer (2%) +MFC (2%)	23	2
2	75%HW+25%SW_Ref4000+Enz+Biopolymer (2%)	21	1,94
3	75%HW+25%SW_Ref4000+Enz+MFC (2%)	25	1,875
4	75%HW+25%SW_Ref4000+Enz	20	1,857
5	90%HW+10%SW_Ref4000+Enz+Biopolymer (2%)+MFC (2%)	19	1,967
6	90%HW+10%SW_Ref4000+Enz+Biopolymer (2%)	15	1,949
7	90%HW+10%SW_Ref4000+Enz+MFC (2%)	22	1,82
8	90%HW+10%SW_Ref4000+Enz	-	-
9	SW_Ref4000+Enz	55	1,92
10	SW+Enz	14	1,925

4.2. Essential oils characterization using GC-MS

Mentha piperita, *Lavandula angustifolia*, and *Citrus limon* essential oils were chosen because they are part of a certain set that is considered CPTG (Certified Pure Test Grade). Since each oil each has unique properties and specific components that have particular characteristics, the characterization of these samples consisted of identifying its main volatile components, using the GC-MS technique.

The essential oils were characterized using GC-MS and the results are presented in tables 4.7, 4.8 and 4.9

4.2.1 *Mentha piperita*

The GC-MS chromatogram obtained is presented in Figure 4.4, in which the peaks presented correspond to the retention time of each compound, some of them showed in Table 4.16.

Table 4.7 - a) Relative chemical composition (%) of *Mentha piperita* L. essential oil b) Menthol Molecular structure in 2D and 3D. Molecules made using ChemDraw ® Professional 16.0 by Moreira, J.

a)

Compound	RI	%
β-pinene	978	1.0
Limonene	1030	2.0
1,8-Cineole	1032	5.5
Menthone	**1151**	**20.8**
Menthofuran	1164	7.3
Neomenthol	1167	3.2
Menthol	**1177**	**35.3**
Terpinen-4-ol	1177	1.3
Pulegone	1234	1.7
Menthyl acetate	1296	7.1
β-Caryophyllene	1420	2.9
Germacrene D	1481	2.0

b)

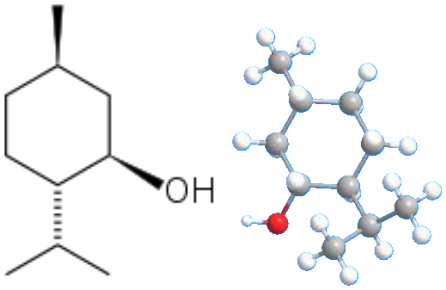

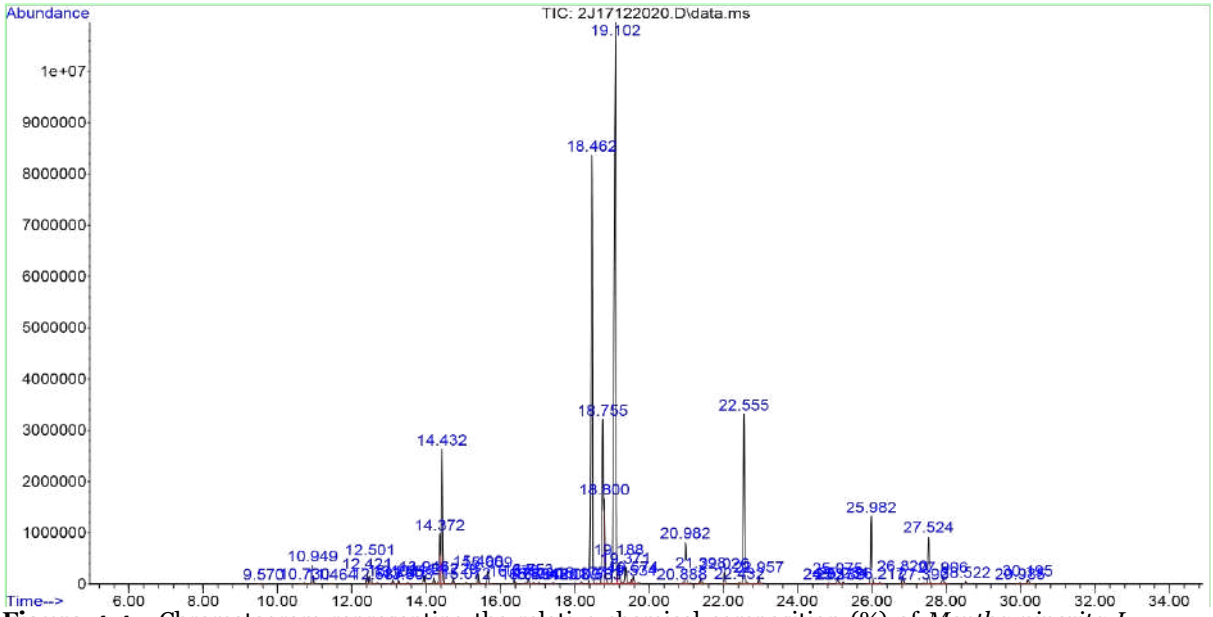

Figure 4.4 - Chromatogram representing the relative chemical composition (%) of *Mentha piperita L.* essential oil

According to the information displayed in table 4.7 and figure 4.4, Menthol constitutes 35.3% of the total components in the essential oil of *Mentha piperita*, while Menthone accounts for 20.8% of the total components.

Table 4.16 simply displays the major components of the sample under analysis. The GC-MS chromatogram obtained is presented in Figure 4.4, in which the peaks presented correspond to the retention time of each compound, some of them showed in Table 4.16.

Menthol (35.3%) and menthone (20.8%), were the two major compounds, with the other components being present trace amounts.

4.2.2 *Lavandula angustifolia*

The GC-MS chromatogram obtained is presented in Figure 4.5, in which the peaks presented correspond to the retention time of each compound, some of them showed in Table 4.8.

Table 4.8 - Relative chemical composition (%) of *Lavandula angustifolia* essential oil

Compound	***RI***	***%***
b-cis-Ocimene	1038	4,41
b-trans-Ocimene	1048	2,33
Linalool	**1099**	**31,76**
Oct-1-en-3-yl-acetate	1110	1,04
Lavandulol	1168	2,01
Terpinen-4-ol	1177	3,86
α-Terpineol	1190	1,70
Linalyl acetate	**1255**	**30,49**
Lavandulyl acetate	1289	5,29
trans-caryophylene	1420	3,81
cis-b-Farnesene	1446	3,04

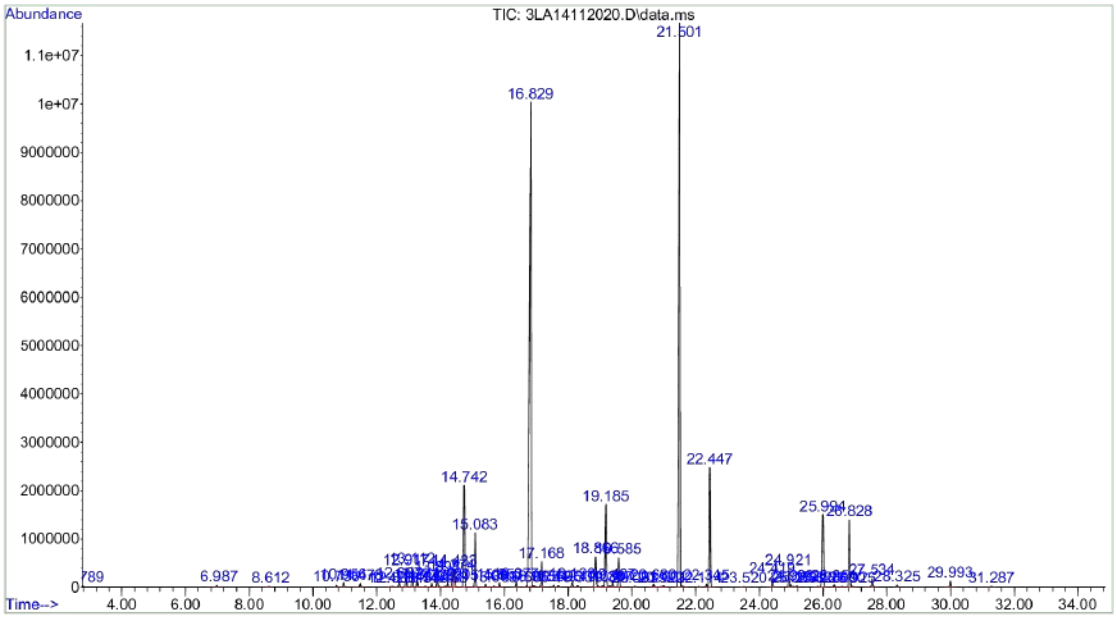

Figure 4.5 - Chromatogram representing the relative chemical composition (%) of *Lavandula angustifolia* essential oil

The essential oil of *Lavandula angustifolia* contains Linalool, which consists of 31.76% of the total components, and linalyl acetate, which makes up 30.49% of the total components, as illustrated in table 4.8 and figure 4.5.

4.2.3 *Citrus limon*

The GC-MS chromatogram obtained is presented in Figure 4.6, in which the peaks presented correspond to the retention time of each compound, some of them showed in Table 4.9.

Table 4.9 - Relative chemical composition (%) of *Citrus Limon* essential oil

Compound	**RI**	**%**
α-Pinene	936	1,86
Sabinene	973	1,98
β-Pinene	**978**	**10,20**
β-Myrcene	989	1,52
Limonene	**1030**	**69,30**
γ-Terpinene	1060	8,53

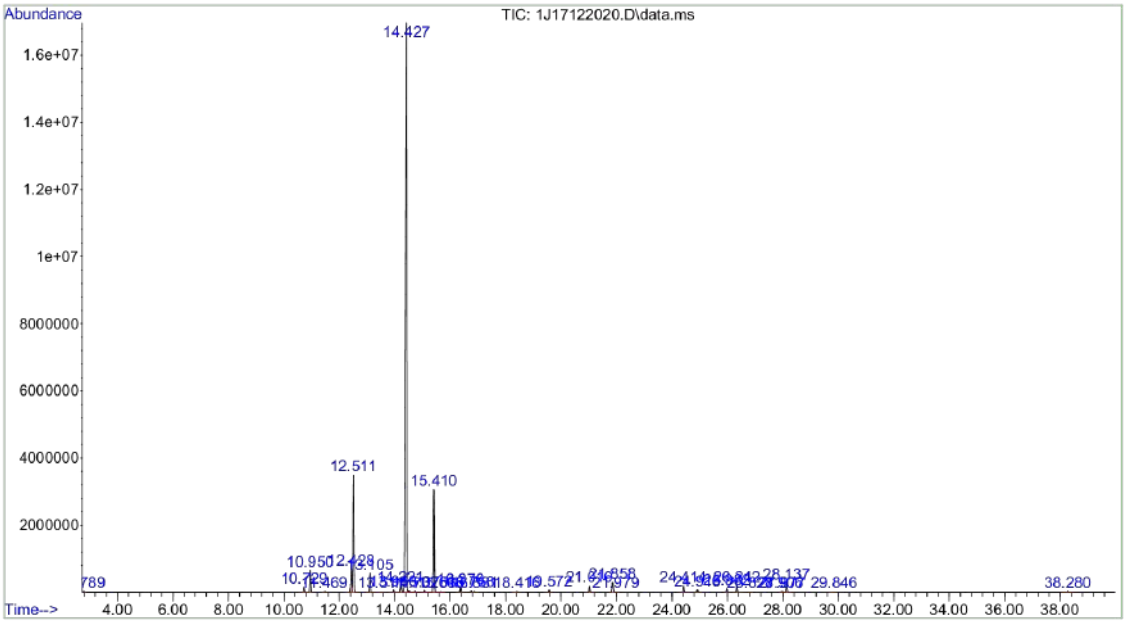

Figure 4.6 - Chromatogram representing the relative chemical composition (%) of *Citrus limon* essential oil

According to table 4.9 and figure 4.6, the *Citrus limon* essential oil contains limonene, which represents up 69.30% of the total components, and **β**-Pinene, which constitutes 10.20% of the total components.

4.3. Dermic delivery systems characterization

4.3.1. Structural properties

4.3.1.1 Characterization of the DDS fiber-based matrix structures

It was made a study where long cellulosic fibers that were subjected to mechanical treatment as described in ISO 5264/2:2011, with the same intensity, 1,6 N. Changing the number of revolutions from zero to 6000. The results in table 4.7 quantify the influence of the mechanical treatment revolutions, which are characterized in terms of porosity, thickness, and density of the cellulosic paper structures. As can be seen in Table 4.7 presents the results of the DDS characterization. The main objective was to study how the mechanical treatment that was performed in softwood fiber through PFI can affect the structural properties. The complete characterization table is presented in Appendix B1 for consultation.

Table 4.10 - Physical characterization of cellulose structures containing mechanically refined softwood fiber

Softwood Fiber PFI beating (Revolutions)	*Porosity (%)*	*Tissue Thickness (µm)*	*Structure Density (g/cm3)*
0	90,3 ± 1,22	138,854 ± 19,638	0,144 ± 0,018
500	89,55 ± 1,21	124,600 ± 12,276	0,157 ± 0,018
1000	89,188 ± 1,261	126,867 ± 16,058	0,162 ± 0,019
1500	89,579 ± 1,342	128,176 ± 28,058	0,156 ± 0,020
2000	89,306 ± 1,165	120,083 ± 15,732	0,160 ± 0,017
3000	82,589 ± 4,160	113,483 ± 44,523	0,261 ± 0,062
4000	72,926 ± 19,463	91,710 ± 38,195	0,406 ± 0,292
6000	79,217 ± 6,071	96,857 ± 32,230	0,312 ± 0,091

Values reported are the mean ± standard deviations.

Regarding table 4.10, the variation in porosity may be due to the production of fines and broken fibers. As expected, the findings of the Schopper-Riegler Degree help to confirm this, as the ºSR provided a high value of 74, as shown in table 4.5.

4.3.1.2 Structure Characterization of Assays containing mixtures of Mechanical and enzymatical treatment

The mechanical process results indicate that beating and enzymatical treatment of the fibers, it was realized in various assays, containing mixtures to see how that would affect the physical properties. To optimize the structures, several tests were carried out on the combination of cellulosic fibers, which consist of those subjected to mechanical treatment and those that were subjected to enzymatic treatment. The table 4.11 shows the influence on the porosity, thickness, and density of cellulosic structures.

Table 4.11 - Physical characterization of cellulose structures in different assays

Assay Description	*Porosity (%)*	*Tissue Thickness (µm)*	*Structure Density (g/cm3)*
75%HW+25%SW_Ref4000+Enz+Biopolymer (2%) +MFC (2%)	88,212±1,481	131,358±36,225	0,177±0,022
75%HW+25%SW_Ref4000+Enz+Biopolymer (2%)	88,403±1,669	127,564±51,189	0,174±0,025
75%HW+25%SW_Ref4000+Enz+MFC (2%)	88,837±1,606	128,426±33,838	0,167±0,024
75%HW+25%SW_Ref4000+Enz	89,163±0,711	112,894±9,421	0,163±0,011
90%HW+10%SW_Ref4000+Enz+Biopolymer (2%)+MFC (2%)	90,144±0,754	115,878±8,738	0,148±0,011
90%HW+10%SW_Ref4000+Enz+Biopolymer (2%)	91,066±0,782	146,452±17,101	0,134±0,012
90%HW+10%SW_Ref4000+Enz+MFC (2%)	88,017±1,031	110,160±9,642	0,180±0,015
SW_Ref4000+Enz	80,736±4,194	93,919±32,000	0,289±0,063
SW+Enz	86,847±2,120	146,462±64,663	0,197±0,032

Values reported are the mean ± standard deviations.

It can be observed in table 4.11 how the mixtures previously described in the experimental set influence the structural properties shown in. In the SW Ref4000+Enz test, for instance, it was determined that the enzymatic treatment enhanced the porosity and thickness of the structures while decreased their density.

It is also confirmed that the SW Ref4000+Enz test increased the porosity and thickness of the structures, indicating that the enzymatic treatment reduced their density in contrast to the SW Ref4000, as shown in table 4.10.

In addition, it can be observed from the mixtures created in this experiment that the additives contribute positively regardless of the amounts of fibers used. The mixtures of 90%HW+10%SW Ref4000+Enz+Biopolymer (2%)+MFC (2%) and 90%HW+10%SW Ref4000+Enz+Biopolymer (2%) stand out as having the maximum porosity (90.144±0.754 and 91.066±0.782) and lowest tissue densities (0.148±0.011 and 0.134±0.012), respectively.

4.3.1.3 Structure Characterization of Hardwood Fiber (Eucalyptus fiber)

Table 4.12 showed, cellulosic structures containing hardwood fibers were produced according to ISO 5269/1 without the use of any additive This assay was conducted so that the fibers could be characterized at a later time, taking into consideration the fact that this would serve as a point of comparison following the addition of the emulsion.

Table 4. 12 - Structure Characterization of Hardwood Fiber (Eucalyptus fiber)

	Hardwood Fiber
Weight (g)	0,681±0,283
Area (m^2)	0,02138±0
Grammage (g/m^2)	31,845±13,243
Tissue Thickness(mm)	0,135±0,043
Tissue Thickness (µm)	135,378±43,455
Bulk (cm^3/g)	4,432±0,582
Structure Density (g/cm^3)	0,229±0,0294
Density/1,5	0,153±0,0196
Porosity	0,847±0,0196
Porosity (%)	84,710±1,958

Values reported are the mean ± standard deviations.

4.3.1.4 Structure Characterization of Hardwood Fiber (Eucalyptus fiber) containing peppermint essential oil emulsion

The emulsion was added as the cellulosic structures were developed, or rather, it was completely integrated into the structure.

Table 4.13 - Structure Characterization of Hardwood Fiber (Eucalyptus fiber) containing peppermint essential oil emulsion

	Hardwood Fiber + Emulsion
Weight (g)	0,481±0,267
Area (m^2)	0,02138±0
Grammage (g/m^2)	22,484±12,511
Tissue Thickness(mm)	0,105±0,032
Tissue Thickness (µm)	104,706±32,033
Bulk (cm^3/g)	4,941±0,641
Structure Density (g/cm^3)	0,206±0,034
Density/1,5	0,138±0,023
Porosity	0,862±0,023
Porosity (%)	86,235±2,259

Values reported are the mean ± standard deviations.

As illustrated in tables 4.11 and 4.12, there is a decrease in tissue thickness and a decrease in structure density. When these structures were characterized, they were found to be smoother than a typical 20 g/m^2 structure.

The structures were manufactured after, and although though the grammage was just 20g/m^2, they were left attached to the blotter to mimic a layered system that could be applied to the skin due to its slickness. Figure 4.7 illustrates this distinction between the blotter and the cellulose structure.

Figure 4. 7 - Emulsified cellulosic structure attached to the blotter to mimic a layered system that could be applied to the skin as a dermic system.

4.3.1.5 Structure Characterization of mixture containing softwood fiber, microcrystalline cellulose and chitosan

As chitosan is widely used because it is as abundant as cellulose and also has the advantages of being biodegradable, biocompatible, and innocuous (Arias et al., 2021) to see if these had an influence on the structural characterization parameters as an additive, as shown in table 4.14.

Table 4.14 - Structure Characterization of Softwood fiber (SW) with the additives Microcrystalline Cellulose and Chitosan

	SW + CelMC + Chitosan
Weight (g)	1,334±0,012
Area (m^2)	0,02138±0
Grammage (g/m^2)	62,404±0,564
Tissue Thickness(mm)	0,231±0,007
Tissue Thickness (µm)	230,8±7,085
Bulk (cm^3/g)	3,698±0,0914
Structure Density (g/cm^3)	0,271±0,007
Density/1,5	0,180±0,005
Porosity	0,820±0,005
Porosity (%)	81,964±0,453

Values reported are the mean ± standard deviations.

The chitosan did not have much influence as an additive in this assay. In order to be able to draw correct conclusions, an experimental plane had to be defined, with the use of various concentrations, and, after characterizing the structures, analyzing whether or not chitosan would actually alter the characterization of the cellulosic structure, showing benefits for the controlled release of active molecules in cellulosic matrixes. However, work has been developed in the area of microencapsulation in how the characteristics of the same can be for controlled release with essential oils (Arias et al., 2021).

4.3.1.6 Structure characterization of bleached and non-bleached softwood

The mechanical treatment of softwood fiber that had been bleached (SW) and softwood fiber that had not been bleached (NSW) was done in a second series of experiments conducted after this investigation. The objective with this experimental set would be to visualize possible differences in characterization or behavior when the active molecules, in this case the essential oils were applied to the same. In the characterization, as can be

seen in tables 4.15 and 4.16, it is possible to verify a decrease in porosity with the increase in mechanical treatment, as it was also shown in table 4.10. Regarding the application of essential oils in these structures, these facts will be discussed further throughout the text, especially in section 4.3.4.

Table 4. 15 - Structure characterization of softwood fibers refined mechanically

	Porosity (%)	*Tissue Thickness (µm)*	*Structure Density (g/cm³)*
SW_Ref_2500	70,71±1,075	143,7±5,964	0,439±0,0161
SW_Ref_4500	57,840±0,666	100,1±1,370	0,632±0,00998
SW_Ref_7500	45,428±1,681	76,8±2,348	0,819±0,0252

Values reported are the mean ± standard deviations.

Table 4. 16 - Structure characterization of non-bleached softwood fibers mechanically refined

	Porosity (%)	*Tissue Thickness (µm)*	*Structure Density (g/cm³)*
NSW_Ref_2500	73,970±1,761	162,6±9,617	0,390±0,0264
NSW_Ref_4500	69,474±1,152	141,4±6,995	0,458±0,0173
NSW_Ref_7500	45,428±1,681	76,8±2,348	0,819±0,0252

Values reported are the mean ± standard deviations.

In the experiments involving the unbleached softwood, a minor change in porosity, tissue thickness, and structure density is observed between the 2500 and 4500 revolution mechanical treatment tests. As with 7500 Revolutions, the porosity falls below 50%, indicating that it would not be an appropriate form for applying the active molecules, as there are fewer pores in which they may be kept.

4.3.2. Morphological characterization using image analysis by SEM

The SEM technique was used to visualize the structural properties, allowing for more information by viewing the arrangement of the porous 3D network. Thus, the differences between structures constructed of mechanically polished softwood and those constructed of a blend of softwood and hardwood in various proportions can be studied. They were examined and magnified at different magnifications (from 50x to 1000x).

4.3.2.1 Softwood Fiber Refined at 4000 Revolutions + Enzyme

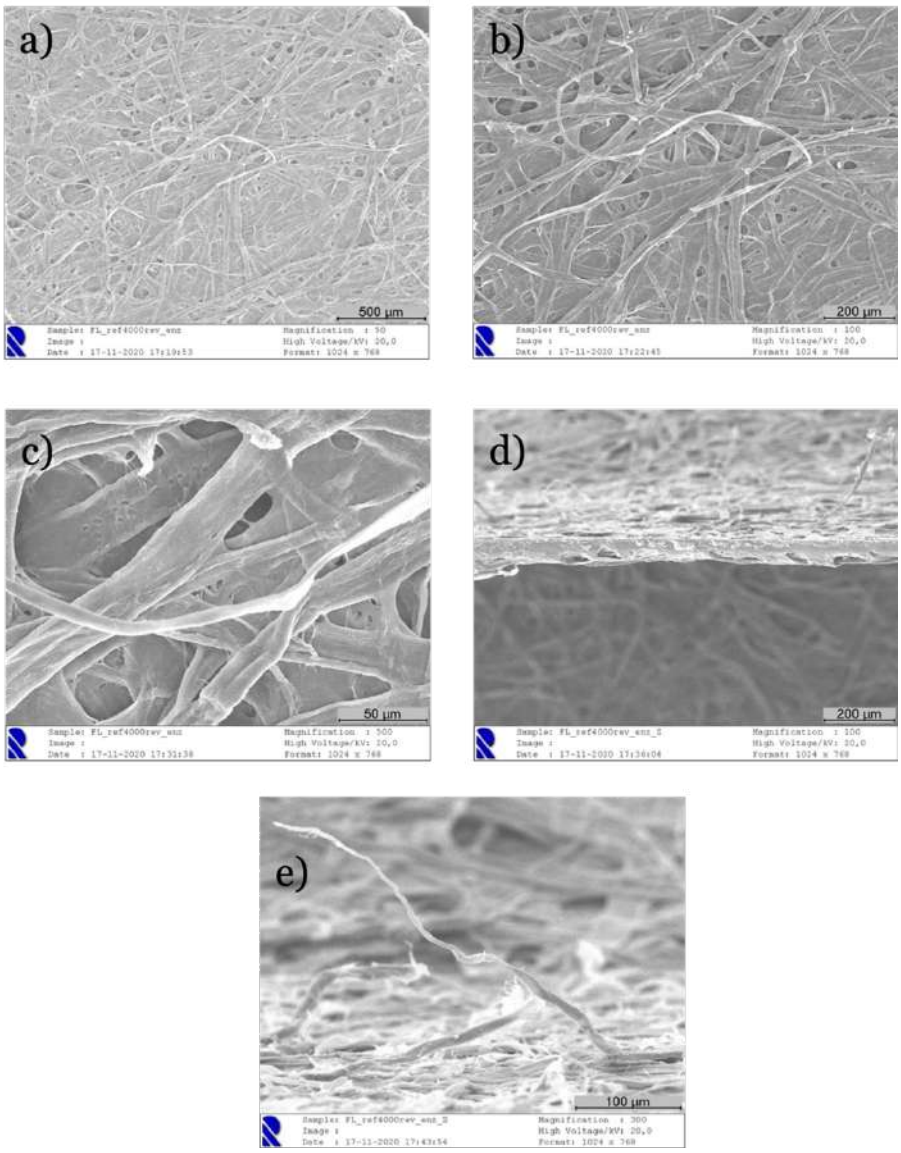

Figure 4.8 - SEM images of Softwood fiber refined at 4000 Revolutions + Enzyme magnified at 50x (a), 100x (b), 500x (c), 100 x in the Z axis(d) and 300x in the Z axis (e).

As can be visualized in Figure 4.8, the structure has a wide variety of pores, but what stands out most in this figure is how potent the enzymatic treatment can be on cellulosic fibers, affecting their thickness, variety of pores, and, as seen in Figure 4.13(e), the fibrillation that occurs in the cellulosic matrix, making it a clear alternative for other types of treatment.

4.3.2.2 75% Hardwood Fiber+25% Softwood Fiber

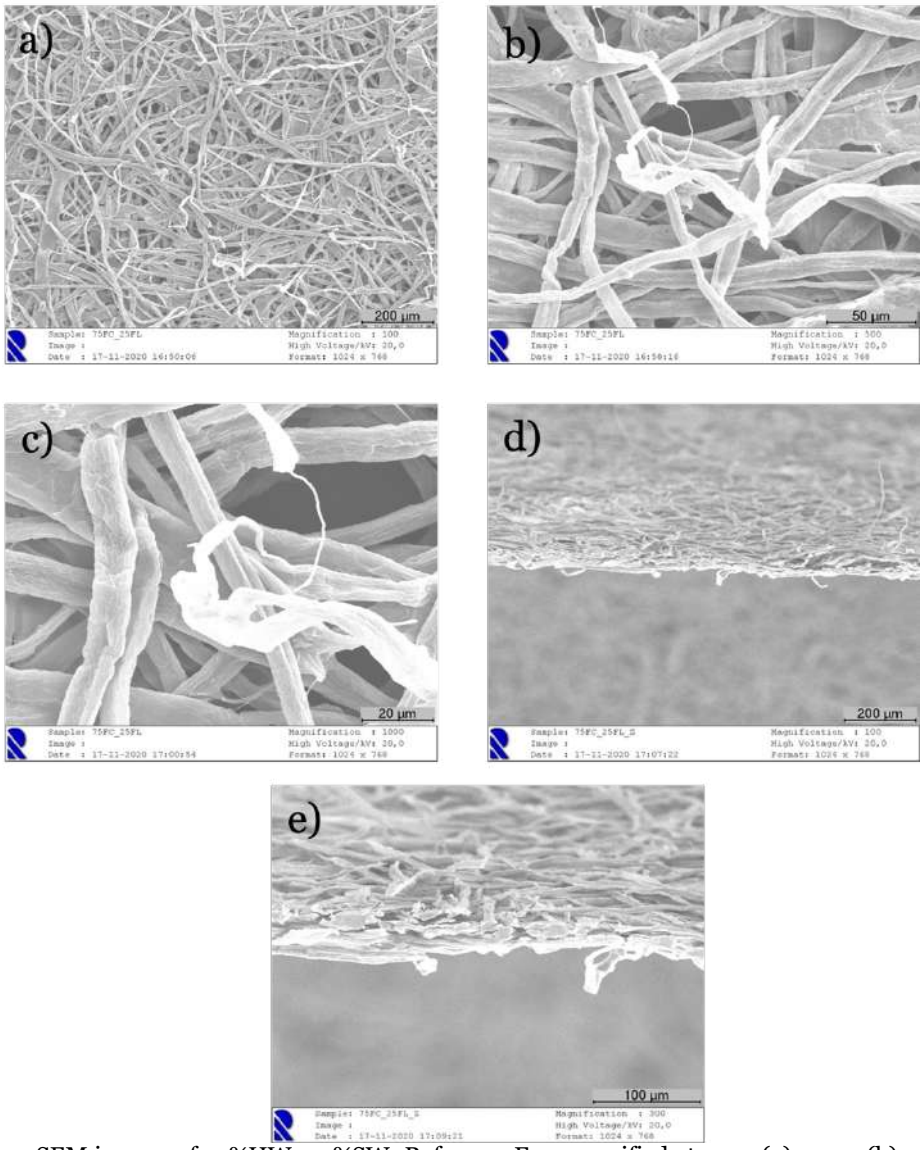

Figure 4.9 - SEM images of 75%HW+25%SW_Ref4000+Enz magnified at 100x (a), 500x (b), 1000x (c), 100 x in the Z axis(d) and 300x in the Z axis (e).

Due to the fact that it is made up of a range of fibers, the structure has a greater variety of pores, as can be seen in figure 4.9. In spite of the fact that the fiber that has been treated enzymatically only accounts for 25% of the total, its impact on the structure is clear. The enzymatic treatment causes fibrillation, which adds to a higher pore variation, which, in turn, has the potential to contribute to a greater retention of the active chemical of interest.

4.3.2.3 75% Hardwood Fiber+25% Softwood Fiber + Biopolymer

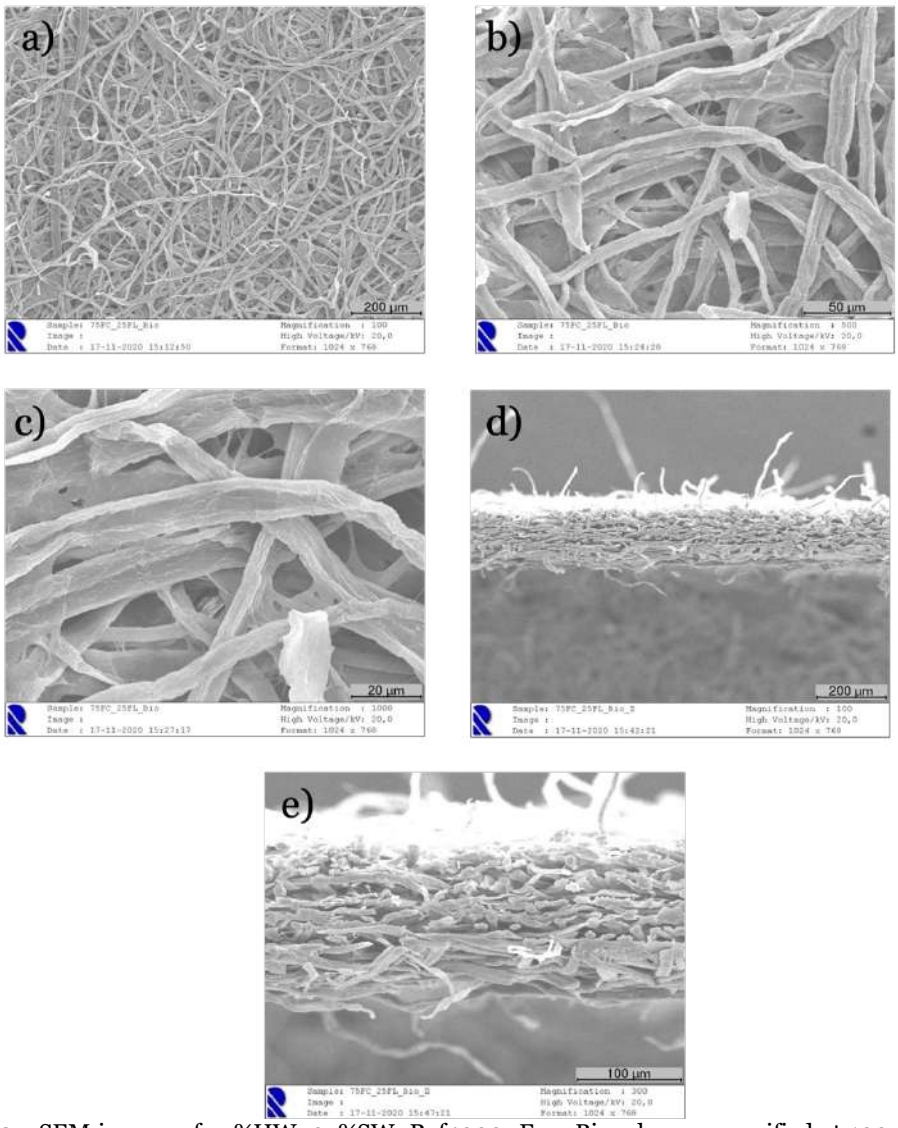

Figure 4.10 - SEM images of 75%HW+25%SW_Ref4000+Enz+Biopolymer magnified at 100x (a), 500x (b), 1000x (c), 100 x in the Z axis(d) and 300x in the Z axis (e).

In addition to being structure porous because of the enzymatic treatment and the fiber mixture, but it is also porous since biopolymer was used in the manufacturing process. This can be seen in figure 4.10. Throughout the various phases of the figure, it is clear to visualize how a diversity of pores (figures 4.10 (b) and (c)) can be transposed into a fine structure (figure 4.10(d)), and in which one can see how significantly a structure cellulosic structure can be complex, due to the deposition of cellulosic fibers that it appears to have, therefore creating diversity with each structure created (figure 4.10 (e)).

4.3.2.4. 75% Hardwood Fiber+25% Softwood Fiber + MFC

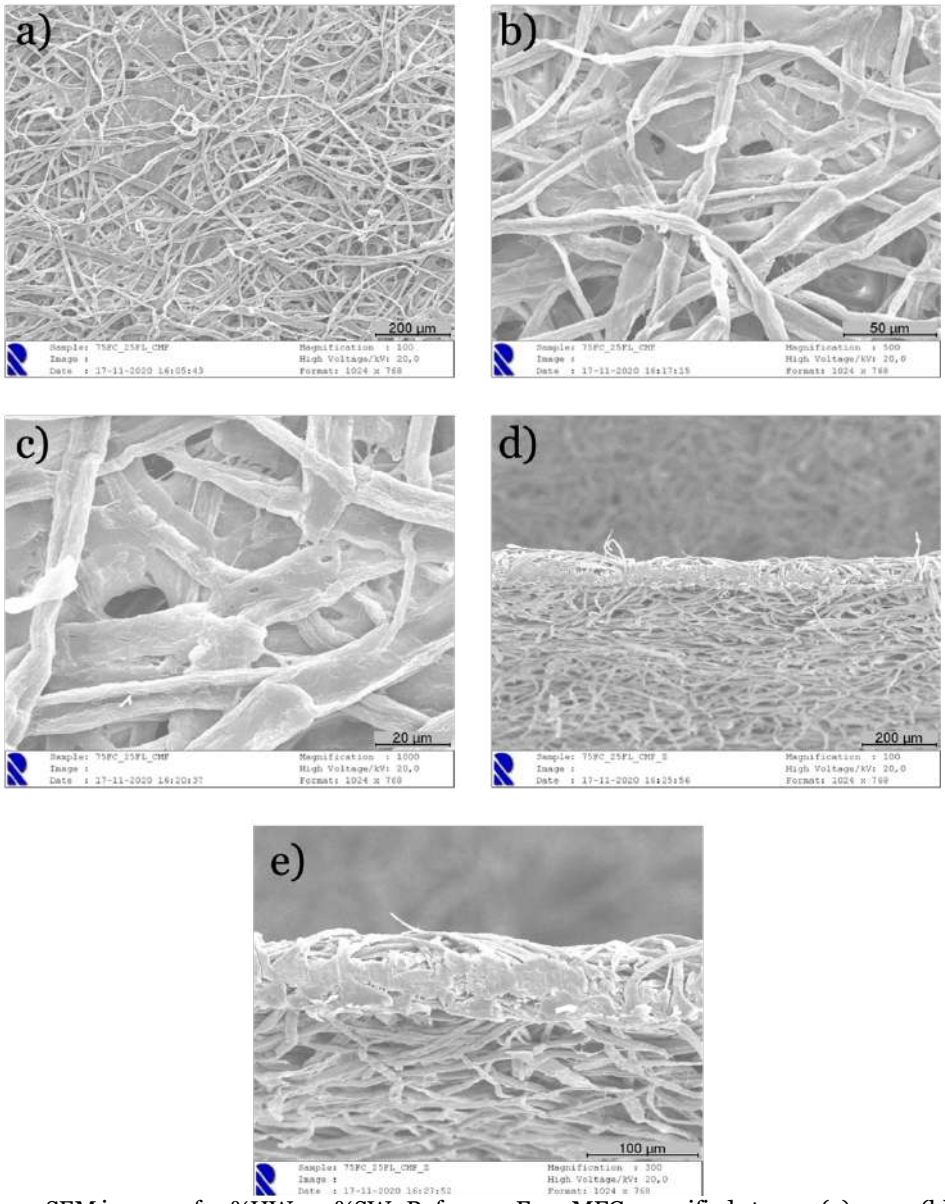

Figure 4.11 - SEM images of 75%HW+25%SW_Ref4000+Enz+MFC magnified at 100x (a), 500x (b), 1000x (c), 100 x in the Z axis(d) and 300x in the Z axis (e).

The utilization of MFC, in addition to the enzymatic treatment and fiber combination, results in the structure exhibiting a wide range of pores, as shown in figure 4.11. These variety of pores are present not just due to the fiber mixture but also due to the addition of MFC. In this particular example, it is conceivable to picture how a variety of pores (as seen in figures 4.11(b) and (c)) can be converted into an exceedingly intricate fine structure (as seen in figure 4.11(d)).

4.3.2.5 75% Hardwood Fiber+25% Softwood Fiber + Biopolymer + MFC

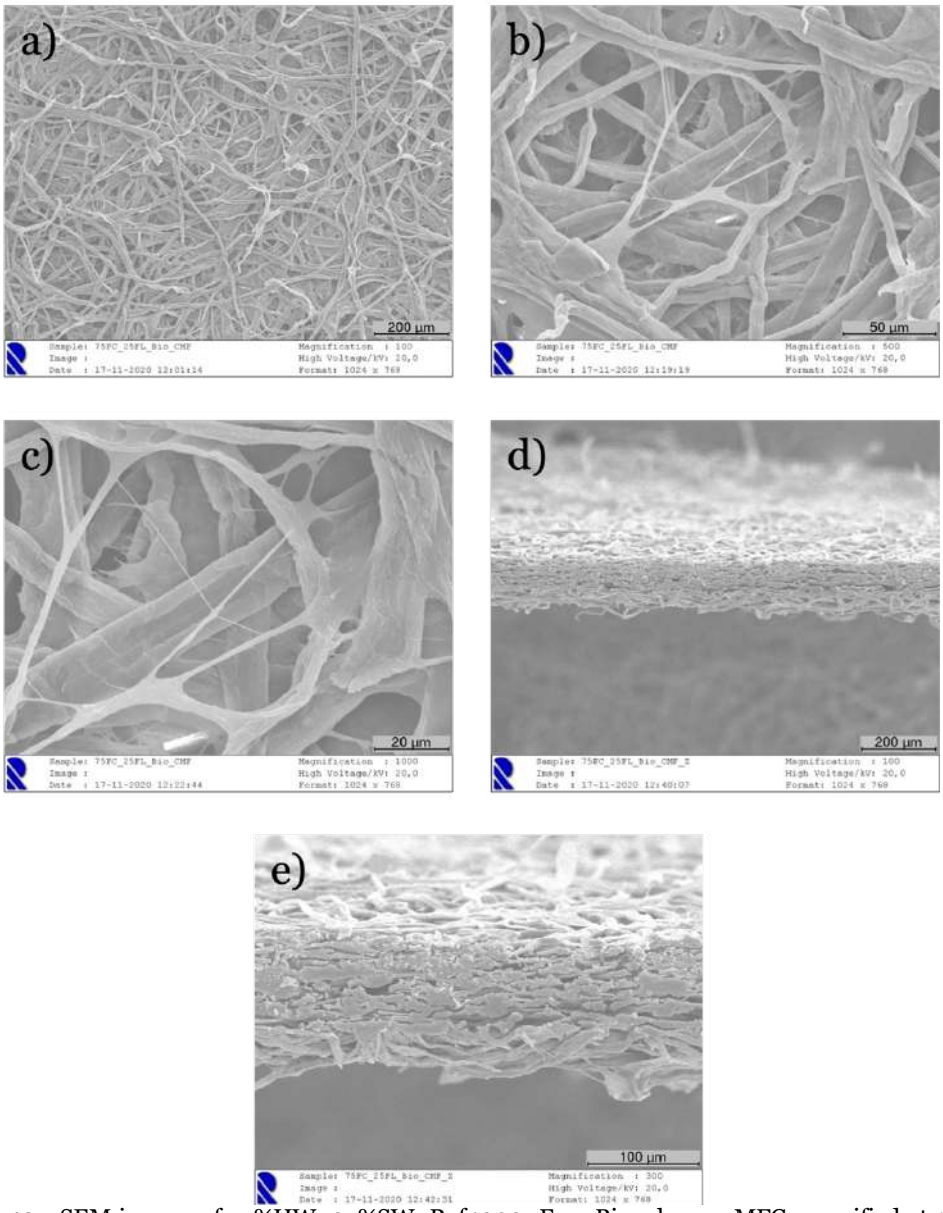

Figure 4.12 - SEM images of 75%HW+25%SW_Ref4000+Enz+Biopolymer+MFC magnified at 100x (a), 500x (b), 1000x (c), 100 x in the Z axis(d) and 300x in the Z axis (e).

Visualizing figure 4.12, in which there is a combination of all the factors used in the previous examples, it can be seen their harmony with each other, due to the formation of a cellulosic structure with complex and interconnected pores (figure 4.12 (b) and (c)), and at the same time a thin, compact, fibrillated structure capable of retaining active molecules of interest (figure 4.12 (d) and (e))

4.3.3. Chemical characterization using FTIR-ATR

A characterization of various samples using Fourier-transform infrared spectroscopy was done using FTIR with attenuated total reflectance (FTIR-ATR).

Figure 4.13 shows the comparison of the Pinus Pinaster fiber-made structure used to manufacture the cellulosic structures with the essential oil. Figure 4.13 shows the cellulosic structure without any addition of oil (green) while shows the same structure after the addition of essential oil from *Mentha piperita* (red).

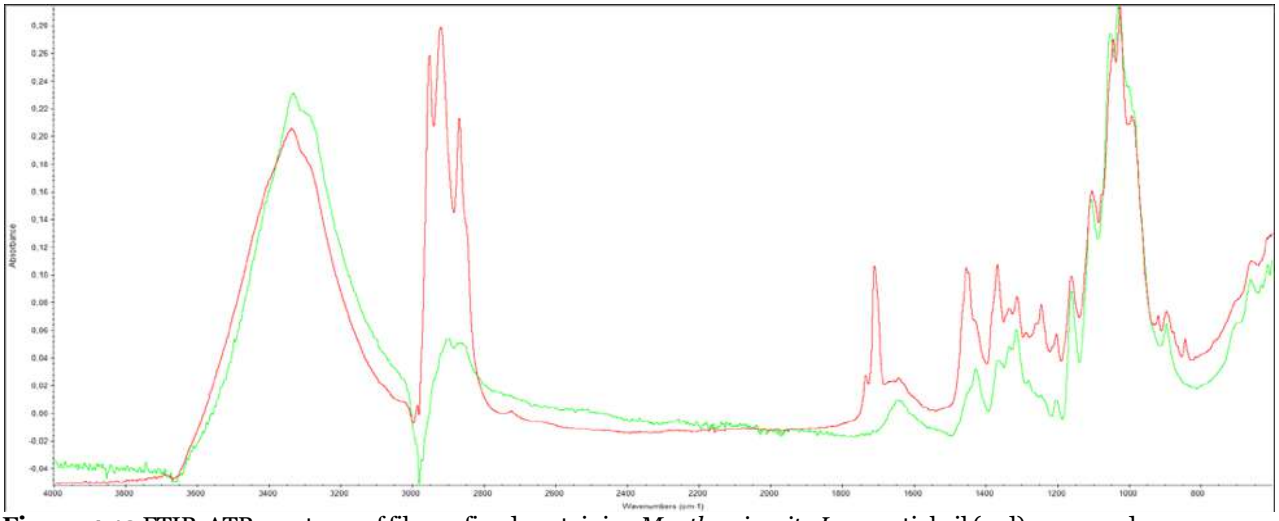

Figure 4.13 FTIR-ATR spectrum of fiber refined containing *Mentha piperita L.* essential oil (red) compared with the fibrous matrix without essential oil (Green).

With this overlap of spectra in figure 4.13 it is possible to clearly visualize the presence of the essential oil in the range of 3600~3000cm^{-1}, since the band corresponding to the OH groups is superior to that of cellulose, which by itself has many bonds by hydrogen. The difference between the two samples is noticed at 2600~3000 cm^{-1}, which shows the presence of CH bonds.

4.3.4 Kinetic studies using FTIR-ATR

Kinetic studies were carried out on the structures with the various refinements, in bleached fiber and unbleached fiber. For this study, softwood bleached, and softwood unbleached *Pinus pinaster* cellulosic structures were used, which were mechanically treated at 2500, 4500 and 7500 revolutions respectively. The objective would be to verify the controlled release of the essential oil using the FTIR-ATR technique and verify the influence of mechanical treatment on the controlled release.

The study consisted of dividing the structure into 4 zones, in which a drop of peppermint essential oil was placed. This test was carried out on softwood structures refined at 2500 and 4500 and 7500, bleached and unbleached, without the emulsion. Measurements

were performed every 3 minutes. Figure 4.14 depicts, in schematic form, how the kinetic investigations were conducted.

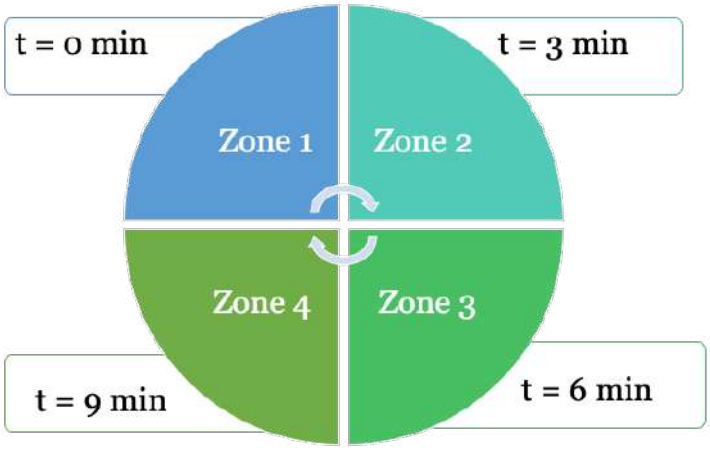

Figure 4. 14 - Schematic illustration how the kinetic studies were conducted

To aid comprehension of the kinetic assays, Table 4.17 is provided. This will allow for a more precise analysis of the times used in kinetics, considering the multiplicity of superimposed variables.

Table 4. 17 - Assay description with corresponded times for the FTIR-ATR kinetics

Assay Description	*Time correspondence*
t0	0 min
t1	3 min
t2	6 min
t3	9 min

The remaining of the tests are placed in Appendix D, where it can seen how mechanical treatment can affect the variation in essential oil retention.

4.3.4.1 Softwood Bleached fiber refined 4500 revolutions

The FTIR-ATR spectra from kinetic studies using softwood bleached cellulose refined at 4500 rev are presented in Figure 4.15. Dark blue is equivalent to SW without EO. Red. light green, light blue, and pink are the colors which correspond to (t0), (t1), (t2), and (t3) assays, respectively.

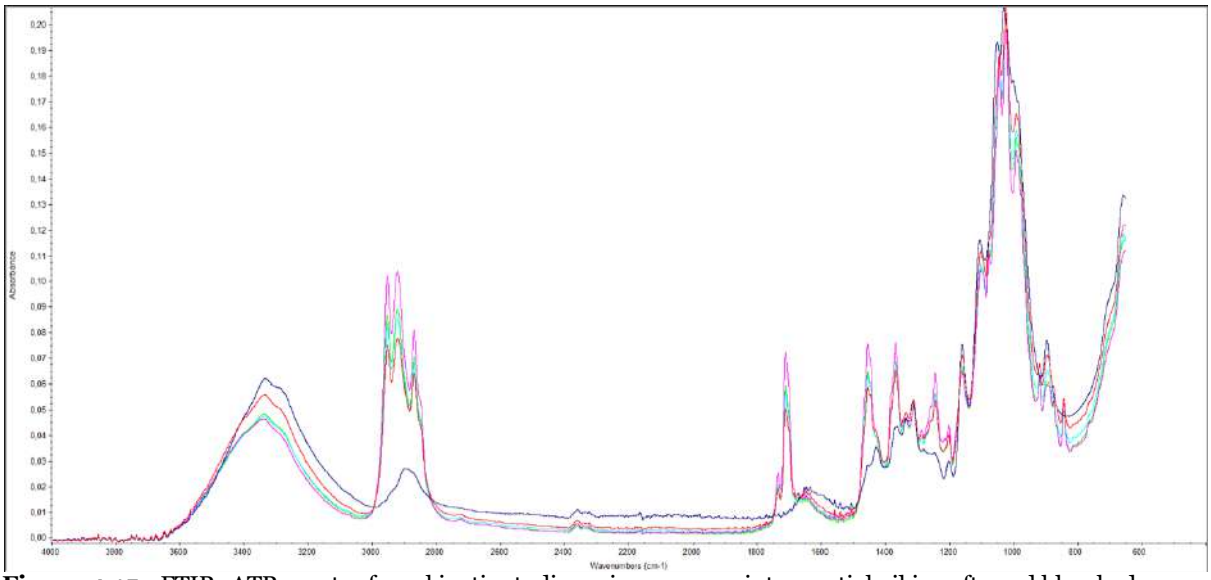

Figure 4.15 - FTIR- ATR spectra from kinetic studies using peppermint essential oil in softwood bleached cellulose refined at 4500 rev. Dark blue corresponds SW without EO. The colors Red(t0), light green(t1), light blue(t2) and pink(t3), represent each time studied in the kinetic assay.

The band corresponding to the O-H groups seems to be increasing in the 3000~2800 cm^{-1} region, indicating that a controlled release is taking place. This release is lower in t0 and more prevalent in t3, with an absorbance of 0,10, approximately .
Because the molecules tend to form hydrogen bonds, the dark blue spectrum, which corresponds to softwood without essential oil, also exhibits a modest peak in the same range.

4.3.4.2 Softwood Bleached fiber refined at 7500 revolutions

The FTIR-ATR spectra from kinetic studies using softwood bleached cellulose refined at 7500 rev are presented in Figure 4.16. Red, purple, light green, and light blue are the colors which correspond to (t0), (t1), (t2), and (t3) assays, respectively .

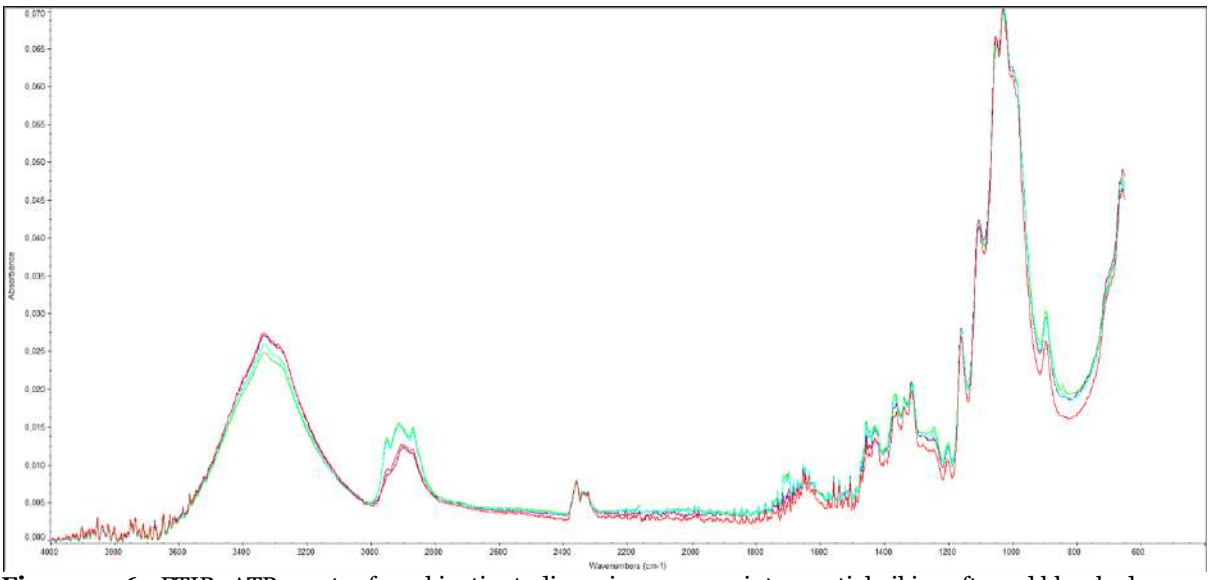

Figure 4.16 - FTIR- ATR spectra from kinetic studies using peppermint essential oil in softwood bleached cellulose refined at 7500 rev. The colors Red(t0), purple(t1), light green(t2) and light blue(t3), represent each time studied in the kinetic assay.

The band corresponding to the O-H groups appears to be growing in the 3000–2800 cm^{-1} region, indicating that a controlled release is taking place. This release is lower in t0 and more prevalent in t3, with an absorbance of 0,015 , approximately.

As illustrated in the region 3000~2800 cm-1, the band corresponding to the O-H groups increases, indicating that a controlled release is taking place, as it is less in t0 and greater in t3, as the assay with SW ref4500

However, the absorbency is significantly lower than that of softwood ref 4500 rev. This is due to the process of mechanical treatment. As the porosity decreases, it becomes increasingly complex for the active molecule to leave the cellulose matrix.

4.3.4.3 Non-bleached softwood fiber refined at 4500 revolutions

The FTIR-ATR spectra from kinetic studies using softwood unbleached cellulose refined at 4500 rev are presented in Figure 4.17. Red is equivalent to SW without EO. Light green, light blue, purple and pink are the colors which correspond to (t0), (t1), (t2), and (t3) assays, respectively.

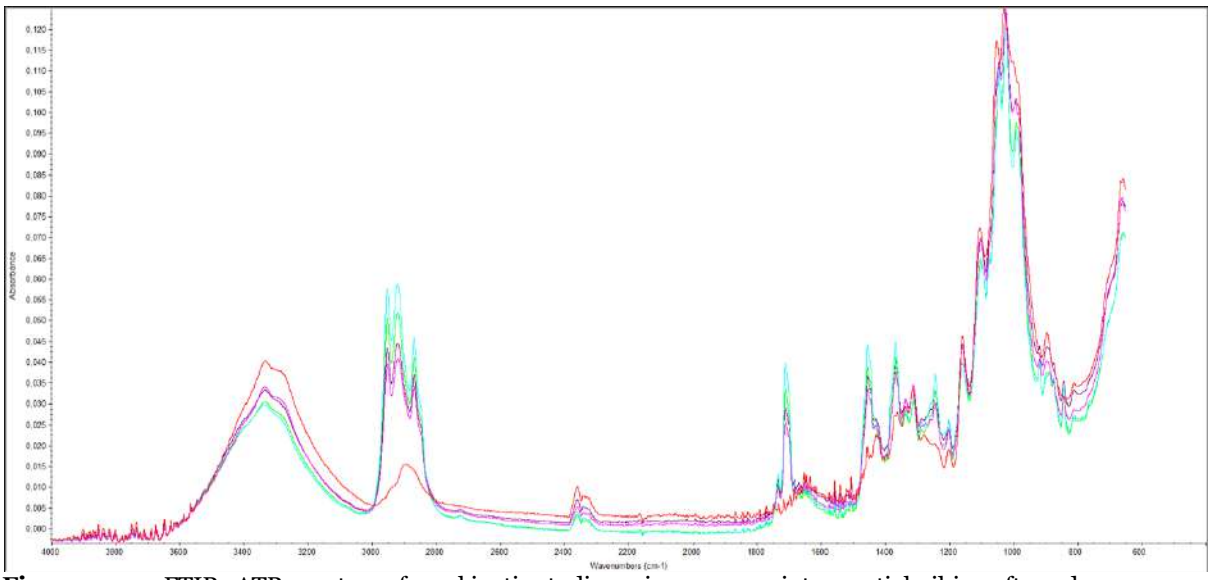

Figure 4.17 - FTIR- ATR spectrum from kinetic studies using peppermint essential oil in softwood non-bleached cellulose refined at 4500 revs. Red corresponds NSW without EO. Light green(t0), light blue(t1), purple(t2) and pink(t3), represent each time studied in the kinetic assay.

As observed in the region 3000~2800 cm-1, the spectrum corresponding to the O-H groups increases, indicating that a controlled release is taking place, as it is less in t0 and greater in t3.

Since molecules tend to form hydrogen bonds, the red spectrum, which corresponds to softwood without essential oil, also has a minor peak in the same range.

The absorbency of t3 , however, is much lower (0.060) than that of softwood ref 4500 rev. This may be because the cellulosic structure was not bleached. As the structure is unbleached, it turns out to be more complex due to the presence of lignin, which might limit the release of the essential oil.

4.3.4 4Non-bleached softwood fiber refined at 7500 revolutions

The FTIR-ATR spectra from kinetic studies using softwood bleached cellulose refined at 4500 rev are presented in Figure 4.18. Red is equivalent to SW without EO. Dark blue, Light green, pink, and light blue are the colors which correspond to (t0), (t1), (t2), and (t3) assays, respectively.

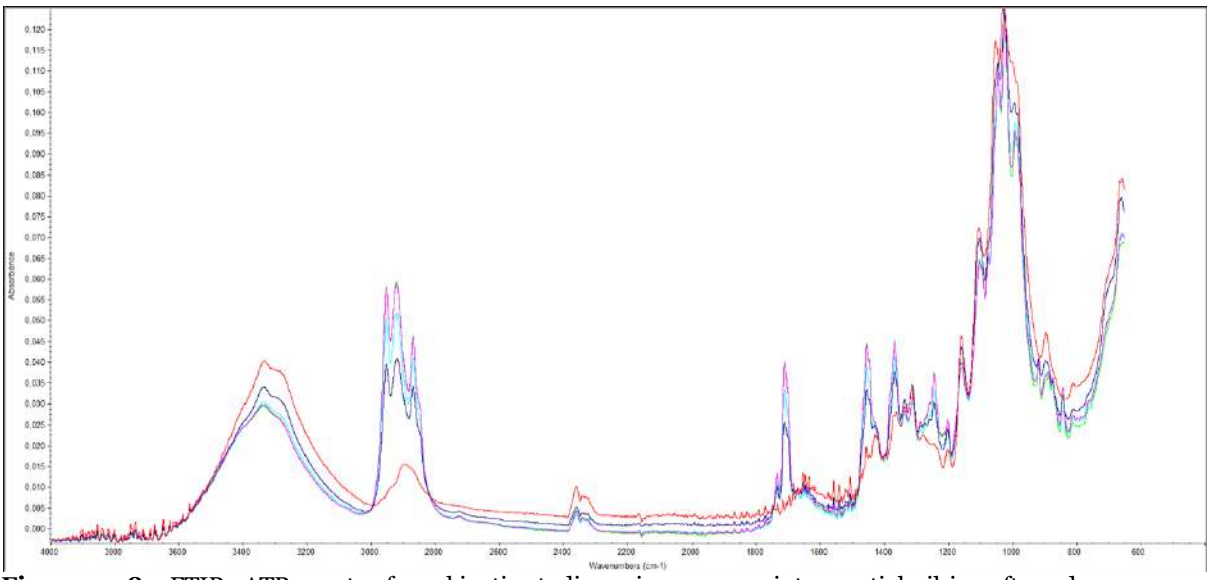

Figure 4.18 - FTIR- ATR spectra from kinetic studies using peppermint essential oil in softwood non-bleached cellulose refined at 7500 rev. Red corresponds NSW without EO. Dark blue(t0), light green(t1), pink(t2) and light blue(t3), represent each time studied in the kinetic assay.

However, the absorbency of t2 is considerably lower (0.060) than that of softwood ref 4500 rev. This could be due to the cellulosic structure not being bleached. In this instance, the structure is unbleached, which makes it more complicated due to the presence of lignin, which may restrict the release of essential oil. As this is also the highest mechanical treatment, 7500 rev. The result was completely unexpected, as the highest absorbency point occurred at one of the earliest times (t1 and t2), whereas it was anticipated that it would occur at one of the latest times(t3).

With this, is possible to conclude that comparing the different times of refining at 2500 and 4000 revolutions reveals a decrease in the band of OH groups, which may indicate a gradual release of *Mentha piperita* essential oil. The mechanical treatment at 4500 revolutions seems to be optimal for producing the prototype, as the progressive release appears to be more uniform.

In the case of the improvements that happened at 7500 revolutions, it was found that the opposite occurred; specifically, the band of OH groups in the unbleached softwood fiber increased. Due to the length of time, it took for the oil to be absorbed by the structure, the spectra obtained as a consequence of this experiment indicate that the optimal time for mechanically refining the fiber has long since passed. This conclusion can be drawn by observing the results acquired.

4.3.5 Carboxymethylcellulose assays

The objective of producing this carboxymethylcellulose gel was to simulate a second layer, and subsequently to conduct a kinetics study similar to conclude whether there were any variations in the controlled release of peppermint oil. The kinetic study consists of pouring a drop of *Mentha piperita* essential oil in a cellulosic structure, immediately adding CMC hydrogel on top, and collecting measurements every three minutes, as described in table 4.17, located in subsection 4.3.4. The cellulosic structures are softwood, bleached and non-bleached, not subjected to any kind of treatment. The structures were produced according to ISO Norm 5269/1.
There were made 4 suspensions containing carboxymethylcellulose, in order to obtain a hydrogel. In two of these suspensions, calcium chloride ($CaCl_2$) was added, which is a crosslinking factor, thus increasing the porous network. All suspensions were made using a stir plate and magnetic stirrer. The volume considered for each suspension was 40 mL, which is the volume contained in a petri dish.

The concentrations considered were:

- 800mg CMC
- 800mg CMC + 200mg $CaCl_2$
- 1600mg CMC
- 1600mg CMC + 400mg $CaCl_2$

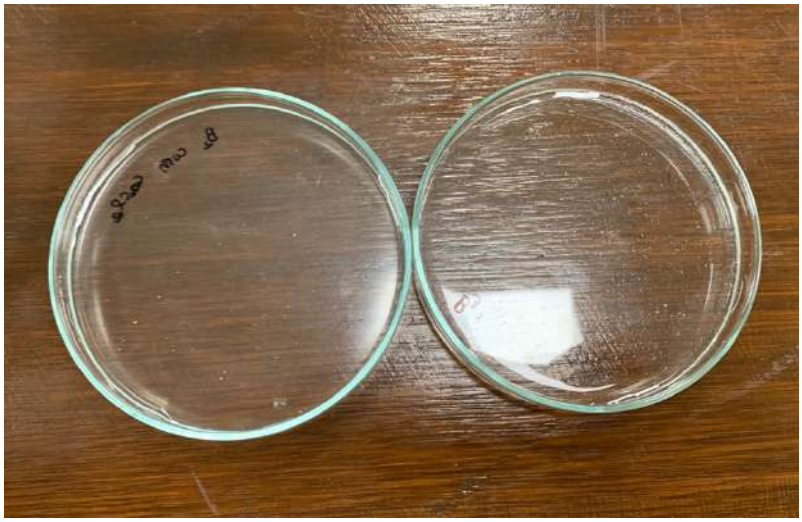

Figure 4.19 - Hydrogel made with 800mg CMC + 200mg CaCl2 (left) and hydrogel made with 800mg CMC (right).

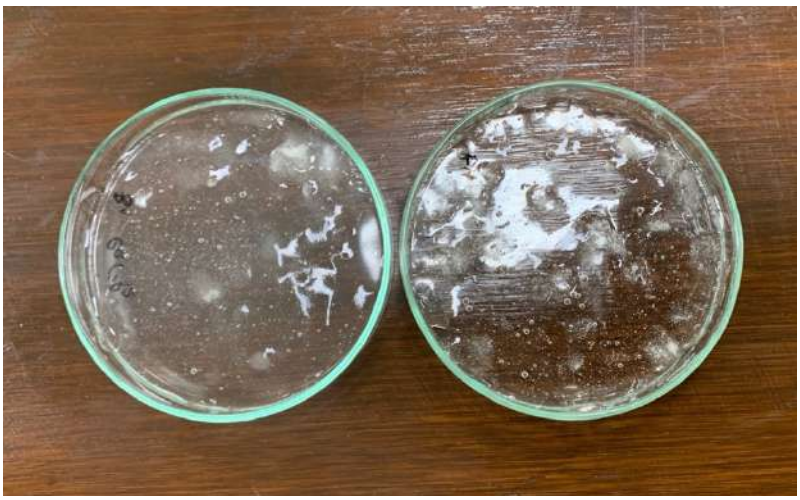

Figure 4.20 - Hydrogel made with 1600mg CMC + 400mg CaCl2 (left) and hydrogel made with 1600mg CMC (right).

The kinetics studies performed are similar to the previous described in subsection 4.3.4, however they were performed at the same point where a drop of peppermint essential oil covered by the CMC hydrogel was placed. Measurements were performed every 3 minutes. A measurement of the CMC hydrogel was also carried out without the presence of the essential oil, for later comparison.

Since there was an overlap of spectra in all of the experiments, it is not possible to differentiate time between them; hence, there is no assay description like there would be in kinetic assays simply having the essential oil and the cellulose matrix. In that scenario, the results of some of the tests will be displayed, while the information regarding the remaining tests can be found in Appendix E.

The objective of this experimental set would be to demonstrate how a top layer can have an effect on the amount of essential oil that is retained. In order to achieve the best results from a dermal application, the active molecule should be kept in the cellulosic matrix for the longest amount of time possible.

4.3.5.1 Kinetic studies using softwood fiber

Softwood bleached cellulose, covered by CMC hydrogel (800 mg)

In figure 4.21 is represented the FTIR- ATR spectra from kinetic studies using peppermint essential oil in softwood bleached cellulose, covered by CMC hydrogel (800 mg).

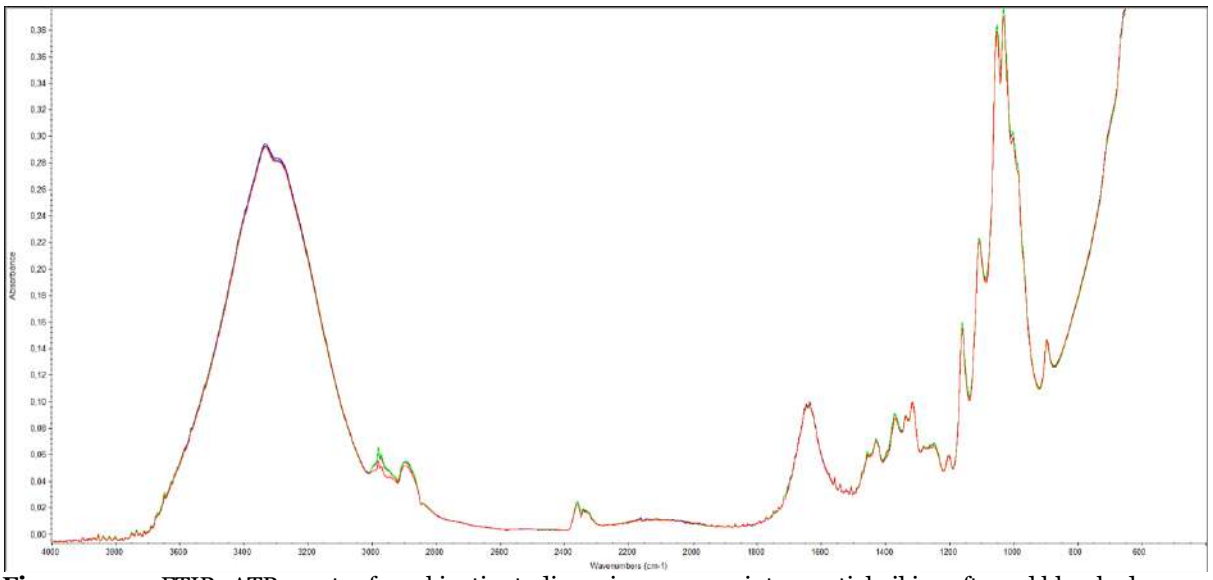

Figure 4.21 - FTIR- ATR spectra from kinetic studies using peppermint essential oil in softwood bleached cellulose, covered by CMC hydrogel (800 mg). All assays represented.

There was no variation in the kinetics illustrated in figure 4.21, except that there were oscillations in the wavelength of the order of 3000cm^{-1}. The region of wavelengths from 3600 cm^{-1}to approximately 3000cm^{-1} remains totally overlapped, suggesting that the gel of CMC acted as a barrier and essential oil might not have been released.

Softwood bleached cellulose, covered by CMC hydrogel (800 mg) and CaCl2 (200mg)

In figure 4.22 is represented the FTIR- ATR spectra from kinetic studies using peppermint essential oil in softwood bleached cellulose, covered by carboxymethylcellulose hydrogel (800 mg) and CaCl2 (200mg).

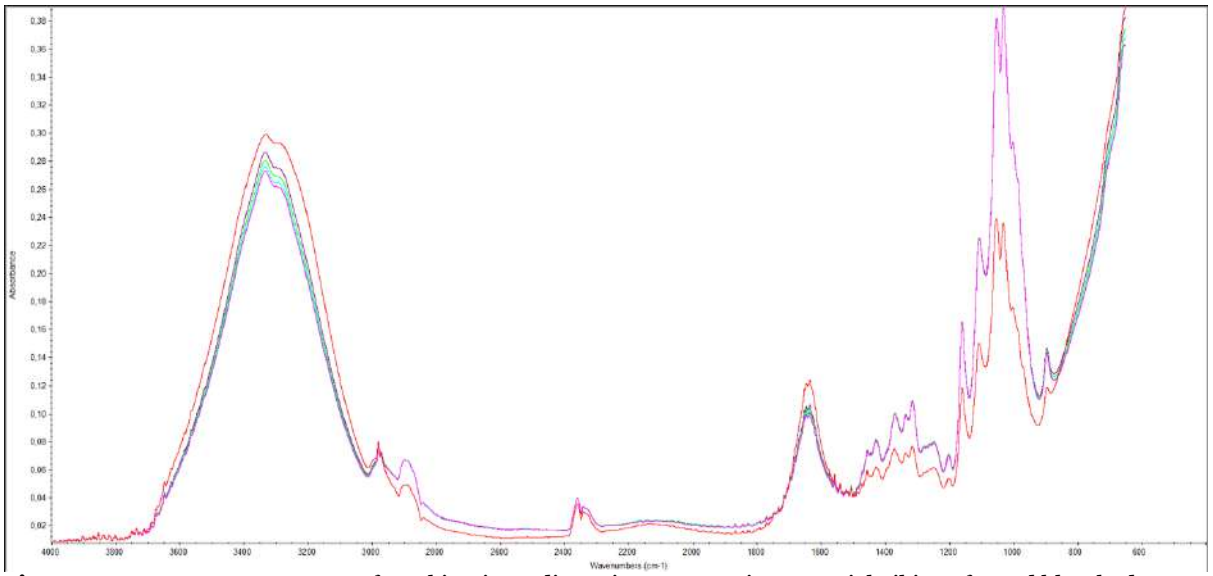

Figure 4.22 - FTIR- ATR spectra from kinetic studies using peppermint essential oil in softwood bleached cellulose, covered by CMC hydrogel (800 mg) and CaCl2 (200mg). All assays represented.

In the kinetics depicted in figure 4.27, the spectra exhibit some variation and are not as overlapped as in figure 4.26. There are higher oscillations in the range of wavelengths between 3600cm^{-1} and about 3000cm^{-1}, suggesting that there was probably some release of essential oil. This could be due to $CaCl_2$ is present.

Softwood bleached cellulose, covered by carboxymethylcellulose hydrogel (1600 mg)

In figure 4.23 is portrayed the FTIR- ATR spectra from kinetic studies using peppermint essential oil in softwood bleached cellulose, covered by CMC hydrogel (1600 mg)

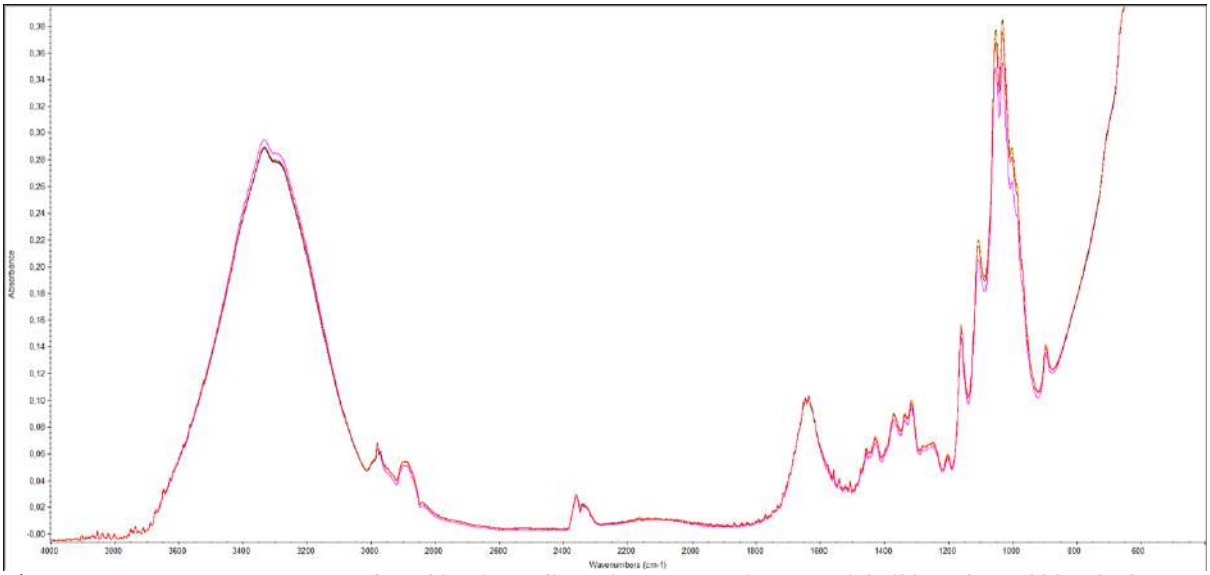

Figure 4.23 - FTIR- ATR spectra from kinetic studies using peppermint essential oil in softwood bleached cellulose, covered by CMC hydrogel (1600 mg). All assays represented.

Softwood bleached cellulose, covered by CMC hydrogel (1600 mg) and CaCl2 (400mg)

In figure 4.24 is represented the FTIR- ATR spectra from kinetic studies using peppermint essential oil in softwood bleached cellulose, covered by CMC hydrogel (1600 mg) and CaCl2 (400mg)

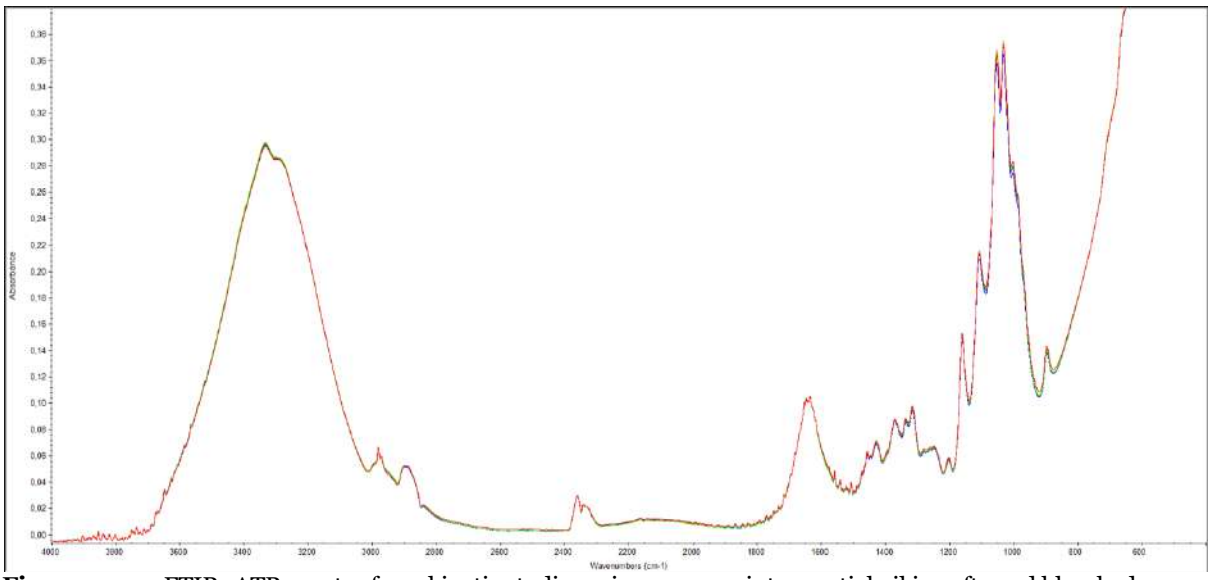

Figure 4.24 - FTIR- ATR spectra from kinetic studies using peppermint essential oil in softwood bleached cellulose, covered by CMC hydrogel (1600 mg) and CaCl2 (400mg). All assays represented.

When the concentration of CMC is increased by a factor of two, either with or without the presence of CaCl2, as seen in Figures 4.23 and 4.24, almost no variation is observed, as shown in Figure 4.26. This may be due to the quantity of CMC. There was no detection of essential oil release during all of the assays.

4.3.5.2 Kinetic assays using non-bleached softwood fiber

Non-bleached softwood cellulose, covered by CMC hydrogel (800 mg)

In figure 4.25 is represented the FTIR- ATR spectra from kinetic studies using peppermint essential oil in softwood non-bleached cellulose, covered by CMC hydrogel (800 mg)

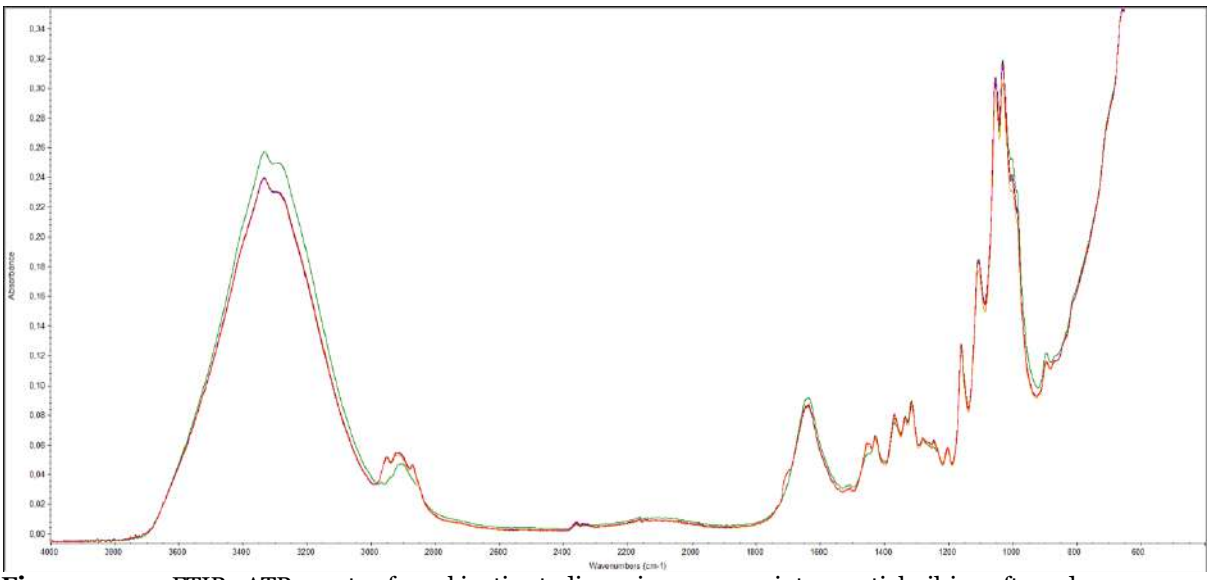

Figure 4.25 - FTIR- ATR spectra from kinetic studies using peppermint essential oil in softwood non-bleached cellulose, covered by CMC hydrogel (800 mg). All assays represented.

Figure 4.25 illustrates a more gradual variation, particularly between the wavelengths 3600~2800 cm^{-1}. This could be owing to the existence of other chemicals in the cellulose matrix, such as lignin.

This may suggest that, when applied as a layer over unbleached softwood, the CMC hydrogel may exhibit a faster release of essential oil.

Non-bleached softwood cellulose, covered by CMC hydrogel (800 mg) and CaCl2 (200mg)

In figure 4.26 is represented a FTIR- ATR spectra from kinetic studies using peppermint essential oil in softwood non-bleached cellulose, covered by CMC hydrogel (800 mg) and CaCl2 (200mg)

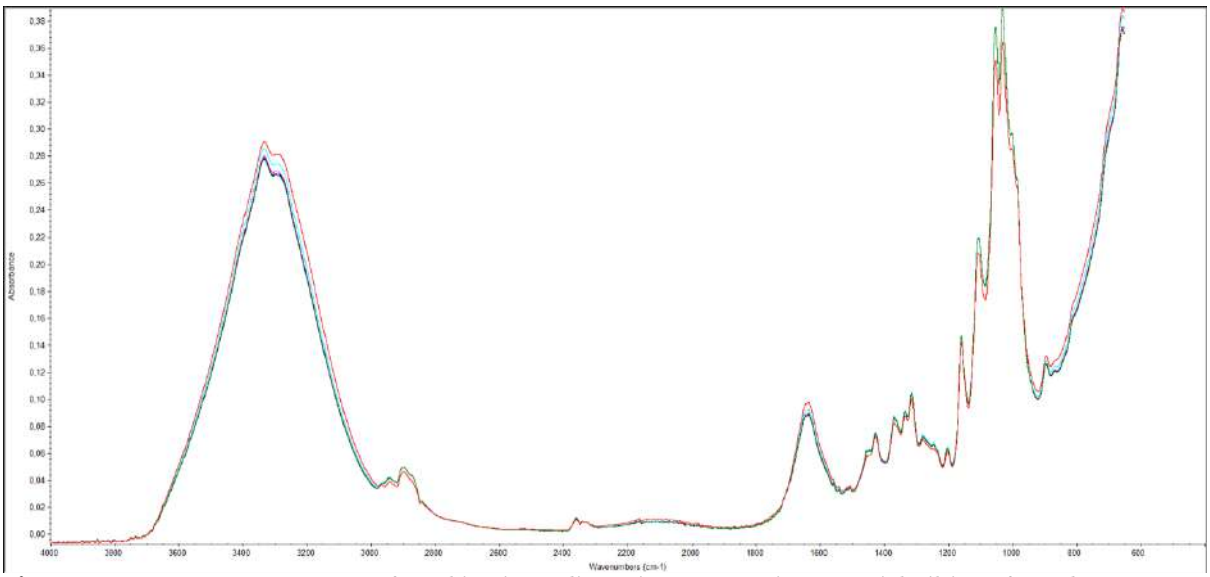

Figure 4.26 - FTIR- ATR spectra from kinetic studies using peppermint essential oil in softwood non-bleached cellulose, covered by CMC hydrogel (800 mg) and CaCl2 (200mg). All assays represented.

Similar to the kinetics presented in subsection 4.3.4, there is a gradual variation in figure 4.26, particularly between the wavelengths 3600-2800 cm^{-1}.
This may suggest that, when applied to unbleached softwood, the conjugation of CMC hydrogel with CaCl2 may result in a gradual release of essential oil.

Non-bleached softwood cellulose, covered by CMC hydrogel (1600 mg)

In figure 4.27 is illustrated a FTIR- ATR spectra from kinetic studies using peppermint essential oil in softwood non-bleached cellulose, covered by CMC hydrogel (1600 mg). All assays represented

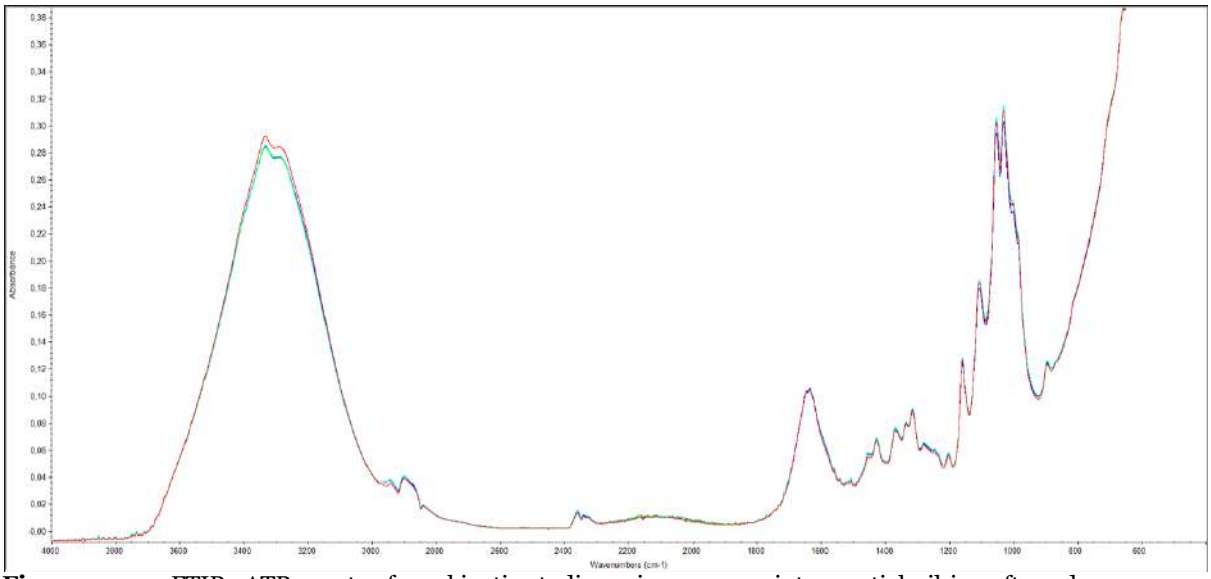

Figure 4.27 - FTIR- ATR spectra from kinetic studies using peppermint essential oil in softwood non-bleached cellulose, covered by CMC hydrogel (1600 mg). All assays represented.

Softwood bleached cellulose, covered by CMC hydrogel (1600 mg) and CaCl2 (400mg)

In Figure 4.28 is represented a FTIR- ATR spectra from kinetic studies using peppermint essential oil in bleached cellulose, covered by CMC hydrogel (1600 mg) and CaCl2 (400mg).

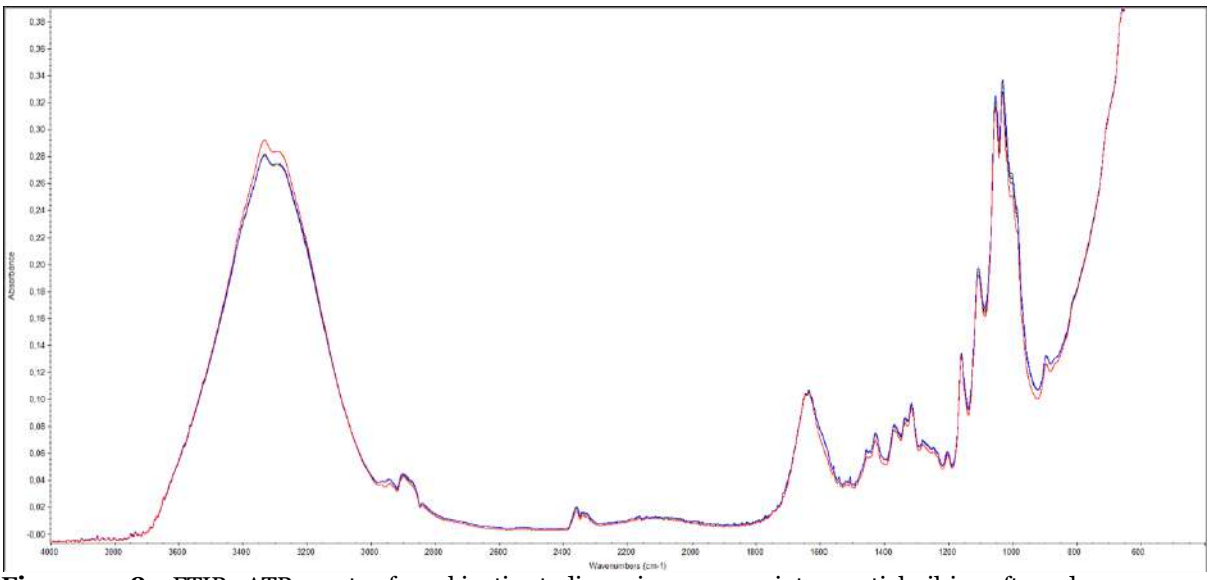

Figure 4.28 - FTIR- ATR spectra from kinetic studies using peppermint essential oil in softwood non-bleached cellulose, covered by CMC hydrogel (1600 mg) and CaCl2 (400mg). All assays represented.

As shown in Figures 4.27 and 4.28, when the CMC concentration is increased by a factor of two, with or without the addition of CaCl2, there is only a small alteration in the spectra. This might be because of how much CMC was used on a lignin-containing cellulose matrix. There might be some interaction that enables a minimal release of essential oil.

With these studies, it can be concluded that the addition of carboxymethylcellulose would be an asset to the drug delivery system. As can be seen along the spectra obtained, they overlap over time, undergoing minimal changes. This may indicate that the layer of CMC hydrogel placed over the structure protects the essential oil from being released. Although the characteristic band of the OH groups is reduced, a slight increase can be observed over time, which may suggest that there is a release of the essential oil. Bearing in mind that the kinetic studies were carried out at 3-minute intervals, it would be indicated to increase this interval to verify if the release of the essential oil is more pronounced. The mixture of CMC hydrogel (800 mg) and CaCl2(200mg) correlated more closely with the kinetics calculated in 4.3.4. .Since one of the of the objectives is the creation of the dermal system was the gradual and controlled release of essential oil, is important to supplement the study, in which additional CMC concentrations can be studied in order to have a better understanding of the influence that it may have as a potential second layer in a dermal system.

4.4 Analysis of commercial products (Benchmark marketing)

Taking into consideration that our prototype dermic system was composed of a cellulose matrix that was emulsified with essential oils, various commercial items were analyzed for their similarities and differences.

As the variety of emulsions and gels on the market increases, it is important to compare the emulsion that was produced and incorporated into the cellulosic matrix for the dermal system with similar products currently available on the market. In a similar manner, an examination of existing structures is also necessary. This analysis is interesting since it enables the optimization of the cellulose matrix dermic system.

4.4.1 Analysis of essential oils and comparison with commercial products

The emulsion and gel used in this comparison are both from the Czech Republic-based Manufaktura brand, which emphasizes utilizing products that are as natural as possible. Because they use plants from their own country, the choosing of this brand was also founded on sustainability. Additionally, this brand's dermatologist-tested lavender emulsion and mint gel were chosen. The dermatologically certified products' composition is included in Appendix F.

Using FTIR-ATR, a Manufacktura lavender emulsion was compared to a drop of lavender essential oil (Lavandula angustiolia) from the experimental set used throughout the entirety of this research.
A Manufacktura brand gel containing plants was also analyzed in order to be able to compare with the hydrogel produced in the laboratory. The tests were performed on softwood bleached fiber and softwood unbleached fiber, without any treatment. The outcomes of some FTIR-ATR experiments are shown in Appendix G.

4.4.1.1 Softwood Bleached fiber

Comparison of isolated bleached fiber, lavender essential oil and commercial emulsion

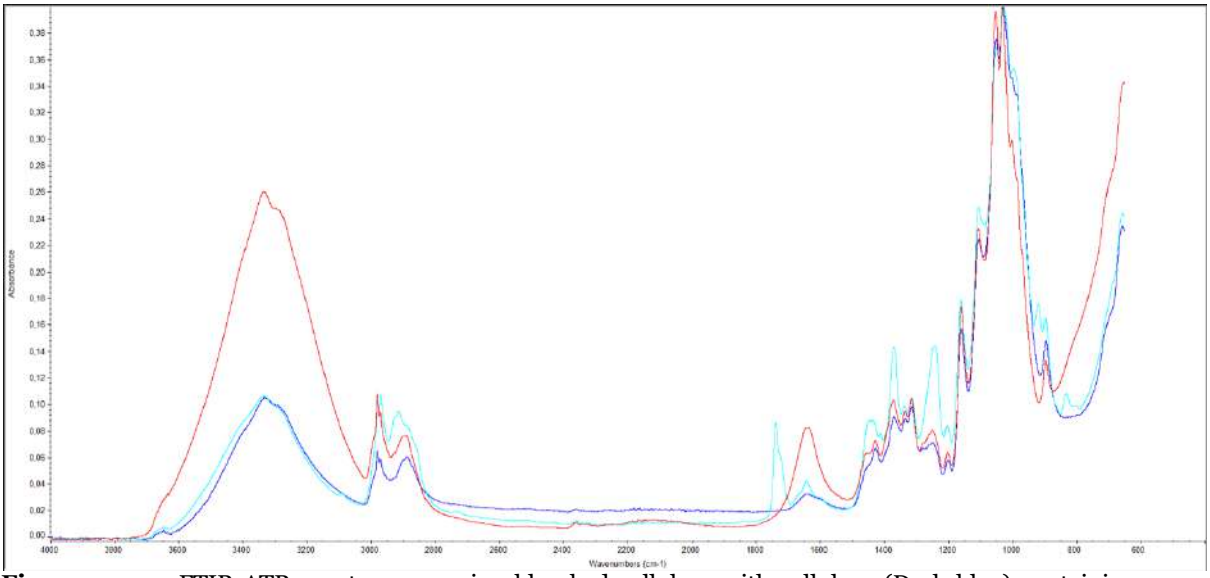

Figure 4.29 - FTIR-ATR spectra comparing bleached cellulose with cellulose (Dark blue) containing lavender essential oil (light blue) and commercial emulsion with lavender(red), represent each assay.

When looking at the SW alongside the essential oil of *Lavandula angustifolia* and the commercial emulsion, it is possible to see concurrent peaks, which are the principal constituents of lavender. Is possible to see in the range of 1800~1700 cm^{-1} what could be a C=O stretch, which may correspond to linalyl acetate, one of the major components of *Lavandula angustiolia* essential oil. There is also an intensification in the peaks of the commercial emulsion, particularly in the range that corresponds to OH groups and CH groups, and this intensification can be exacerbated by the other compounds that compose the emulsion.

Softwood fiber bleached with commercial gel

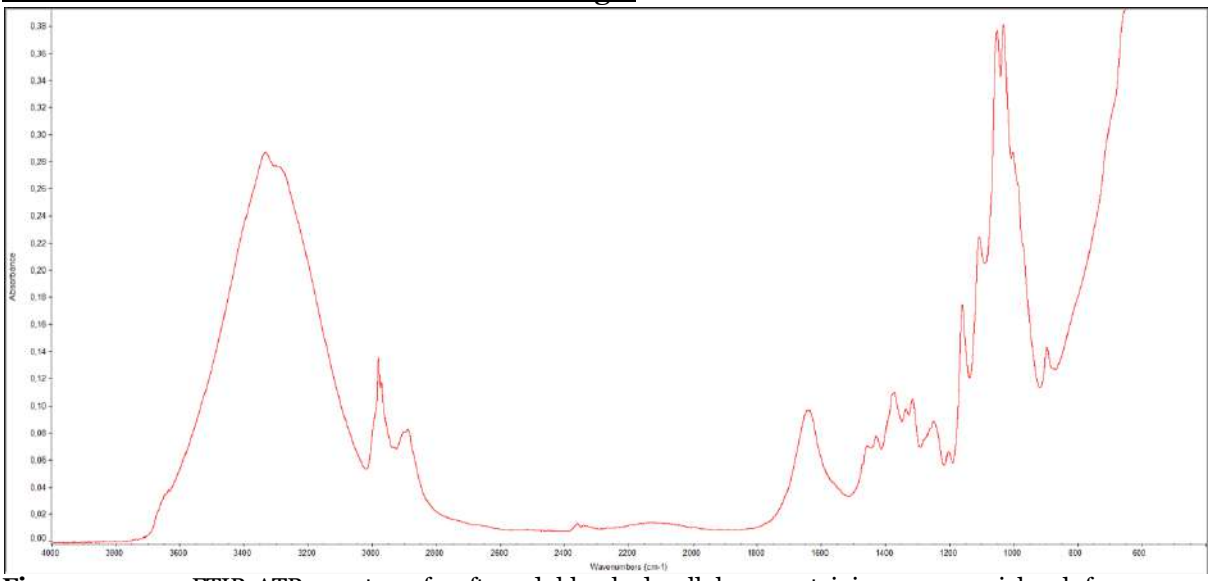

Figure 4.30 - FTIR-ATR spectra of softwood bleached cellulose containing commercial gel from Manufacktura.

Noting that the commercial gel described in appendix F it has menthol in its constituent. Figure 4.30 depicts a highly pronounced and sharp peak in the 3000 cm^{-1} zone, which could be the OH groups, since the gel has menthol as a major component, or can be the combination of mint present in the commercial gel with the SW, due to the higher cellulose's capacity to generate hydrogen bond.

4.4.1.2 Non-bleached Softwood fiber

Comparison between isolated fiber, fiber with lavender oil and fiber with commercial oil

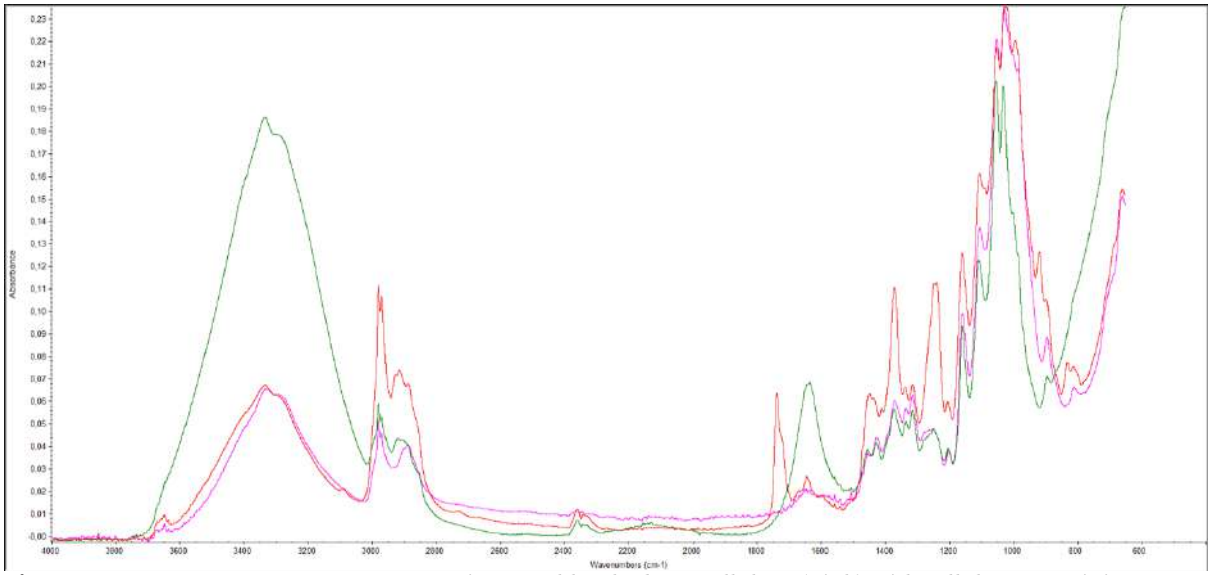

Figure 4.31 - FTIR-ATR spectrum comparing non-bleached SW cellulose (Pink) with cellulose containing lavender essential oil(Red) and commercial emulsion with lavender(Green) represent each assay.

When examining the NSW alongside the essential oil of Lavandula angustifolia and the commercial emulsion, it is possible to observe peaks that correspond to lavender's primary ingredients. It is possible to observe a C=O stretch between 1800 and 1700 cm^{-1}, which may correlate to linalyl acetate, one of the principal components of the essential oil of Lavandula angustifolia. There is also an amplification of the peaks in the commercial emulsion, notably in the range corresponding to OH and CH groups, and this intensification can be increased by the other compounds that make up the emulsion. However, the absorbency in the region of 3000 to 2800 cm-1 is much greater than the SW assay. This could be due to the fiber was not bleached. As the structure is unbleached, it turns out to be more complicated due to the presence of lignin, which might impede the release of the essential oil.

Unbleached fiber with commercial gel

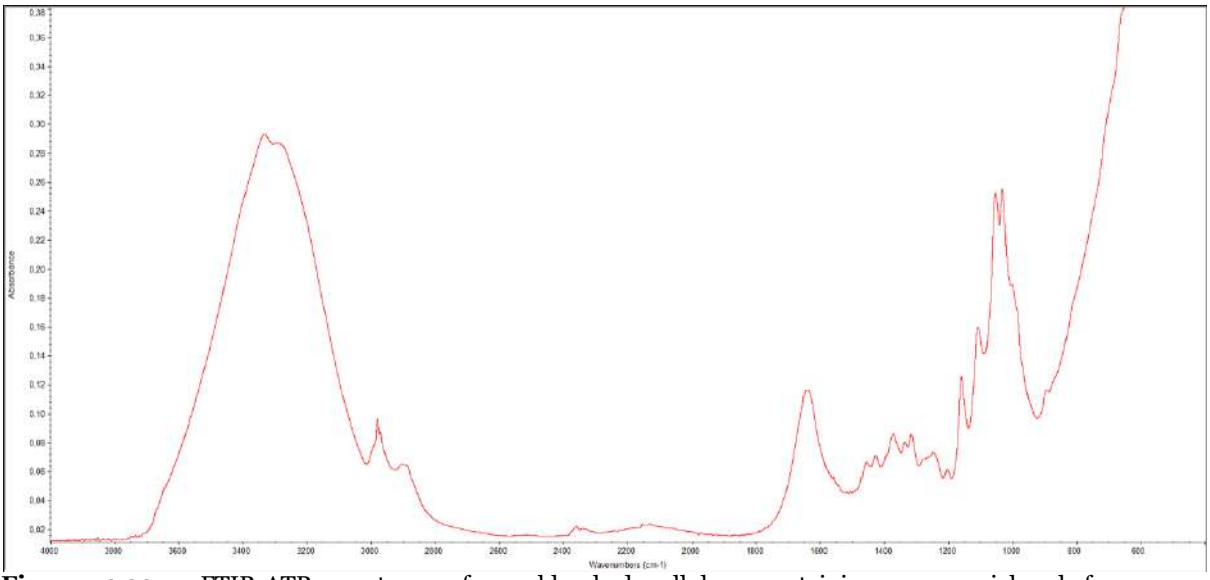

Figure 4.32 - FTIR-ATR spectrum of non-bleached cellulose containing commercial gel from Manufacktura.

Noting that menthol is present in the commercial gel detailed in Appendix F. Figure 4.32 illustrates a highly noticeable and sharp peak in the 3000 cm^{-1} range, which might be the OH groups, since menthol is a large component of the gel, or it could be the combination of mint present in the commercial gel with the NSW, due to the higher cellulose's propensity to create hydrogen bonds.

4.4.2 Structural analysis and comparison

The structural analysis comprises both biodegradable and non-biodegradable structures, and these structures can be contrasted with the laboratory-produced cellulose matrix structure. In this instance, brand names will not be mentioned as they are well-known, and the primary purpose is to compare structures composition. The structures were designated Biod MKT1, biod MKT2, and nonbiod MKT3 for this purpose.
Since the selected products are bleached, the analysis was conducted only in comparison to bleached softwood fiber.

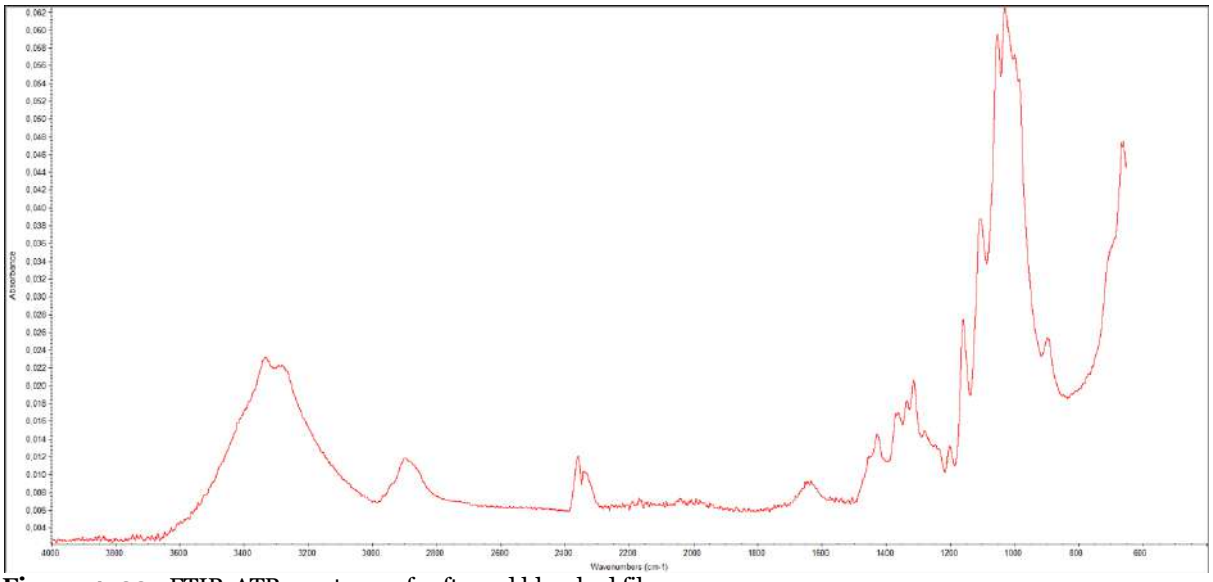

Figure 4. 33 - FTIR-ATR spectrum of softwood bleached fiber

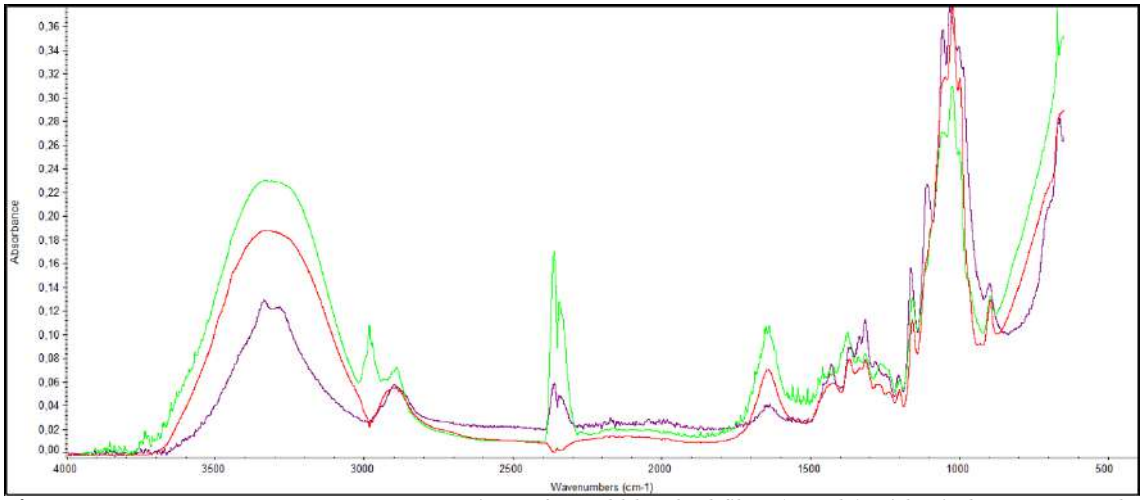

Figure 4. 34 - FTIR-ATR spectrum comparing softwood bleached fiber (Purple) with Biod_MKT1 sample (Green) and Biod_MKT2 sample (Red) represent each assay.

Regarding structural properties, figures 4.33 and 4.34 demonstrate that the structures are biodegradable, as both Biod MKT1 and Biod MKT2 samples have the same structural basis, with many peaks highlighted in Biod MKT1, such as in the range of 3000~2800

cm^{-1} and approximately 2400 cm^{-1}, which may be due to the addition of active components to the structure.

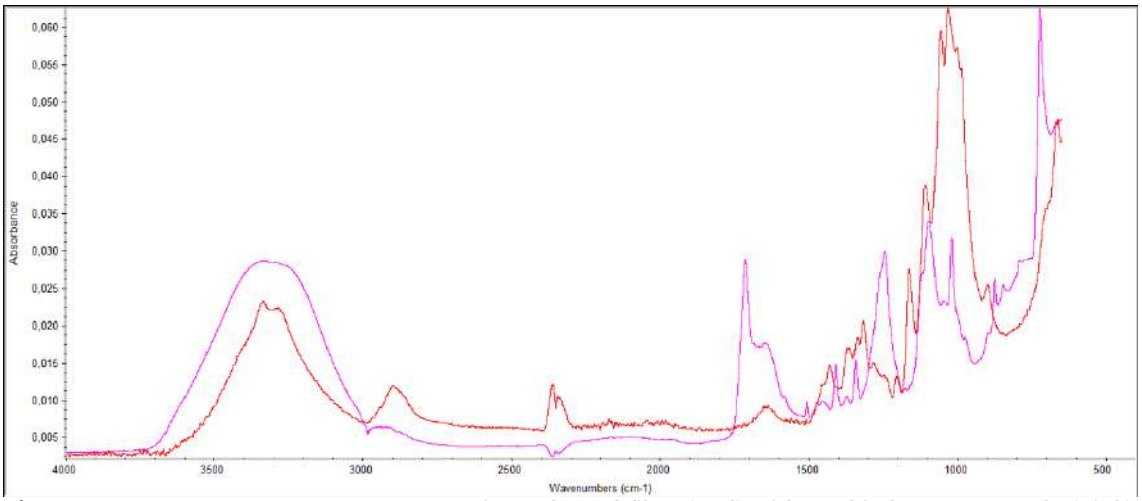

Figure 4. 35 - FTIR-ATR spectrum comparing softwood fiber (Red) with nonbiod_MKT3 sample (Pink) represent each assay.

Regarding the structural properties, figure 4.35 indicates that the structures may not be biodegradable since they lack a cellulose-like FTIR-ATR spectrum. However, there is a peak at approximately 1600 cm^{-1}, which may be due to a C=O stretch, which can correlate to an ester group. This data may suggest that polyester is present in this structure.

4.5. Computational Simulation studies for structure optimization

In order to build drug delivery systems that fulfill desired functionality, improving structural qualities is essential. A polymeric system's 3D structure, porosity, thickness, and relative bonding area are crucial for enhancing the transport and release capabilities of delivery systems. A polymeric DDS's 3D structure and porosity play an important role in determining how effectively it will perform in regard to drug release and transport. (Y. R. Bhardwaj et al., 2014) Single fibers are deposited one at a time to create the structure. The fiber adapts to the underlying structure depending on its location, size, and flexibility. To simulate the production of the structure, fibers are randomly positioned and oriented in the current work's x-y plane. A suitable geographical distribution can be used to simulate the structure orientation. The model's output is a 3D structure made up of filled and empty voxels that contains data about each fiber. It is possible to compute the paper thickness (local and average), porosity (interfiber and global), relative bonded area, coverage, and the number of crossings per fiber from the created structure.

When simulating cellulosic matrices on a computer, there are several chances to change the porosity, fiber length, and fiber flexibility using the MATLAB® simulator. This has the benefit of allowing for the simultaneous simulation of multiple experiments, preserving laboratory resources as well as the time required to develop the structures and characterize them, a procedure that was evident throughout this work.

Despite functioning independently, the simulator requires information from the structures created in the laboratory, which must be added to it. In this case, MORFi provides information about what can be used as an input for the simulation, such as the fiber length.

Eucalyptus fibers, from Hardwoods (HW), also designated by short fibers, and *Pinus* and *Picea* fibers, from Softwoods (SW), also designated by long fibers, are the major Cellulose constituents of Tissue Materials . In this study (Neiva et al., 2015)the main properties of the most significant eucalyptus species are presented.
In the DDS for demic application investigated in this work, both HW fibers and SW are very important, since SW fibers provide strength to the structure and HW fibers contribute to softness.

Using the simulator, it was possible to make a complete study of the fiber parameters that have an influence in the DDS porosity.
In this section of the results four representative case studies are presented, chosen to have different fiber length (30 and 40 voxel length) and fiber flexibility (1 and 4) where 1 denotes a rigid fiber and 4 represents the most flexible fiber. The following examples are representative of untreated HW and SW Fibers (4.5.1 and 4.5.2), and the same fibers after mechanical or enzymatical processing, with a change in fiber flexibility, and the structure DSS porosity (4.5.3 and 4.5.4).
Porosity is defined by the quocient between the volume of the void or empty Spaces and the total volume of the structure, as seen in the following equation:

$$Porosity\ (\%) = 100 \times \left(1 - \frac{\rho_{structures}}{\rho_{cellulose}}\right) \quad (2)$$

For each case study, three images were taken for each simulation: the first image represents the beginning of the structure's fiber deposition, the second image shows an intermediate perspective, and the third image illustrates the final fiber deposition.

4.5.1 Simulation of fiber deposition of Hardwood Fibers without mechanical or enzymatic treatment

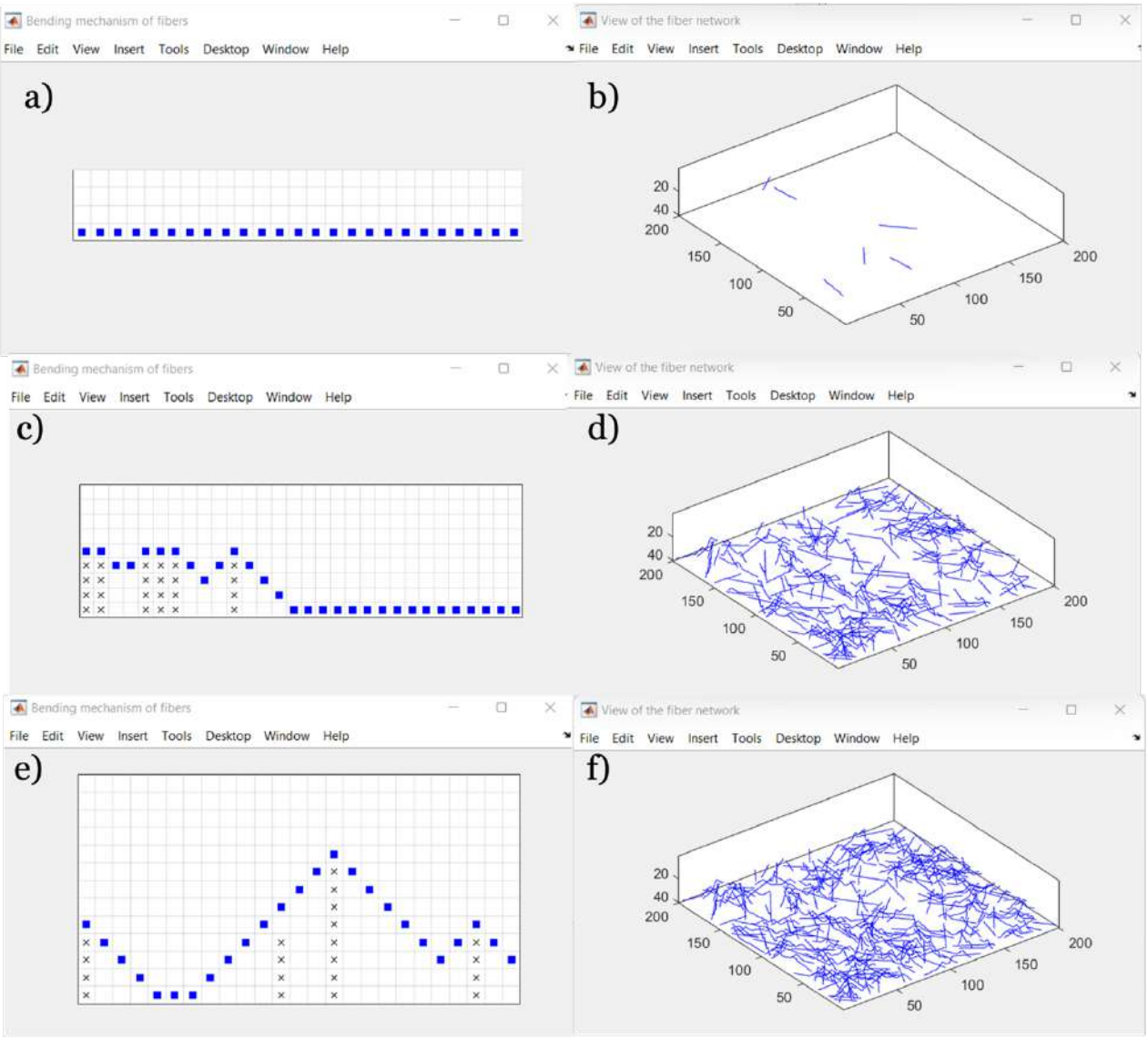

Figure 4. 36 - Illustration of the MATLAB simulation process, demonstrating the start, intermediate, and end of the fiber deposition process in which (a), (c), and (e) indicate the fiber deposition and (b), (d), and (f) represent the visualization of the area in 3 dimensions. The simulation represents a HW fiber that has a length of 30 voxels and a low flexibility (1/4).

4.5.2 Simulation of fiber deposition of Softwood Fibers without mechanical or enzymatic treatment

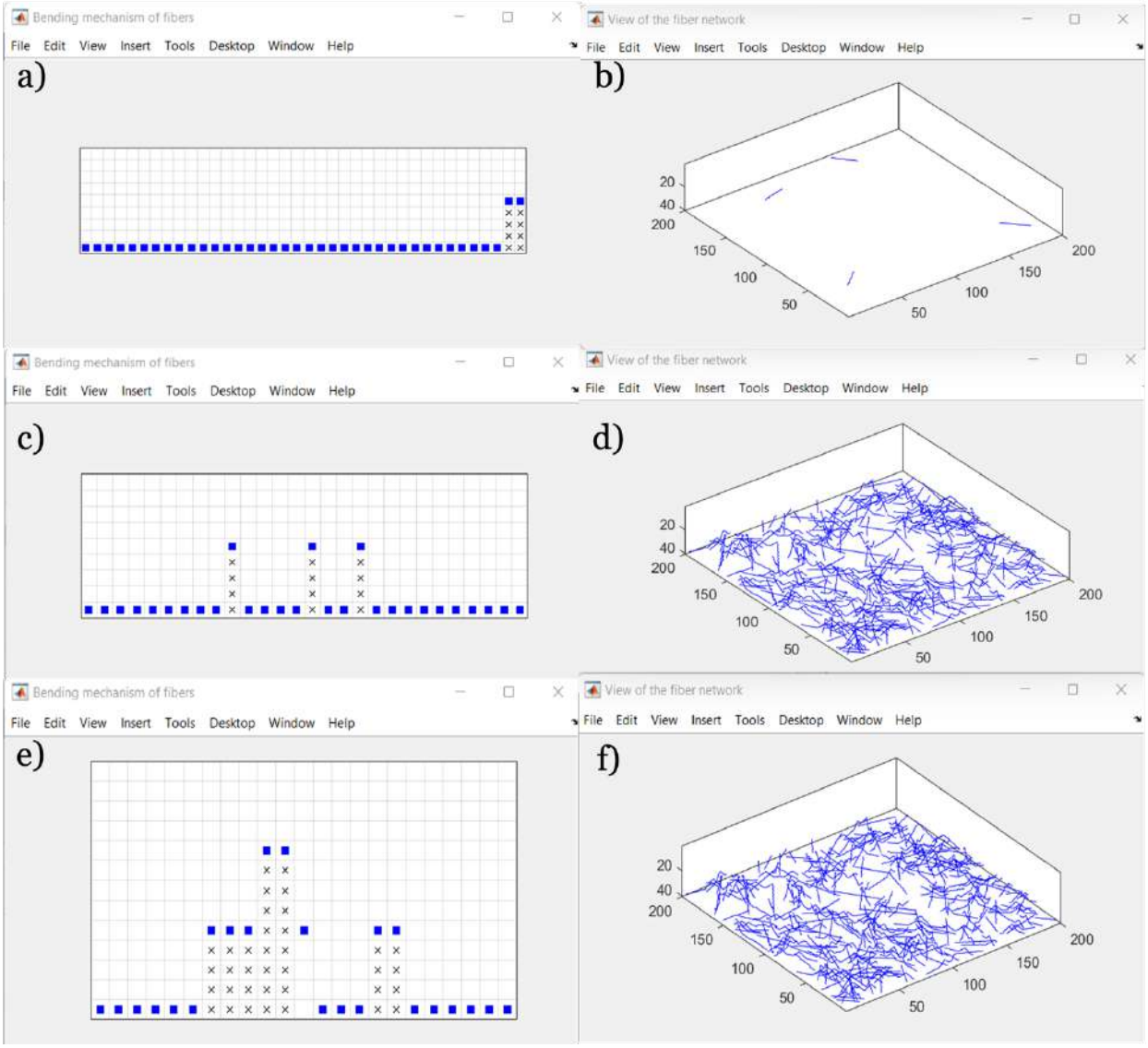

Figure 4. 37 - Illustration of the MATLAB simulation process, demonstrating the start, intermediate, and end of the fiber deposition process. in which (a), (c), and (e) indicate the fiber deposition and (b), (d), and (f) represent the visualization of the area in 3 dimensions. The simulation represents a SW fiber that has a length of 40 voxels and a low flexibility (1/4).

As can be observed in low flexibility (1/4), whether in the length with represent HW or SW non treated, it can be seen that the fibers appear to be straighter in the initial simulation (figures 4.36 and 4.37). It is possible to see that the deposition of fibers is significantly more linear all the throughout the process, which results in a structure that is considerably more rigid. If this structure were to be developed in the laboratory, it would not be as smooth, which is not the most optimal for a dermal system.

4.5.3 Simulation of fiber deposition of Hardwood fibers with flexibility increased due to enzymatic or mechanical processes

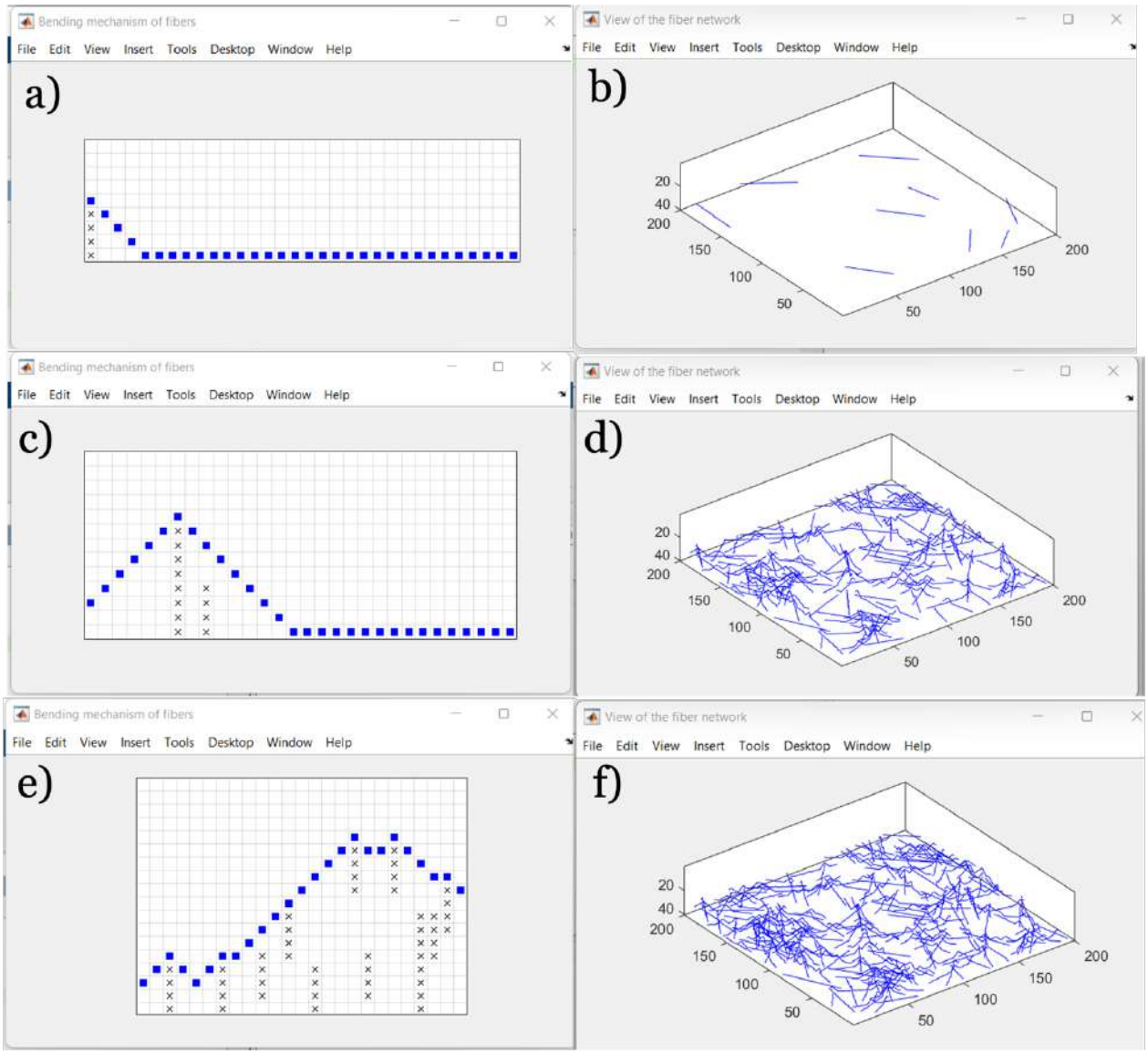

Figure 4. 38 - Illustration of the MATLAB simulation process, demonstrating the start, intermediate, and end of the fiber deposition process. in which (a), (c), and (e) indicate the fiber deposition and (b), (d), and (f) represent the visualization of the area in 3 dimensions. The simulation represents a HW fiber that has a length of 30 voxels and a high flexibility (4/4).

4.5.4 Simulation of fiber deposition Softwood fibers with flexibility increased due to enzymatic or mechanical processes

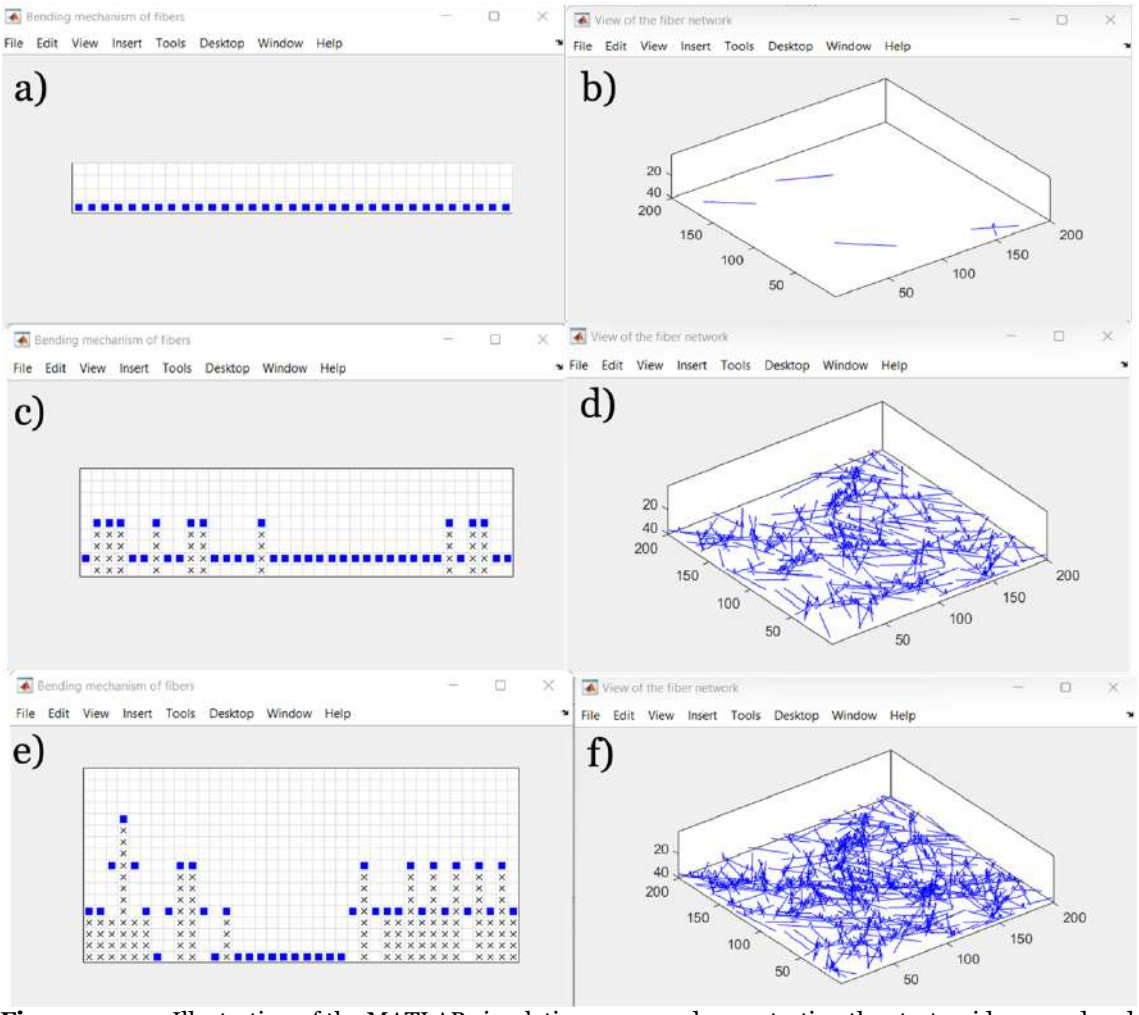

Figure 4. 39 - Illustration of the MATLAB simulation process, demonstrating the start, midway, and end of the fiber deposition process. in which (a), (c), and (e) indicate the fiber deposition and (b), (d), and (f) represent the visualization of the area in 3 dimensions. The simulation represents a SW fiber that has a length of 40 voxels and a high flexibility (4/4).

In the initial simulation (figures 4.38 and 4.39.), it can be seen that the fibers in elevated flexibility (4/4), whether in the length of HW or SW, appear to be straighter than it is in low flexibility (1/4). This model is different because the deposition of fibers is much more fluid than the previous that represented low flexibility, adapting to the other fibers, leading to a softer and more flexible structure. This structure would be softer and the most suitable for a dermal system if it were developed in a laboratory.

4.5.5 - Simulation of fiber mixture deposition

Considering that fiber combinations were created throughout the course of this experiment, a simulation of, certain simulations were conducted using HW and SW mixtures and ranging the flexibility 1 to 4—where 1 denotes a rigid fiber and 4 represents the most flexible fiber.

In this example, scenarios will be simulated where both have low flexibility (1/4), where there will be a mixture of flexibilities, and finally, there will simulated be a combination of HW and SW with both high flexibility of both 4 of flexibility.

4.5.5.1 - Simulation of fiber mixture deposition representing low flexibility

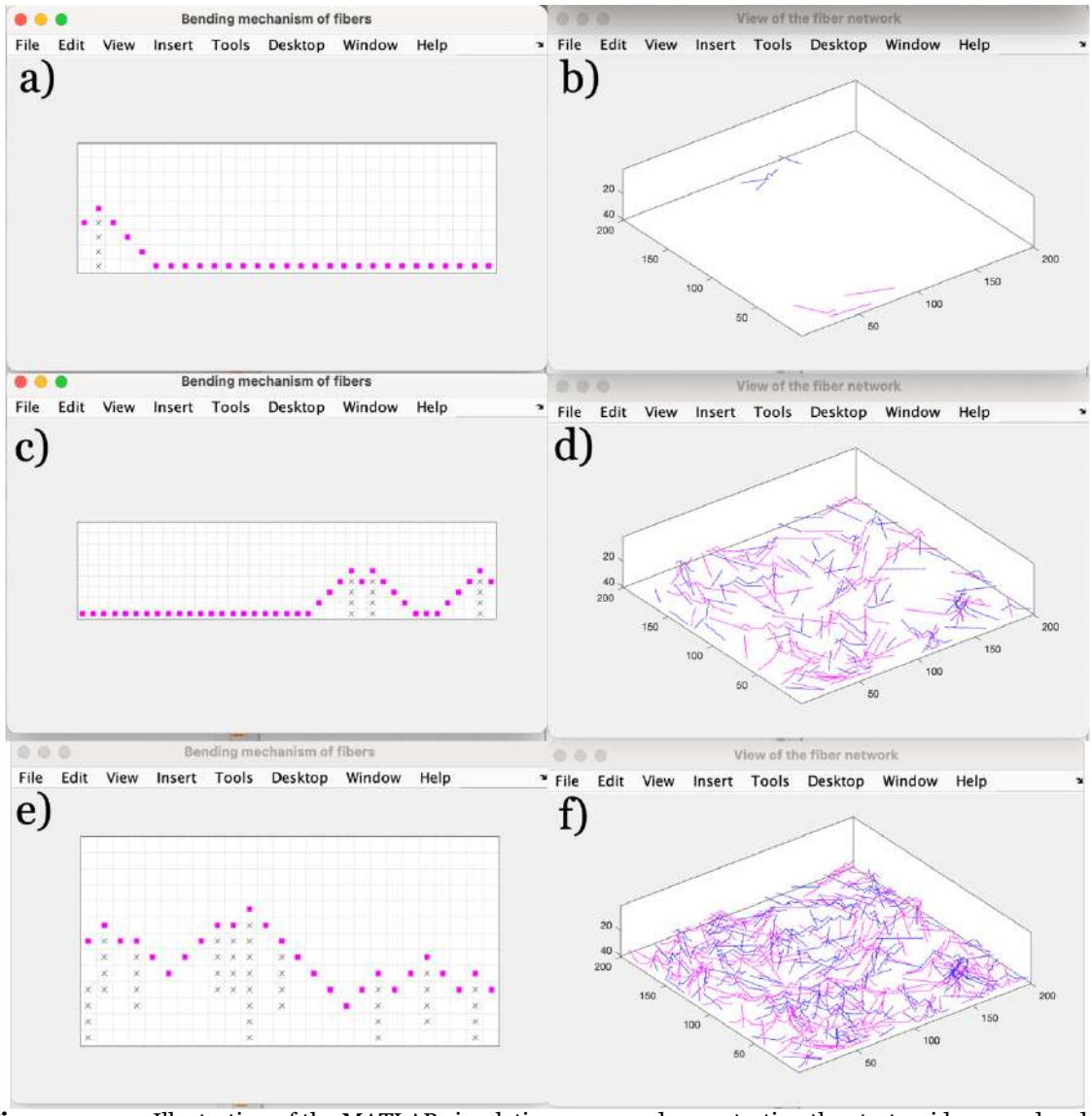

Figure 4. 40 - Illustration of the MATLAB simulation process, demonstrating the start, midway, and end of the fiber deposition process. in which (a), (c), and (e) indicate the fiber deposition and (b), (d), and (f) represent the visualization of the area in 3 dimensions. The simulation represents fiber mixture of HW and SW that has a low flexibility (1/4)

4.5.5.2 - Simulation of fiber mixture deposition with mixed flexibility

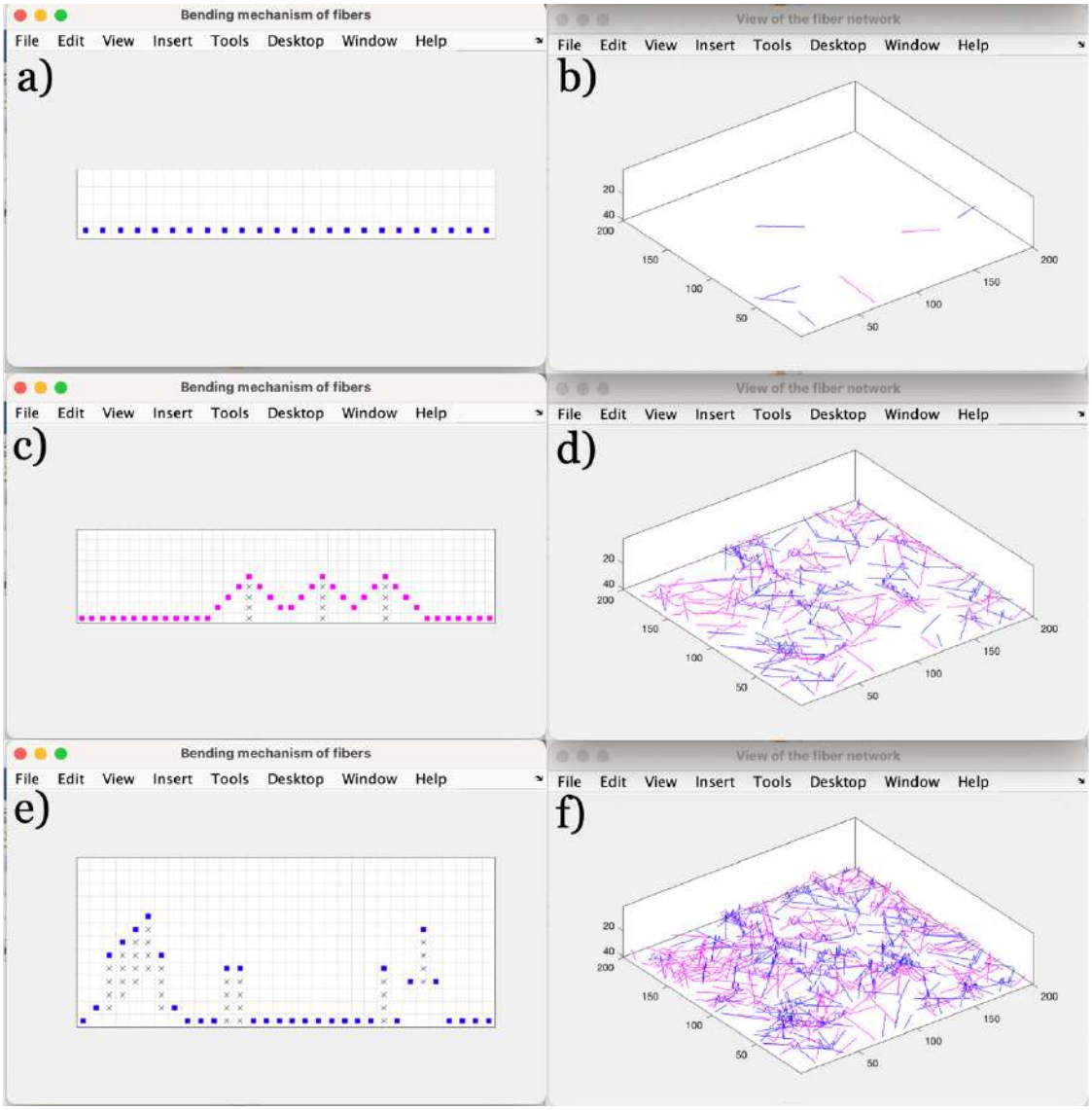

Figure 4. 41 -Illustration of the MATLAB simulation process, demonstrating the start, midway, and end of the fiber deposition process. in which (a), (c), and (e) indicate the fiber deposition and (b), (d), and (f) represent the visualization of the area in 3 dimensions. The simulation represents fiber mixture of HW and SW that has a mixture of high and low flexibility (1/4) and (4/4)

4.5.5.3 - Simulation of fiber mixture deposition with high flexibility (treated mechanically or enzymatically)

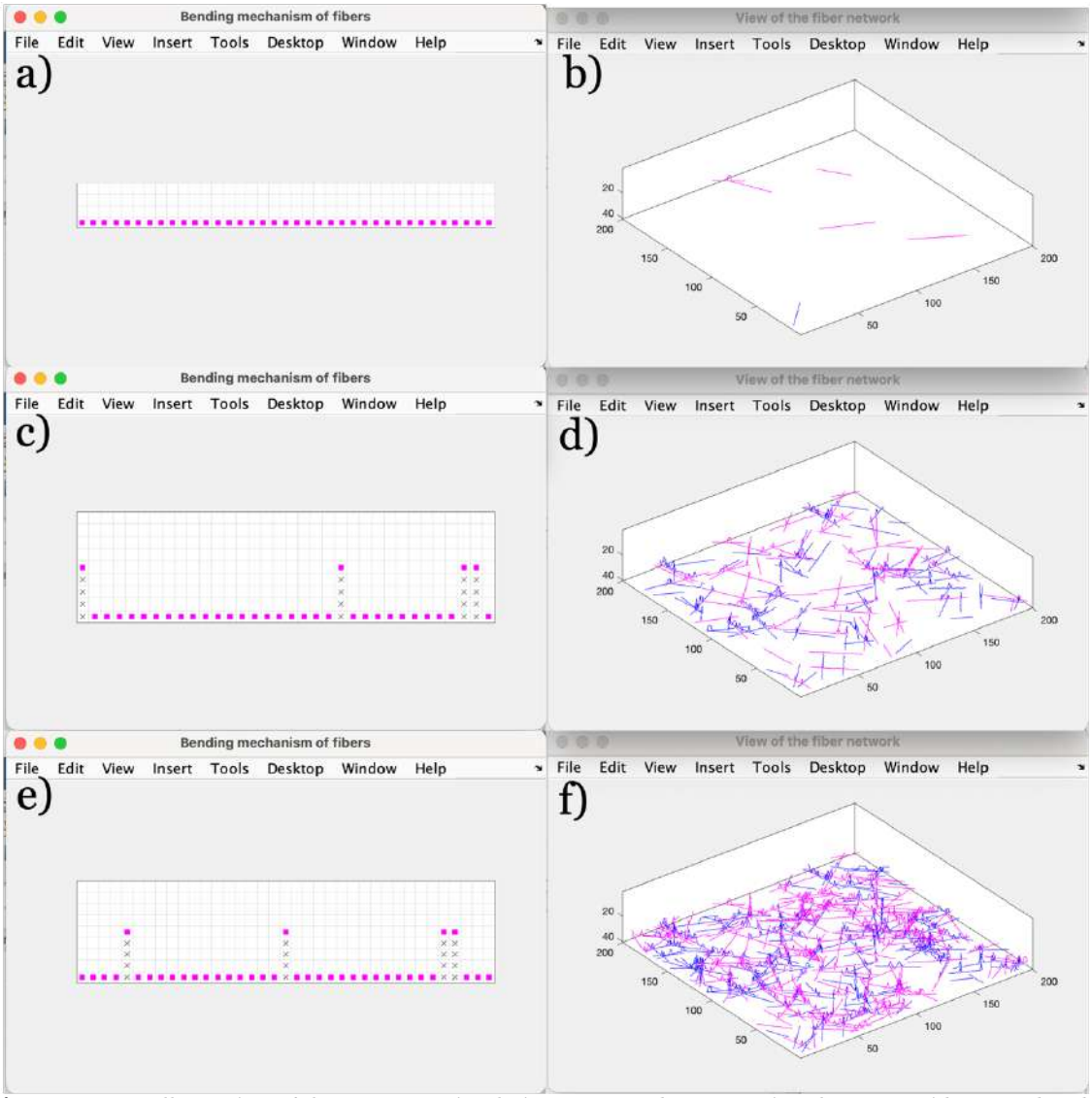

Figure 4. 42 - Illustration of the MATLAB simulation process, demonstrating the start, midway, and end of the fiber deposition process. in which (a), (c), and (e) indicate the fiber deposition and (b), (d), and (f) represent the visualization of the area in 3 dimensions. The simulation represents fiber mixture of WF and SW that has a high flexibility (4/4)

These simulations of fiber blends are used to illustrate a range of possible applications. The variable component in this example was flexibility, which led to the creation of three distinct structures: one that might be more rigid (figure 4.40), one that might be intermediate (figure 4.41), and one that might be soft because the two fibers employed in the simulation had higher flexibility (Figure 4.42). Although it is made very clear that fiber flexibility will be influenced as a factor, which is also obvious in the structures replicated in the lab, it will also have an impact on all other aspects of the structure, including grammage, porosity, and density of the cellulosic matrix, among others.

Chapter V

Conclusions and Futures perspectives

5. Conclusions and Future perspectives

The primary objective was to create systems that can store and then release active molecules by employing a three-dimensional polymeric matrix that is based on cellulose fibers and it is composed of an optimized formulation of different fibers and biopolymer additives. To achieve this goal, it was necessary to conduct research into various fibers derived from various pulps. A wide range of results from the several experimental sets that were carried out, have been presented and discussed along this work, and can be summarized as following.

The study of the characteristics of various types of mechanical softwood cellulosic fiber processing, as well as the characterization of mixtures of mechanically and enzymatically processed cellulose matrices. The mechanic treatment and enzymatic treatment have shown that variation in porosity may be a consequence of the production of fines and broken fibers.

The mixture of fibers 90%HW+10%SW Ref4000+Enz+Biopolymer (2%) +MFC (2%) have presented the highest porosity (90.144±0.754 and 91.066±0.782) and the lowest tissue densities (0.148±0.011 and 0.134±0.012), respectively.

In addition to that, a prototype constructed of hardwood fiber was used in order to apply an emulsion that included the essential oil of *Mentha piperita*. The mask prototype produced present optimized properties of strength, smoothness, stability, and retention of the therapeutic molecules.

Both biometric studies using MorFi, and the research of laboratory-built buildings were utilized to carry out this evaluation. The study of laboratory-built structures allows for the determination of the thickness variation, which in turn determines the porosity variation.

With the mechanical treatment it has presented that when compared a SW sample without refinement, intensive refining (6000 revolutions) decreased the length weighted in length by 13%, coarseness by 21%, kinked fibers by 15%, curl by 7%, while increased macrofibrils rate by 117%, and fines content by 77%.

As, with the fiber mixtures it had shown that enzymatic treatment in SW fiber increased the length weighted in length by 2%, coarseness by 18%, kinked fibers by 11%, macrofibrils rate by 7%, and fines content by 56% compared to the SW sample without refinement.

Lastly, SW that had mechanical treatment (4000 rev) and enzymatic treatment increased length weighted in length by 3% and decreased coarseness by 5%, kinked fibers by 1%, curl by 2%, macrofibrils rate by 25%, and fines content by 12%.

Images were also acquired through the scanning electron microscopy (SEM) study, which enabled us to identify the various types of pores and fibrillation seen in the structures. Because of this, we were able to identify the extent to which mechanical treatment might influence fibrillation. This resulted in the creation of more fibrillated and fine elements, which will have an impact on the structure porosity, and consequently will improve our ability to retain active molecules into our structure. It was possible to observe how additives influence the development of pores when producing a structure, leading to a wide range of potentially unique structures. In addition to this viewing, a characterization of the fiber morphology was performed by using an optical microscope equipped with a camera, as a complementary characterization. These results provide a supplementary perspective on the fibrillation of the cellulose matrix.

Gas chromatography with mass spectrometry (GC-MS), which allowed for the verification of the major components of each essential oil, was undertaken for the purpose of conducting an accurate examination of the essential oils that were included in this experimental set. This allowed for the identification of the essential oil constituents with the highest composition. Menthol constitutes 35.3% in the essential oil of *Mentha piperita*, and Menthone consists of 20.8%. For *Lavandula angustifolia*, linalool and linalyl acetate are both found in the essential oil of. Linalool consisting of 31.76% and 30.4%, respectively. And Citrus limon essential oil does have limonene, which composes 69.30% of the components, and β-pinene, which constitutes 10.20% of the essential oil.

After the cellulose matrix and oils had been described in the appropriate manner, an FTIR-ATR characterization was performed. This allowed for the development of kinetic tests that demonstrated the release of the active molecules over time, as would be predicted, as well as the ability to confirm the existence of the essential oil within the cellulosic structure. Additionally, this allowed for the development of kinetic tests that demonstrated the release of the active molecules over time. The band of OH groups decreased at 2500 and 4000 revolutions, indicating a gradual release of *Mentha piperita* essential oil. The progressive release feels more consistent around 4500 revolutions, which makes it ideal for prototyping.

A benchmark marketing analysis was carried out, which consisted of comparing our prototype to a few products that are already on the market. Because of this, we have information about what is already available, and an important weak point in the products available is their non biodegradability. Using cellulose and biopolymer additives as well, we present solutions not only to improve softness and strength properties, but also biodegradable materials, a plus to our prototypes.

When looking at the NSW along with the essential oil of Lavandula angustifolia and the commercial emulsion, you can see peaks that correspond to lavender's main ingredients. Between 1800 and 1700 cm^{-1}, you can see a C=O stretch, which may be linalyl acetate, which is one of the main parts of the essential oil of Lavandula angustifolia. There is also an increase in the intensity of the peaks in a commercial emulsion, especially in the range where OH and CH groups are observed. This can be made even wider by the other compounds in the emulsion. But the absorbency between 3000 and 2800 cm-1 is much higher than what the SW assay shows.

Regarding Structural properties, it can be concluded that both Biod MKT1 and Biod MKT2 samples indicate that the structures are biodegradable due having the same structural base, and Biod MKT1 has several peaks in the range of 3000~2800 cm-1 and 2400 cm-1, which may be attributed to active components.

While lacking a cellulose-like FTIR-ATR spectrum, nonbiod MKT3 may not be biodegradable. However, a peak at 1600 cm-1 may indicate a C=O stretch and an ester group. This indicates polyester in this structure.

Finally, but not least, the employment of a computer model that has been tested and proven effective in the past constitutes a significant contribution made by this project. This model enabled the modeling of a wide variety of cellulosic matrices with fibers in varying proportions. We were also able to modify the input parameters, such as fiber length, width, and thickness, as well as its flexibility and collapsibility dimensions. The porosity of the three-dimensional network is essential for optimizing the function of transport and controlled release of active molecules, and the computational simulation model provides an important tool to go further in the structure porosity optimization. This is highly significant since it enables the modeling of a number of different options, which helps optimize DDS transport structures and controlled release while also contributing to the conservation of resources, with less laboratory work.

It can be concluded that, when fibers present lower flexibility, whether HW or SW, fiber deposition is more linear, resulting in a more porous and different structure. Fibers with elevated flexibility behave distinct because the fibers are more fluid, bend easily and adapt to each other, creating a softer and more flexible structure. If produced in a laboratory, this structure would be soft and ideal for a dermal system. The use of optimization studies of the pore dimension and the 3D porous network using computational simulation is an important tool to achieve the optimum porosity faster, saving experimental resources.

As general conclusion, the development of dermal DDS system incorporating essential oils, using ecologically friendly and biodegradable items, was successful and all the stages required for their development were completed, and the goals stablished for this work were accomplishment.

For future prospects, it would be fascinating to develop other prototypes using essential oils and other active molecules, such as CBD oil, that is currently investigated in the FibEnTech Research Unit. Other objective possible is to create other biodegradable multi-layering systems, for dermic medicinal potential applications. It would also be complementary to run a microbiological investigation on them, to stablish the conditions to ensure that there is no development of bacteria or fungi in the dermic cellulosic dermal application known by their antibacterial and antifungal activities. Developing a transdermal system that has the capability of releasing active molecules to the systemic stream would also be an interesting project. All of these projects would involve using cellulose-based materials, and other biodegradable polymers, in order to be as environmentally friendly as is humanly possible.

Chapter VI
Bibliography

Abeer, M. M., Mohd Amin, M. C. I., & Martin, C. (2014). A review of bacterial cellulose-based drug delivery systems: Their biochemistry, current approaches and future prospects. *Journal of Pharmacy and Pharmacology*, *66*(8), 1047–1061. https://doi.org/10.1111/jphp.12234

Abitbol, T., Rivkin, A., Cao, Y., Nevo, Y., Abraham, E., Ben-Shalom, T., Lapidot, S., & Shoseyov, O. (2016). Nanocellulose, a tiny fiber with huge applications. *Current Opinion in Biotechnology*, *39*(I), 76–88. https://doi.org/10.1016/j.copbio.2016.01.002

Ahmad, U., Ahmad, Z., Khan, A., Akhtar, J., Singh, S., & Ahmad, F. (2018). Strategies in Development and Delivery of Nanotechnology Based Cosmetic Products. *Drug Research*, *68*(10), 545–552. https://doi.org/10.1055/a-0582-9372

Alankar, S. (2009). A review on peppermint oil. *Asian Journal of Pharmaceutical and Clinical Research*, *2*(2), 27–33.

Alava, M., & Niskanen, K. (2006). The physics of paper. *Reports on Progress in Physics*, *69*(3), 669–723. https://doi.org/10.1088/0034-4885/69/3/R03

AL-Jabri, N. N., & Hossain, M. A. (2018). Chemical composition and antimicrobial potency of locally grown lemon essential oil against selected bacterial strains. *Journal of King Saud University - Science*, *30*(1), 14–20. https://doi.org/10.1016/j.jksus.2016.08.008

Angioni, A., Barra, A., Coroneo, V., Dessi, S., & Cabras, P. (2006). Chemical composition, seasonal variability, and antifungal activity of Lavandula stoechas L. ssp. stoechas essential oils from stem/leaves and Flowers. *Journal of Agricultural and Food Chemistry*, *54*(12), 4364–4370. https://doi.org/10.1021/jf0603329

Arafa, M. G., & Ayoub, B. M. (2017). DOE Optimization of Nano-based Carrier of Pregabalin as Hydrogel: New Therapeutic & Chemometric Approaches for Controlled Drug Delivery Systems. *Scientific Reports*, *7*(1), 41503. https://doi.org/10.1038/srep41503

Arias, M. J. L., López, A., Vilaseca, M., Vallès, B., Prieto, R., Simó, M., Valle, J. A. B., Valle, R. D. C. S. C., Bezerra, F. M., & Bellalta, J. P. (2021). Influence of Chitosan Characteristics in the Microencapsulation of Essential Oils. *Journal of Biomedical Science and Engineering*, *14*(03), 119–129. https://doi.org/10.4236/jbise.2021.143012

Asbahani, A. el, Miladi, K., Badri, W., Sala, M., Addi, E. H. A., Casabianca, H., Mousadik, A. el, Hartmann, D., Jilale, A., Renaud, F. N. R., & Elaissari, A. (2015). Essential oils: From extraction to encapsulation. In *International Journal of Pharmaceutics*,(483, 1–2), 220–243. Elsevier B.V. https://doi.org/10.1016/j.ijpharm.2014.12.069

Bajpai, P. (1999). Application of Enzymes in the Pulp and Paper Industry. *Biotechnology Progress*, *15*(2), 147–157. https://doi.org/10.1021/bp990013k

Baptista-Silva, S., Borges, S., Ramos, O. L., Pintado, M., & Sarmento, B. (2020). The progress of essential oils as potential therapeutic agents: a review. *Journal of Essential Oil Research*, *32*(4), 279–295. https://doi.org/10.1080/10412905.2020.1746698

Bedoya-Serna, C. M., Dacanal, G. C., Fernandes, A. M., & Pinho, S. C. (2018). Antifungal activity of nanoemulsions encapsulating oregano (Origanum vulgare) essential oil: in vitro study and application in Minas Padrão cheese. *Brazilian Journal of Microbiology*, *49*(4), 929–935. https://doi.org/10.1016/j.bjm.2018.05.004

ben Hsouna, A., ben Halima, N., Smaoui, S., & Hamdi, N. (2017). Citrus lemon essential oil: Chemical composition, antioxidant and antimicrobial activities with its preservative effect against Listeria monocytogenes inoculated in minced beef meat. *Lipids in Health and Disease*, *16*(1), 1–11. https://doi.org/10.1186/s12944-017-0487-5

Beuther, P. D., Veith, M. W., & Corp, K. (2009). Sources of Variability in Testing Absorptive Rate of Tissue Paper. *Tappi Engineering Pulping and Environmental Conference*, 907–952.

Bhardwaj, K., Islam, M. T., Jayasena, V., Sharma, B., Sharma, S., Sharma, P., Kuča, K., & Bhardwaj, P. (2020). Review on essential oils, chemical composition, extraction, and utilization of some conifers in Northwestern Himalayas. In *Phytotherapy Research* (Vol. 34, Issue 11, pp. 2889–2910). John Wiley and Sons Ltd. https://doi.org/10.1002/ptr.6736

Bhardwaj, Y. R., Pareek, A., Jain, V., & Kishore, D. (2014). Chemical delivery systems and soft drugs: Retrometabolic approaches of drug design. *Saudi Pharmaceutical Journal*, *22*(4), 290–302. https://doi.org/10.1016/j.jsps.2013.04.004

Bos, J. D., & Meinardi, M. M. H. M. (2000). The 500 Dalton rule for the skin penetration of chemical compounds and drugs. *Experimental Dermatology*, *9*(3), 165–169. https://doi.org/10.1034/j.1600-0625.2000.009003165.x

Butun, S., Ince, F. G., Erdugan, H., & Sahiner, N. (2011). One-step fabrication of biocompatible carboxymethyl cellulose polymeric particles for drug delivery systems. *Carbohydrate Polymers*, *86*(2), 636–643. https://doi.org/10.1016/j.carbpol.2011.05.001

Çakaloğlu, B., Özyurt, V. H., & Ötleş, S. (2018). Cold press in oil extraction. A review. *Ukrainian Food Journal*, *7*(4), 640–654. https://doi.org/10.24263/2304-974X-2018-7-4-9

Caraschi, J. C., & Campana Filho, S. P. (1999). Influência do grau de substituição e da distribuição de substituintes sobre as propriedades de equilíbrio de carboximetilcelulose em solução aquosa. *Polímeros*, *9*(2), 70–77. https://doi.org/10.1590/S0104-14281999000200015

Chakar, F. S., & Ragauskas, A. J. (2004). Review of current and future softwood kraft lignin process chemistry. *Industrial Crops and Products*, *20*(2), 131–141. https://doi.org/10.1016/j.indcrop.2004.04.016

Ciolacu, D. E., Nicu, R., & Ciolacu, F. (2020). Cellulose-Based Hydrogels as Sustained Drug-Delivery Systems. *Materials*, *13*(22), 5270. https://doi.org/10.3390/ma13225270

Conceição, E. L. T., Curto, J. M. R., Simões, R. M. S., & Portugal, A. A. T. G. (2010). Coding a Simulation Model of the 3D Structure of Paper. *Computational Modeling of Objects Represented in Images: Second International Symposium, CompIMAGE 2010, Buffalo, NY, USA, May 5-7, 2010. Proceedings*, 299–310. https://doi.org/10.1007/978-3-642-12712-0_27

Curto, J. M. R., Conceição, E. L. T., Portugal, a. T. G., & Simões, R. M. S. (2011). Three-dimensional modelling of fibrous materials and experimental validation. *Materialwissenschaft Und Werkstofftechnik*, *42*(5), 370–374. https://doi.org/10.1002/mawe.201100790

Curto, J. M. R., Costa, A. P., Amaral, M. E., Ferreira, J. S., Costa, V. L. D., Martins, N. v, Videira, P. E. M., Morais, F. P., Sousa, A. R. L., Conceição, E. L. T., Portugal, A. T. G., Simões, R. M. S., & Santos Silva, M. J. (2016). The Importance of Optimizing the 3D Structure When Developing Cellulosic Materials for Medical Applications: The Case of Drug Delivery Systems (DDS). *XXIII TECNICELPA - Conferência Internacional Da Floresta, Pasta e Papel*, 1–8.

Curto, J. M. R., Hekmati, A. H., Drean, J. Y., Conceição, E. L. T., Portugal, A. T. G., Simões, R. M. S., & Santos Silva, M. J. (2011). Three Dimensional (3D) Polyamide-6-Nanowebs Modeling and Simulation. *11th World Textile Conference, Autex 2011, Mulhouse, France*, *2*, 639–643.

Curto, J. M. R., Rodrigues, T. I. F., & Santos Silva, M. J. (2015). Optimization of fibrous structures with cellulose fibres, polyacrylamide polymers and CaCO3 fillers. *Materialwissenschaft Und Werkstofftechnik*, *46*(4–5), 434–439. https://doi.org/10.1002/mawe.201500418

Dawidowicz, A., Rado, E., Wianowska, D., Mardarowicz, M., & Gawdzik, J. (2008). Application of PLE for the determination of essential oil components from Thymus vulgaris L. *Talanta*, *76*(4), 878–884. https://doi.org/10.1016/j.talanta.2008.04.050

de Assis, T., Huang, S., Driemeier, C. E., Donohoe, B. S., Kim, C., Kim, S. H., Gonzalez, R., Jameel, H., & Park, S. (2018). Toward an understanding of the increase in enzymatic hydrolysis by mechanical refining. *Biotechnology for Biofuels*, *11*(1), 289. https://doi.org/10.1186/s13068-018-1289-3

Demuner, I. F., Borges Gomes, F. J., Gomes, J. S., Coura, M. R., Borges, F. P., Macedo Ladeira Carvalho, A. M., & Silva, C. M. (2021). Improving kraft pulp mill sustainability by lignosulfonates production from processes residues. *Journal of Cleaner Production*, *317*, 128286. https://doi.org/10.1016/j.jclepro.2021.128286

Efentakis, M., Vlachou, M., & Choulis, N. H. (1997). Effects of Excipients on Swelling and Drug Release from Compressed Matrices. *Drug Development and Industrial Pharmacy*, *23*(1), 107–112. https://doi.org/10.3109/03639049709148487

Fearon, O., Kuitunen, S., Ruuttunen, K., Alopaeus, V., & Vuorinen, T. (2020). Detailed Modeling of Kraft Pulping Chemistry. Delignification. *Industrial & Engineering Chemistry Research*, *59*(29), 12977–12985. https://doi.org/10.1021/acs.iecr.0c02110

Ferreira, J. S., Curto, J. M. R., Simões, R. M. S., & Silva, M. J. S. (2016). 3D Computational simulation of Drug Delivery Systems (DDS) made from Carboxymethyl Cellulose (CMC). *1st Symposium of FibEnTech-Fibrous Materials and Environmental Technologies Research Unit, Universidade Da Beira Interior, Covilhã, Portugal*, 91–94.

Ferrer, A., Pal, L., & Hubbe, M. (2017). Nanocellulose in packaging: Advances in barrier layer technologies. *Industrial Crops and Products*, *95*, 574–582. https://doi.org/10.1016/j.indcrop.2016.11.012

Hadgraft, J. (2004). Skin deep. *European Journal of Pharmaceutics and Biopharmaceutics*, *58*(2), 291–299. https://doi.org/10.1016/j.ejpb.2004.03.002

Hajhashemi, V., Ghannadi, A., & Sharif, B. (2003). Anti-inflammatory and analgesic properties of the leaf extracts and essential oil of Lavandula angustifolia Mill. *Journal of Ethnopharmacology*, *89*(1), 67–71. https://doi.org/10.1016/S0378-8741(03)00234-4

Heyden, S. (2000). *Network modelling for the evaluation of mechanical properties of cellulose fibre fluff* [PhD. Thesis]. Lund University.

Jeffries, T.W. (1992). Enzymatic Treatments of Pulps. In: *Emerging Technologies for Materials and Chemicals from Biomass*. In Rowell, R.M., Schultz, T.P., and Narayan, R. (Eds.). *ACS Syposium Series*, American Chemical Society, Washington, DC. pp. 313-329. DOI: 10.1021/bk- 1992-0476.ch018

Jorfi, M., & Foster, E. J. (2015). Recent advances in nanocellulose for biomedical applications. *Journal of Applied Polymer Science*, *132*(14), 1–19. https://doi.org/10.1002/app.41719

Kalemba, D., & Synowiec, A. (2020). Agrobiological interactions of essential oils of two menthol mints: Mentha piperita and mentha arvensis. In *Molecules,* 25(1). MDPI AG. https://doi.org/10.3390/molecules25010059

Kamel, S., Ali, N., Jahangir, K., Shah, S. M., & El-Gendy, A. A. (2008). Pharmaceutical significance of cellulose: A review. *Express Polymer Letters*, *2*(11), 758–778. https://doi.org/10.3144/expresspolymlett.2008.90

Kenealy, W.R., and Jeffries, T.W. (2003). Enzyme Processes for Pulp and Paper: A Review of Recent Developments. In Goodell, B. (Ed.). *Wood deterioration and preservation: advances in our changing world*. ACS Syposium Series, American Chemical Society, Washington, DC. pp. 210-239. DOI: 10.1021/bk-2003-0845.ch012

Kim, S., Kim, J.-H., Jeon, O., Kwon, I. C., & Park, K. (2009). Engineered polymers for advanced drug delivery. *European Journal of Pharmaceutics and Biopharmaceutics*, *71*(3), 420–430. https://doi.org/10.1016/j.ejpb.2008.09.021

Klemm, D., Cranston, E. D., Fischer, D., Gama, M., Kedzior, S. A., Kralisch, D., Kramer, F., Kondo, T., Lindström, T., Nietzsche, S., Petzold-Welcke, K., & Rauchfuß, F. (2018). Nanocellulose as a natural source for groundbreaking applications in materials science: Today's state. *Materials Today*, *21*(7), 720–748. https://doi.org/10.1016/j.mattod.2018.02.001

Klimek-szczykutowicz, M., Szopa, A., & Ekiert, H. (2020). Citrus limon (Lemon) phenomenon—a review of the chemistry, pharmacological properties, applications in the modern pharmaceutical, food, and cosmetics industries, and biotechnological studies. *Plants*, *9*(1). https://doi.org/10.3390/plants9010119

Koulivand, P. H., Khaleghi Ghadiri, M., & Gorji, A. (2013). Lavender and the nervous system. *Evidence-Based Complementary and Alternative Medicine*, *2013*. https://doi.org/10.1155/2013/681304

Lavoine, N., Desloges, I., Dufresne, A., & Bras, J. (2012). Microfibrillated cellulose - Its barrier properties and applications in cellulosic materials: A review. *Carbohydrate Polymers*, *90*(2), 735–764. https://doi.org/10.1016/j.carbpol.2012.05.026

Li, X. M., Tian, S. L., Pang, Z. C., Shi, J.-Y., Feng, Z.-S., & Zhang, Y.-M. (2009). Extraction of Cuminum cyminum essential oil by combination technology of organic solvent with low boiling point and steam distillation. *Food Chemistry*, *115*(3), 1114–1119. https://doi.org/10.1016/j.foodchem.2008.12.091

Lin, N., & Dufresne, A. (2014). Nanocellulose in biomedicine: Current status and future prospect. *European Polymer Journal*, *59*, 302–325. https://doi.org/10.1016/j.eurpolymj.2014.07.025

Martins, V. D. F., Cerqueira, M. A., Fuciños, P., Garrido-Maestu, A., Curto, J. M. R., & Pastrana, L. M. (2018). Active bi-layer cellulose-based films: development and characterization. *Cellulose*, *25*(11), 6361–6375. https://doi.org/10.1007/s10570-018-2021-y

Mishra, R. K., Sabu, A., & Tiwari, S. K. (2018). Materials chemistry and the futurist eco-friendly applications of nanocellulose: Status and prospect. *Journal of Saudi Chemical Society*, *22*(8), 949–978. https://doi.org/10.1016/j.jscs.2018.02.005

Mogoşanu, G. D., Grumezescu, A. M., Bejenaru, L. E., & Bejenaru, C. (2016). Natural and synthetic polymers for drug delivery and targeting. In *Nanobiomaterials in Drug Delivery* (pp. 229–284). Elsevier. https://doi.org/10.1016/B978-0-323-42866-8.00008-3

Moon, R. J., Martini, A., Nairn, J., Simonsen, J., & Youngblood, J. (2011). Cellulose nanomaterials review: structure, properties and nanocomposites. *Chemical Society Reviews*, *40*(7), 3941. https://doi.org/10.1039/c0cs00108b

Morais, F. P., Carta, A. M. M. S., Amaral, M. E., & Curto, J. M. R. (2020a). 3D Fiber Models to Simulate and Optimize Tissue Materials. *BioResources*, *15*(4), 8833–8848. https://doi.org/10.15376/biores.15.4.8833-8848

Morais, F. P., Carta, A. M. M. S., Amaral, M. E., & Curto, J. M. R. (2020b). Cellulose fiber enzymatic modification to improve the softness, strength, and absorption properties of tissue papers. *BioResources*, *16*(1), 846–861. https://doi.org/10.15376/biores.16.1.846-861

Morais, F. P., & Curto, J. M. (2018). Design of Porous Nano Cellulose Based Biopolymers for Nanomedicine Applications. *Current Scientific Research in Biomedical Sciences Research Article*, *2018*(1), 180003. https://chembiopublishers.com/CSRBS/

Morais, F. P., & Curto, J. M. R. (2022). "3D computational simulation and experimental validation of structured materials: Case studies of tissue papers. *BioResources*, *17*(3), 4206–4225. https://doi.org/10.15376/biores.17.3.4206-4225

Morais, F. P., Simões, R. M. S., & Curto, J. M. R. (2020). Biopolymeric Delivery Systems for Cosmetic Applications Using Chlorella vulgaris Algae and Tea Tree Essential Oil. *Polymers*, *12*(11), 2689. https://doi.org/10.3390/polym12112689

Moreira, J., Lopes, C., Lis Arias, M.-J., Silva, L., & Curto, J. (2022). Development of Biodegradable, Cellulose-Based, Essential Oil and Chitosan Drug Delivery Systems for Cosmetic Mask Applications. *In 1st International FibEnTech Congress (FibEnTech21) New Opportunities for Fibrous Materials in the Ecological Transition, KnE Materials Science*, 63–71. https://doi.org/10.18502/kms.v7i1.11609

Moulton, S. E., & Wallace, G. G. (2014). 3-dimensional (3D) fabricated polymer based drug delivery systems. *Journal of Controlled Release*, *193*, 27–34. https://doi.org/10.1016/j.jconrel.2014.07.005

Mura, S., Nicolas, J., & Couvreur, P. (2013). Stimuli-responsive nanocarriers for drug delivery. *Nature Materials*, *12*(11), 991–1003. https://doi.org/10.1038/nmat3776

Mutlu-Ingok, A., Devecioglu, D., Dikmetas, D. N., Karbancioglu-Guler, F., & Capanoglu, E. (2020). Antibacterial, antifungal, antimycotoxigenic, and antioxidant activities of essential oils: an updated review. In *Molecules*, 25 (20). MDPI AG. https://doi.org/10.3390/molecules25204711

Nehme, R., Blel, W., Montillet, A., Bellettre, J., & Marchal, L. (2021). Production of oil in water emulsions in microchannels at high throughput: Evaluation of emulsions in view of cosmetic, nutraceutical or pharmaceutical applications. *Chemical Engineering and Processing - Process Intensification*, *161*. https://doi.org/10.1016/j.cep.2021.108301

Neiva, D., Fernandes, L., Araújo, S., Lourenço, A., Gominho, J., Simões, R., & Pereira, H. (2015). Chemical composition and kraft pulping potential of 12 eucalypt species. *Industrial Crops and Products*, *66*, 89–95. https://doi.org/10.1016/j.indcrop.2014.12.016

Nicu, R., Ciolacu, F., & Ciolacu, D. E. (2021). Advanced Functional Materials Based on Nanocellulose for Pharmaceutical/Medical Applications. *Pharmaceutics*, *13*(8), 1125. https://doi.org/10.3390/pharmaceutics13081125

Niskanen, K. J., & Alava, M. J. (1994). Planar random networks with flexible fibers. *Physical Review Letters*, *73*(25), 3475–3478. https://doi.org/10.1103/PhysRevLett.73.3475

Nóbrega, K. C., & Amorim, L. V. (2015). Influência da massa molar de CMC no comportamento reológico e de filtração de suspensões argilosas. *Cerâmica*, *61*(360), 399–408. https://doi.org/10.1590/0366-69132015613601904

Orchard, A., & van Vuuren, S. (2017). Commercial Essential Oils as Potential Antimicrobials to Treat Skin Diseases. In *Evidence-based Complementary and Alternative Medicine* (Vol. 2017). Hindawi Limited. https://doi.org/10.1155/2017/4517971

Owen, A., Rannard, S., Bawa, R., & Feng, S.-S. (2016). Interdisciplinary nanomedicine publications through interdisciplinary peer-review. *Journal of Interdisciplinary Nanomedicine*, *1*(1), 4–8. https://doi.org/10.1002/jin2.1

Parry, A. (2016). Nanocellulose and its Composites for Biomedical Applications. *Current Medicinal Chemistry*, *24*(5), 512–528. https://doi.org/10.2174/0929867323666161014124008

Pavlačková, J., Kovacsová, K., Radiměřský, P., Egner, P., Sedlaříková, J., & Mokrejš, P. (2018). Stability and in vivo efficiency of natural cosmetic emulsion systems with the addition of vegetable oils. *Brazilian Journal of Pharmaceutical Sciences*, *54*(3). https://doi.org/10.1590/s2175-97902018000317693

Pavoni, L., Perinelli, D. R., Bonacucina, G., Cespi, M., & Palmieri, G. F. (2020). An Overview of Micro- and Nanoemulsions as Vehicles for Essential Oils: Formulation, Preparation and Stability. *Nanomaterials*, *10*(1), 135. https://doi.org/10.3390/nano10010135

Provatas, N., & Uesaka, T. (2003). Modelling Paper Structure and Paper-Press Interactions. *Journal of Pulp and Paper Science*, *29*, 332–340.

Prusinowska, R., & Śmigielski, K. B. (2014). Composition, biological properties and therapeutic effects of lavender (Lavandula angustifolia L). A review. *Herba Polonica*, *60*(2), 56–66. https://doi.org/10.2478/hepo-2014-0010

Przybysz, P., Kuncewicz, C., & Rieger, F. (2014). A New Device for Characterisation of the Drainage Kinetics of Fibrous Suspensions Under Gravity. *Chemical and Process Engineering*, *35*(4), 409–420. https://doi.org/10.2478/cpe-2014-0031

Rajnish, K. N., Samuel, M. S., John J, A., Datta, S., Chandrasekar, N., Balaji, R., Jose, S., & Selvarajan, E. (2021). Immobilization of cellulase enzymes on nano and micro-materials for breakdown of cellulose for biofuel production-a narrative review. *International Journal of Biological Macromolecules*, *182*, 1793–1802. https://doi.org/10.1016/j.ijbiomac.2021.05.176

Rao, Y. M., Veni, J. K., & Jayasagar, G. (2001). Formulation and Evaluation of Diclofenac Sodium Using Hydrophilic Matrices. *Drug Development and Industrial Pharmacy*, *27*(8), 759–766. https://doi.org/10.1081/DDC-100107239

Rassem, H. H., Nour, A. H., & Yunus, R. M. (2016). Techniques for extraction of essential oils from plants: A review. *Australian Journal of Basic and Applied Sciences*, *10*(16), 117–127.

Řebíčková, K., Bajer, T., Šilha, D., Ventura, K., & Bajerová, P. (2020). Comparison of Chemical Composition and Biological Properties of Essential Oils Obtained by Hydrodistillation and Steam Distillation of Laurus nobilis L. *Plant Foods for Human Nutrition*, *75*(4), 495–504. https://doi.org/10.1007/s11130-020-00834-y

Sabbagh, F., & Kim, B. S. (2022). Recent advances in polymeric transdermal drug delivery systems. *Journal of Controlled Release*, *341*, 132–146. https://doi.org/10.1016/j.jconrel.2021.11.025

Safari, J., & Zarnegar, Z. (2014). Advanced drug delivery systems: Nanotechnology of health design A review. *Journal of Saudi Chemical Society*, *18*(2), 85–99. https://doi.org/10.1016/j.jscs.2012.12.009

Santner, T. J., Williams, B. J., & Notz, W. I. (2003). *The Design and Analysis of Computer Experiments*. Springer New York. https://doi.org/10.1007/978-1-4757-3799-8

Shaaban, H. A. E., El-Ghorab, A. H., & Shibamoto, T. (2012). Bioactivity of essential oils and their volatile aroma components: Review. *Journal of Essential Oil Research*, *24*(2), 203–212. https://doi.org/10.1080/10412905.2012.659528

Simões, S., Figueiras, A., & Veiga, F. (2012). Modular Hydrogels for Drug Delivery. *Journal of Biomaterials and Nanobiotechnology*, *03*(02), 185–199. https://doi.org/10.4236/jbnb.2012.32025

Sindhu, K. A., Prasanth, R., & Thakur, V. K. (2014). Medical Applications of Cellulose and its Derivatives: Present and Future. In *Nanocellulose Polymer Nanocomposites* (pp. 437–477). John Wiley & Sons, Inc. https://doi.org/10.1002/9781118872246.ch16

Singh, R., Kumar, M., Mittal, A., & Mehta, P. K. (2016). Microbial enzymes: industrial progress in 21st century. *3 Biotech*, *6*(2), 174. https://doi.org/10.1007/s13205-016-0485-8

Sood, S., Gupta, V. K., Agarwal, S., Dev, K., & Pathania, D. (2017). Controlled release of antibiotic amoxicillin drug using carboxymethyl cellulose-cl-poly(lactic acid-co-itaconic acid) hydrogel. *International Journal of Biological Macromolecules*, *101*, 612–620. https://doi.org/10.1016/j.ijbiomac.2017.03.103

Sun, Y., Su, J., Liu, G., Chen, J., Zhang, X., Zhang, R., Jiang, M., & Qiu, M. (2017). Advances of blood cell-based drug delivery systems. *European Journal of Pharmaceutical Sciences*, *96*, 115–128. https://doi.org/10.1016/j.ejps.2016.07.021

Tongnuanchan, P., & Benjakul, S. (2014). Essential Oils: Extraction, Bioactivities, and Their Uses for Food Preservation. *Journal of Food Science*, *79*(7), 1231–1249. https://doi.org/10.1111/1750-3841.12492

Tsai, M. L., Wu, C. T., Lin, T. F., Lin, W. C., Huang, Y. C., & Yang, C. H. (2013). Chemical composition and biological properties of essential oils of two mint species. *Tropical Journal of Pharmaceutical Research*, *12*(4), 577–582. https://doi.org/10.4314/tjpr.v12i4.20

Ulker, Z., & Erkey, C. (2014). An emerging platform for drug delivery: Aerogel based systems. *Journal of Controlled Release*, *177*, 51–63. https://doi.org/10.1016/j.jconrel.2013.12.033

Valle, J. A. B., Valle, R. de C. S. C., Bierhalz, A. C. K., Bezerra, F. M., Hernandez, A. L., & Lis Arias, M. J. (2021). Chitosan microcapsules: Methods of the production and use in the textile finishing. In *Journal of Applied Polymer Science*, 138(21). John Wiley and Sons Inc. https://doi.org/10.1002/app.50482

van Gheluwe, L., Chourpa, I., Gaigne, C., & Munnier, E. (2021). Polymer-Based Smart Drug Delivery Systems for Skin Application and Demonstration of Stimuli-Responsiveness. *Polymers*, *13*(8), 1285. https://doi.org/10.3390/polym13081285

Varshney, V. K., & Naithani, S. (2011). Chemical Functionalization of Cellulose Derived from Nonconventional Sources. In *Cellulose Fibers: Bio- and Nano-Polymer Composites* (pp. 43–60). Springer Berlin Heidelberg. https://doi.org/10.1007/978-3-642-17370-7_2

Villanova, J. C. O., Oréfice, R. L., & Cunha, A. S. (2010). Aplicações farmacêuticas de polímeros. *Polímeros*, *20*(1), 51–64. https://doi.org/10.1590/S0104-14282010005000009

Vlaia, L., Coneac, G., Olariu, I., Vlaia, V., & Lupuleasa, D. (2016). Cellulose-Derivatives-Based Hydrogels as Vehicles for Dermal and Transdermal Drug Delivery. In S. B. Majee (Ed.), *Emerging Concepts in Analysis and Applications of Hydrogels* (1st ed., pp. 159–200). InTech. https://doi.org/10.5772/63953

Yang, S., Yang, B., Duan, C., Fuller, D. A., Wang, X., Chowdhury, S. P., Stavik, J., Zhang, H., & Ni, Y. (2019). Applications of enzymatic technologies to the production of high-quality dissolving pulp: A review. *Bioresource Technology*, *281*, 440–448. https://doi.org/10.1016/j.biortech.2019.02.132

Yen, H. Y., & Lin, Y. C. (2017). Green extraction of Cymbopogon citrus essential oil by solar energy. *Industrial Crops and Products*, *108*, 716–721. https://doi.org/10.1016/j.indcrop.2017.07.039

Yu, R., Chen, H., Chen, T., & Zhou, X. (2008). Modeling and simulation of drug release from multi-layer biodegradable polymer microstructure in three dimensions. *Simulation Modelling Practice and Theory*, *16*(1), 15–25. https://doi.org/10.1016/j.simpat.2007.09.008

Zhang, C., Mo, J., Fu, Q., Liu, Y., Wang, S., & Nie, S. (2021). Wood-cellulose-fiber-based functional materials for triboelectric nanogenerators. *Nano Energy*, *81*, 105637. https://doi.org/10.1016/j.nanoen.2020.105637

Appendix

Appendix A. Publications List

A1. Full papers in proceedings/conferences/symposium books with scientific peer review and publication with ISBN:

Moreira, J., Lopes, C., Lis Arias, M.-J., Silva, L., & Curto, J. (2022). Development of Biodegradable, Cellulose-Based, Essential Oil and Chitosan Drug Delivery Systems for Cosmetic Mask Applications. 1st International FibEnTech Congress (FibEnTech21) New opportunities for fibrous materials in the ecological transition, *KnE Materials Science*, *7*(1), 63–71. https://doi.org/10.18502/kms.v7i1.11609

A2. Poster communications:

Won 1st prize in poster communication in: VIII Ciclo de Conferências da Faculdade de Ciências Ensino Pós-Pandemia: O Novo Amanhã", University of Beira Interior, Covilhã, Portugal, Sep 23-24, 2022.

Moreira, J., Curto, J., Development of dermic application systems made from micro/nano cellulose biopolymeric materials with 3D porosity simulation to optimize the retention and release of essential oils biomolecules, in VIII Ciclo de Conferências da Faculdade de Ciências "Ensino Pós-Pandemia: O Novo Amanhã", University of Beira Interior, Covilhã, Portugal, Sep 23-24, 2022. (Poster presentation and Abstract in conference book).

Saraiva, P.N.C., Moreira, J., Lopes, C., Silva, L., Curto, J.M.R., Drug Delivery Systems (DDS) for oral and dermic applications using Cannabis fibers and Essential Oils, in Encontro com a Ciência e Tecnologia em Portugal 2022, CCL, Lisbon, Portugal, May 16-18, 2022.

Moreira, J., Curto, J., Development of dermic application systems made from micro/nano cellulose biopolymeric materials with 3D porosity simulation to optimize the retention and release of essential oils biomolecules, in: VII Ciclo de Conferências da Faculdade de Ciências "Novos desafios no Ensino Aprendizagem", University of Beira Interior, Covilhã, Portugal, Sep 24-25, 2021. (Poster presentation and Abstract in conference book).

A3. Oral comunications:

Moreira, J., Lopes, C., Lis Arias, M.-J., Silva, L., & Curto, J. (2022). Development of Biodegradable, Cellulose-Based, Essential Oil and Chitosan Drug Delivery Systems for Cosmetic Mask Applications. 1st International FibEnTech Congress (FibEnTech21) New opportunities for fibrous materials in the ecological transition*, KnE Materials Science*, *7*(1), 63–71. https://doi.org/10.18502/kms.v7i1.11609

Moreira, J., Curto, J., Development of dermic application systems made from micro/nano cellulose biopolymeric materials with 3D porosity simulation to optimize the retention and release of essential oils biomolecules, in Polymer Connect, Polymer Science and Composite Materials Conference on 05-07 July 2021.

Development of Biodegradable Cellulose-based, Essential Oil and Chitosan Drug Delivery Systems (DDS) for cosmetic masks applications

Joana Moreira[1, *], Catarina Lopes[1], Manuel-José Lis Arias[2], Lúcia Silva[1], Joana M.R. Curto[1, *]

[1]FibEnTech, Chemistry Dep., University of Beira Interior, Covilhã, Portugal
[2]POLQUITEX, Chemical Engineering Dep., Universitat Politècnica de Catalunya, Terrassa, Spain

---

Keywords: Biopolymers; Dermic application; Drug Delivery Systems (DDS); Essential Oil; *Mentha piperita*.

Abstract

The goal of this research is the development of cellulose-based biodegradable Drug Delivery Systems (DDS) solutions for cosmetic masks applications. Cellulose-based materials derived from natural renewable sources provide a sustainable alternative to nonwoven cosmetic masks derived from nondegradable fossil-based raw materials. An experimental plan design was executed to assembly the 3D cellulose fibres matrix and the water in oil emulsion comprising the active molecules from *Mentha piperita* L. Two types of biopolymeric additives were used, one derived from a nano/micro fibrillated cellulose pulp and another one including chitosan. A 3D computational simulation study was performed to enhance porosity and strength properties.
The results indicate that the cosmetic face mask optimized prototypes, made from a biodegradable 3D matrix of cellulose fibres, and active molecules, are suitable for dermic use.

Introduction

Cellulose is a polymer, consisting of long chains of glucose anhydride, also known as anhydridoglucose (AGU), which has three hydroxyl groups. These groups give cellulose the ability to make hydrogen bonds, which allows for great stability and resistance [1,2].It is produced by the biosynthesis of plants, animals and bacteria in the Eubacteria domain, it leads to many variations of it [3]. Cellulose is properly structured, as it has crystalline and amorphous areas. Cellulose from plants requires processes to remove lignin and hemicelluloses, which can be tricky to solve experimentally [4]. Cellulose is a renewable source of bio-polymers, being produced by several species, such as plants, animals and bacteria. Cellulose is the structural unit of plants, and is therefore one of the most abundant natural materials [4].

Chitosan is a polysaccharide, vastly abundant like cellulose, becoming an inexpensive resource. Chitosan is derived from organisms such as crustaceans and fungus, and since its common in nature it presents the benefits of being biodegradable, biocompatible and innocuous [5]. Essential oils are multifaceted as they are used in various industries, such as the cosmetic, pharmaceutical and food industries [6]. These are produced by plants and extracted from them, in which many extracts have been recognized as GRAS (Generally Recognized as Safe) [7]. These by-products have anti-inflammatory, antimicrobial and even antiviral properties [8]. Essential oils can be extracted from various parts of the plant such as flowers, fruits, seeds and leaves. Other extractions can be done in a variety of ways, such as solvent extraction and cold pressing [9]. The extraction product's consistency, quantity, and composition can differ depending on environment, soil composition, plant organ, age, and vegetative cycle stage [10]. To obtain the same composition of EOs, they must be harvested under the same conditions, i.e., from the same

organ of the plant, which must be growing in the same soil, atmosphere, and season [11]. Each essential oil is a complex sample, composed by many volatile compounds, mostly terpenes [12]. Monoterpenes are present in all essential oils. They are made up of 10 carbon atoms that are derived from two isoprene units. Monoterpenes may have a straight-chain or a single ring backbone. Because of their smaller size, they respond easily to air and heat, and they degrade faster than their more complex molecules [7]. Due to the high volatility of essential oils, the dermal application in the form of masks has the advantage of storing the therapeutic molecules, prolonging their period of action [13]. The innovation of this project is the development of a cosmetic face mask prototype, made from an optimized 3D matrix, containing micro and nano cellulose fibres, obtained by a combination of mechanical and enzymatic processes, to achieve the desired porosity and strength [14-16]. The biopolymer chitosan is also being investigated as an additive, to promote the controlled release of peppermint active molecules [5].

Material and methods

Bleached and unbleached *Pinus pinaster* and Eucalyptus pulps from FibEnTech (University of Beira Interior) Research Laboratory were used.
In this study hardwood and softwood industrial Kraft pulps processes were disintegrated according to the ISO 5263/1. The fibres' morphological properties were determined automatically by image analysis of a diluted suspension (20 mg/L and 30 mg/L 145 to hardwood and softwood samples, respectively) in a flow chamber in MorFi Fiber Analyzer (TECHPAP, Grenoble, France). After their characterization, the hardwood and soft wood pulps were mixed in different ratios.

The cellulose fibres were modified using enzymatic and mechanical treatments. The mechanical treatment was applied to the kraft pulp using a PFI mill at 500-7500 revolutions, under an intensity of 3,33 N/mm. Enzymatic treatments were performed using an enzyme dosages of 10 g per ton of pulp, for 30 and 60 minutes. The assays were carried out at a consistency of 4%, pH 7, and 40ºC, with continuous mechanical agitation. To stop the reaction sodium hypochlorite was added to the pulp suspension. After these enzymatic treatments, the pulps were mixed in a ratio of 80:20. A more detailed description of this study can be found in the work of Morais et al. [13-15,18].
Different mixtures with additives were made to understand their influence. The micro/ nanofibrillated cellulose (MFC/NFC) was incorporated in a never-dry (slush) bleached eucalyptus kraft pulp, according to loads of 1%, 5%, and 10%. A chitosan additive was also incorporated in the same fiber pulp slurry, at the same dosages. A more detailed description of this study can be found in the master thesis document of the author Moreira, J.
The tissue structures were produced in a batch laboratory sheet former according to an adaptation of ISO 5269/1. The adjustments consisted of the production of structures with a basis weight of 20 g/m² and of 60 g/m² and suppression of the pressing operation.

The prototype mask samples were conditioned at 22±1ºC, with a relative humidity of 50±2%, according to ISO 187. For all assays, the tissue properties for handsheets were measured in terms of structural and functional properties. The basis weight (ISO 12625-6) was obtained by the ratio between the average mass of each structure and the respective area (0,02138 m²). The thickness (ISO 12625-3) was obtained using a Frank-PTI micrometer. The bulk (ISO 12625- 3) was obtained by the quotient between the structure thickness and the basis weight. A water in oil emulsion was prepared using a ratio of 1:4 (w/w) and 3700 rpm. The water phase is a peppermint infusion, and the oil phase is made using a carrier sunflower oil and the *Mentha piperita L.* essential oil. The emulsion was incorporated in the fibre mixture bulk, and the mask prototype was stored between 0ºC and 4ºC [18]. The fibres length, width, coarseness and fine content were characterized using an automated analyser. The essential oil was analysed using Gas Chromatography–Mass Spectrometry (GC-MS). The Gas Chromatography was performed using an Agilent technologies 7890A GC A.01.13 with Agilent Technologies 5975 inert XL MSD with Triple-Axis Detector. SEM images were performed using Hitachi S-2700 (Tokyo, Japan). The structures were cross-sectioned were covered with gold using a Sputter Quorum Q 15 OR ES (Laughton, East Sussex, UK) and analysed at different magnifications. FTIR-ATR was used to analyse the face mask prototypes without and with peppermint essential oil active molecules. The equipment used was a FTIR-ATR Thermo-Nicolet IS10.

The 3D fibrous matrix computational simulation was performed using Matlab®, according to a previously validated model [18,19]. The fibrous material simulation model was used to simulate the deposition of fibres and the assembly of the mask structure prototype.

Results and discussion

The assembly of the mask prototype and its structural hierarchy is presented in Figure 1. Cellulose microcrystalline and chitosan molecular structures are represented in Fig1.b) and c).

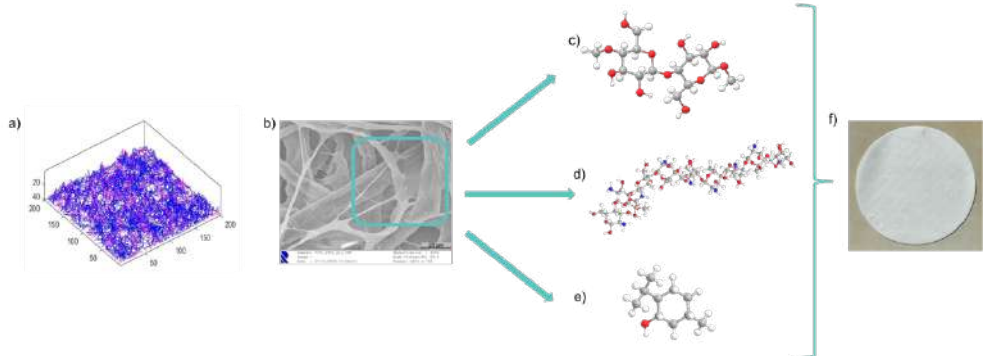

Fig. 1. Visual representation of the mask prototype structural hierarchy. a) Structures obtained by Computational Simulation, representing fibres at the end of their deposition, b) SEM image of the fibrous matrix, c) cellulose, d) chitosan, e) menthol and f) laboratory made mask prototype. Molecules made using ChemDraw ® Professional 16.0 by Moreira, J. Model and computational Simulation by Curto, J.

The fibres morphology and biometry changes with the type of raw-material and the mechanical and enzymatic processes are presented in table 1 and table 2.

Table 1. Biometry of different raw materials and mechanical and enzymatic operations

	Hardwood Fibre	Softwood Fibre	Softwood Fibre + Enzymatic treatment	Softwood Fibre + Mechanical treatment (4000 rev. PFI)	Softwood Fibre + Enzymatic + Mechanical treatment (4000 rev. PFI)
Fibres (million/g)	21,269 ±0,010	4,742 ±0,538	5,542 ±0,265	6,714 ±0,058	6,704 ±0,067
Length weighted in length (mm)	0,793 ±0,003	1,858 ±0,047	1,889 ±0,052	1,693 ±0,026	1,745 ±0,009
Width (µm)	19,3±0,1	30,1±0,2	30,6±0,4	32,3±0,3	32,2±0,1
Coarseness (mg/100 m)	0,0692 ±0,0002	0,2052 ±0,0323	0,1692 ±0,0065	0,1581 ±0,0021	0,1509 ±0,0017
Fine elements (% in length)	36,8±0,2	24,4±21,3	37,9±1,7	42,7±2,2	37,8±1,5

Table 2. Characterization of different raw materials and mechanical and enzymatic operations

	Hardwood Fibre	Softwood Fibre	Softwood Fibre + Enzymatic treatment	Softwood Fibre + Mechanical treatment (4000 rev. PFI)	Softwood Fibre+ Enzymatic+ Mechanical treatment (4000 rev. PFI)	Softwood Fibre + Microcrystalline cellulose+ Chitosan
Porosity (%)	84,710 ±1,96	90,376 ±1,22	86,847 ±2,1	72,926 ±19,46	80,736 ±4,19	81,964 ±0,45
Tissue Thickness (µm)	135,378 ±43,46	138,854 ±0,18	146,462 ±0,031	91,710 ±38,195	93,919 ±32,00	230,800 ±7,085
Sheet Density (g/cm³)	0,229 ±0,039	0,144 ±19,64	0,197 ±64,662	0,406 ±0,291	0,289 ±0,063	0,271 ±0,006
Bulk (cm³/g)	4,432 ±0,58	7,066 ±1,15	5,181 ±0,72	2,945 ±0,921	3,593 ±0,64	3,698 ±0,091
Grammage (g/m²)	31,845 ±13,24	20,080 ±4,06	30,583 ±19,15	36,220 ±24,19	28,815 ±17,48	62,404 ±0,56

To identify the components of *Mentha piperita* essential oil, a Gas Chromatography–Mass Spectrometry (GC-MS) analysis was performed. The results (table 3 and fig.2) indicate that the major component is menthol (35.31%).

Table 3. a) Relative chemical composition (%) of *Mentha piperita L.* essential oil b) Menthol Molecular structure in 2D and 3D. Molecules made using ChemDraw ® Professional 16.0 by Moreira, J.

a)

Compound	RI	%
β-pinene	978	1,0
Limonene	1030	2,0
1,8-Cineole	1032	5,5
Menthone	1151	20,8
Menthofuran	1164	7,3
Neomenthol	1167	3,2
Menthol	1177	35,3
Terpinen-4-ol	1177	1,3
Pulegone	1234	1,7
Menthyl acetate	1296	7,1
β-Caryophyllene	1420	2,9
Germacrene D	1481	2,0

b)

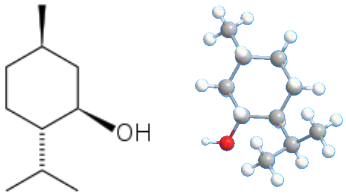

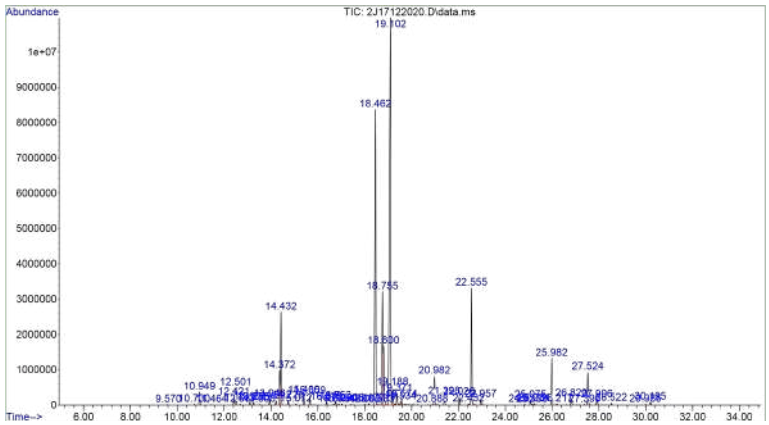

Fig. 2. Chromatogram representing the relative chemical composition (%) of *Mentha piperita L.* essential oil

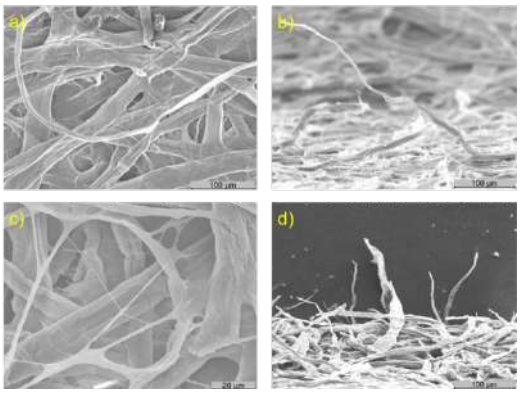

Fig. 3. SEM image of the structures of cellulose that went through enzymatic and mechanical treatment, where it can be visualized (a) how the cellulose fibres deposit (magnification of x300), (b) fibrilization of the fibre (magnification of x300), (c) diversity of pore dimensions (magnification of x1000) and (d) fibre in a z axis (magnification of x300).

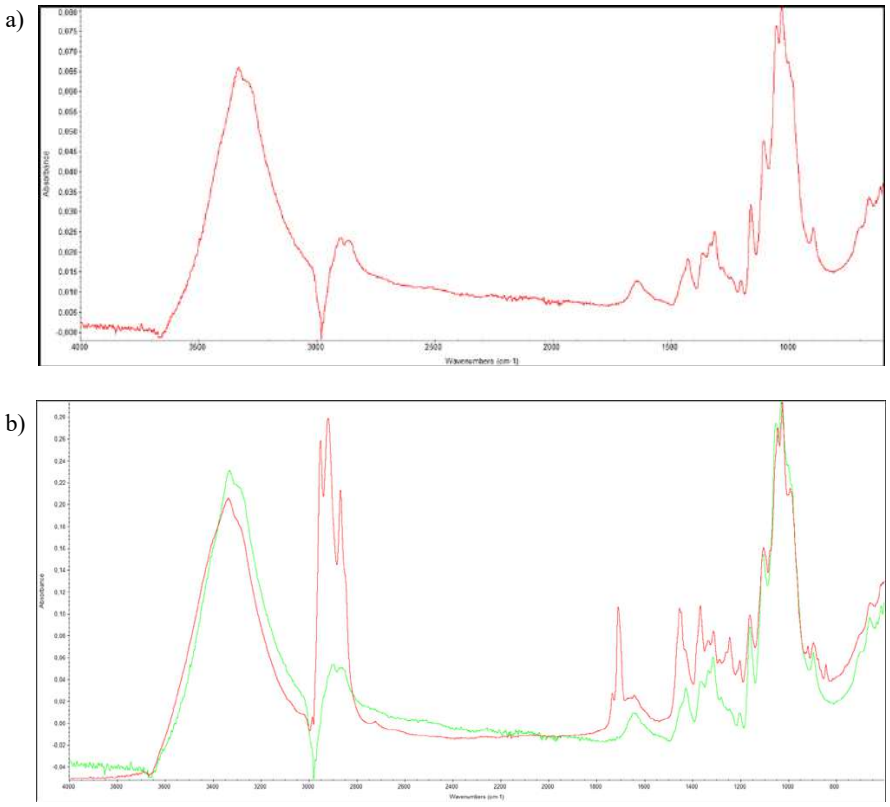

Fig. 4. a) FTIR-ATR spectrum of fibrous matrix without essential oil **b)** FTIR-ATR spectrum of fibre refined containing *Mentha piperita L.* essential oil (red) compared with the fibrous matrix without essential oil (Green).

With this result, we can conclude that after nine months there's still some molecules of peppermint essential oil in the structure, due to the wavelength interval within 2700-3000 cm $^{-1}$.

The results indicate that *Mentha piperita* active molecules are retained in the cellulose fibres porous structure.

Conclusions

A 3D cellulose fibres matrix was used to make a biodegradable *Mentha piperita* Delivery System, suitable for dermic application. With the mechanic and enzymatic treatment is it possible to see many changes, including in porosity and bulk. With SEM images it was possible to visualize the

pore diversity that is present in every structure and also the fibrilization of cellulose fibres that occur with mechanical and enzymatical treatment. FTIR-ATR results indicate that the peppermint essential oil is retained in the fibrous structure, as is possible to visualize the peak in the wavelength 2700-3000 cm $^{-1}$ that represent the OH groups, since the main component of the essential oil is menthol.

References

[1] Lavoine, N., Desloges, I., Dufresne, A., and Bras, J. (2012). Microfibrillated cellulose - Its barrier properties and applications in cellulosic materials: A review. *Carbohydrate Polymers*, *90*(2), 735–764. https://doi.org/10.1016/j.carbpol.2012.05.026

[2] Jorfi, M., and Foster, E. J. (2015). Recent advances in nanocellulose for biomedical applications. *Journal of Applied Polymer Science*, *132*(14), 1–19. https://doi.org/10.1002/app.41719

[3] Abeer, M. M., Mohd Amin, M. C. I., and Martin, C. (2014). A review of bacterial cellulose-based drug delivery systems: Their biochemistry, current approaches and future prospects. *Journal of Pharmacy and Pharmacology*, *66*(8), 1047–1061. https://doi.org/10.1111/jphp.12234

[4] Abitbol, T., Rivkin, A., Cao, Y., Nevo, Y., Abraham, E., Ben-Shalom,T., Lapidot, S., and Shoseyov, O. (2016). Nanocellulose, a tiny fiber with huge applications. *Current Opinion in Biotechnology*, *39*(I), 76–88. https://doi.org/10.1016/j.copbio.2016.01.002

[5] Arias, M., López, A., Vilaseca, M., Vallès, B., Prieto, R., Simó, M., Valle, J., Valle, R., Bezerra, F. and Bellalta, J. (2021). Influence of Chitosan Characteristics in the Microencapsulation of Essential Oils. *Journal of Biomedical Science and Engineering*, 14, 119-129. https://doi.org/10.4236/jbise.2021.143012.

[6] Klimek-Szczykutowicz, M., Szopa, A., and Ekiert, H. (2020). Citrus limon (Lemon) phenomenon—a review of the chemistry, pharmacological properties, applications in the modern pharmaceutical, food, and cosmetics industries, and biotechnological studies. *Plants*, *9*(1). https://doi.org/10.3390/plants9010119

[7] Pavoni, L., Perinelli, D. R., Bonacucina, G., Cespi, M., and Palmieri, G. F. (2020). An Overview of Micro- and Nanoemulsions as Vehicles for Essential Oils: Formulation, Preparation and Stability. Nanomaterials, 10(1), 135. https://doi.org/10.3390/nano10010135

[8] Mutlu-Ingok, A., Devecioglu, D., Dikmetas, D. N., Karbancioglu-Guler, F., and Capanoglu, E. (2020). Antibacterial, antifungal, antimycotoxigenic, and antioxidant activities of essential oils: an updated review. Molecules, 25(20). https://doi.org/10.3390/molecules25204711

[9] Turek, C., and Stintzing, F. C. (2013). Stability of essential oils: A review. Comprehensive Reviews in Food Science and Food Safety, 12(1), 40–53. https://doi.org/10.1111/1541-4337.12006

[10] Angioni, A., Barra, A., Coroneo, V., Dessi, S., and Cabras, P. (2006). Chemical composition, seasonal variability, and antifungal activity of *Lavandula stoechas* L. ssp. *stoechas* essential oils from stem/leaves and flowers. Journal of agricultural and food chemistry, 54(12), 4364–4370. https://doi.org/10.1021/jf0603329

[11] Baptista-Silva, S., Borges, S., Ramos, O. L., Pintado, M., and Sarmento, B. (2020). The progress of essential oils as potential therapeutic agents: a review. *Journal of Essential Oil Research*, *32*(4), 279–295. https://doi.org/10.1080/10412905.2020.1746698

[12] Shaaban, H. A. E., El-Ghorab, A. H., and Shibamoto, T. (2012). Bioactivity of essential oils and their volatile aroma components: Review. *Journal of Essential Oil Research*, *24*(2), 203–212. https://doi.org/10.1080/10412905.2012.659528

[13] Morais, F.M., Simões R.M.S, Curto, J.M., (2020). "Biopolymeric Delivery Systems for Cosmetic Applications Using *Chlorella vulgaris Algae* and Tea Tree Essential Oil", *Polymers*, 12(11). https://doi.org/10.3390/polym12112689

[14] Morais, F.P., Carta, A.M.M.S., Amaral, M.E., Curto, J.M.R. Micro/nano-fibrillated cellulose (MFC/NFC) fibers as an additive to maximize eucalyptus fibers on tissue paper production. *Cellulose,* 28**,** 6587–6605 (2021). https://doi.org/10.1007/s10570-021-03912-9

[15] Morais, F.P., Carta, A.M.M.S., Amaral, M.E., Curto, J.M.R. (2021) Cellulose Fiber Enzymatic Modification to Improve the Softness, Strength, and Absorption Properties of Tissue Papers. *BioResources*, 16, 846-861.

[16] Spiridon, I., Duarte, A. P., and Curto, J. (2003). Influence of xilanase treatment on *Pinus pinaster* kraft pulp. *Cellulose chemistry and technology*, (37 (3-4))

[17] Mota, A.S., Rosário Martins, M., Arantes, S., Lopes, V.R., Bettencourt, E., Pombal, S., Gomes, A.C., Silva, L.A., (2015) Antimicrobial activity and chemical composition of the essential oils of Portuguese *Foeniculum vulgare* fruits, *Natural Product Communications*, 10 (4) 673-676.

[18] Morais F.P., Carta A.M.M.S, Amaral M.E., Curto J.M.R. (2020) 3D Fiber Models to Simulate and Optimize Tissue Materials. *BioResources* 15, 8833-8848

[19] Curto, J.M.R., Conceição, E.L.T., Portugal, A.T.G., and Simões, R.M.S. (2011). Three-dimensional modelling of fibrous materials and experimental validation. *Materialwissenschaft Und Werkstofftechnik*, 42(5), 370–374. https://doi.org/10.1002/mawe.201100790.

DEVELOPMENT OF DERMIC APPLICATION SYSTEMS MADE FROM MICRO/NANO CELLULOSE BIOPOLYMERIC MATERIALS WITH 3D POROSITY SIMULATION TO OPTIMIZE THE RETENTION AND RELEASE OF ESSENTIAL OILS BIOMOLECULES

Joana Moreira [1], Joana Curto[1,2]

1 Fiber Materials and Environmental Technologies Research Unit (FibEnTech-UBI), Dep. Química, Faculdade de Ciências, Universidade da Beira Interior

2 CIEPQPF, Departamento de Engenharia Química, FCTUC, Universidade de Coimbra

Resumo

Num mundo em mudança, onde a preocupação com o meio ambiente está a aumentar, a procura por produtos biodegradáveis e biocompatíveis aumenta. Alguns desses produtos com essas características são as fibras de celulose e os óleos essenciais, pois são biodegradáveis, biocompatíveis e os óleos essenciais possuem efeito terapêutico.

Devido à alta volatilidade dos óleos essenciais, a aplicação cutânea na forma de máscaras com capacidade de armazenar moléculas terapêuticas prolonga seu período de ação, o que é uma vantagem. Nesse sentido, o objetivo deste projeto é criar uma máscara facial cosmética feita de micro/nano celulose modificada utilizando uma combinação de processos químicos, mecânicos e enzimáticos para atingir a porosidade, resistência e suavidade pretendidas.

As fibras de celulose em microescala conferem resistência e estabilidade, enquanto as fibras de celulose em nanoescala contribuem para a criação de uma estrutura com alto grau de retenção e estabilidade de moléculas terapêuticas.

As propriedades terapêuticas da matriz celulósica produzida foi obtida pela adição de óleo essencial de *Mentha piperita* (Hortelã-pimenta) à estrutura porosa. Este foi adicionado por um processo de emulsão, para proteger as moléculas do óleo essencial da oxidação e retardar a sua libertação, garantindo que a mesma seja controlada.

As fibras de celulose, e a matriz por elas formadas, foram caracterizadas morfologicamente por Microscopia Eletrónica de Varrimento. Foi realizada a simulação computacional em 3D das estruturas moleculares e das matrizes porosas.

Além disso, o uso de um simulador computacional validado permite otimizar a porosidade, tamanho e distribuição dos poros e, assim, atingir a cinética de liberação desejada.

Palavras-chave: Óleo essencial e extrato de *Mentha piperita*, micro/nanocelulose, materiais fibrosos, *drug delivery systems*

VIII Ciclo de Conferências da Faculdade de Ciências
Escola e Universidade
29 e 24 setembro 2022
O novo amanhã

Development of dermic application systems made from micro/nano cellulose biopolymeric materials with 3D porosity simulation to optimize the retention and release of essential oils biomolecules

Joana Moreira [1] (joana.maria.moreira@ubi.pt)
Joana Curto [1,2] (joana.curto@ubi.pt)
1 Fiber Materials and Environmental Technologies Research Unit (FibEnTech-UBI), Dep. Química, Faculdade de Ciências, Universidade da Beira Interior
2 CIEPQPF, Departamento de Engenharia Química, FCTUC, Universidade de Coimbra
FACULDADE CIÊNCIAS
Departamento de Química

Introduction

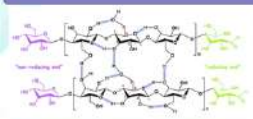

Fig 1. Schematic representation of the chemical structure and intra- and inter-molecular hydrogen bonds in crystalline cellulose (Adapted from Lin and Dufresne 2014)

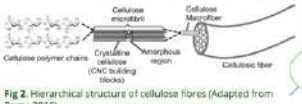

Fig 2. Hierarchical structure of cellulose fibres (Adapted from Parry, 2016)

Cellulose:

- Obtained from plants
- Biopolymer constituted by glucose monomers
- Sustainable
- Biodegradable
- Safe

Micro Cellulose	Nano Cellulose
Obtained by mechanical treatment	Obtained by mechanical and enzymatic treatment
High specific surface area	Retention capacity
High strength	Control of porosity
Biodegradability	

→ Optimized structures

Characteristics/properties:

- Antibacterial;
- Antifungal;
- Anti-inflammatory;
- Antioxidant;
- Wound healing properties (or scab properties);
- Hypotensive/ antidepressant.

Methodology

Enzymatic treatment — Fibrous Structure formation: nano and microfiber — SEM porosity, fiber and pore dimension and distribution

Emulsion containing sunflower oil and the bioactive molecule — Prototype Manufacturing containing biomolecule — Computational Simulation: Computational model developed and implemented in Matlab®

Results

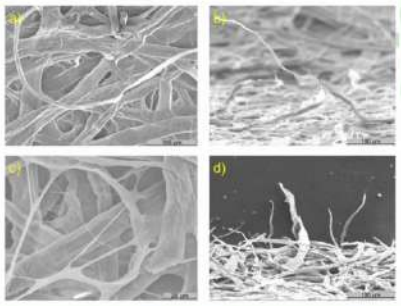

Fig. 3. SEM image of the structures of cellulose that went through enzymatic and mechanical treatment, where it can be visualized (a) how the cellulose fibres deposit (magnification of x300), (b) fibrilization of the fibre (magnification of x300), (c) diversity of pore dimensions (magnification of x1000) and (d) fibre in a z axis (magnification of x300).

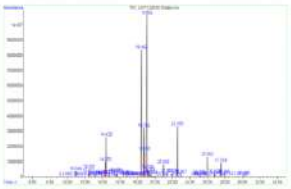

Fig 4. Chromatogram representing the relative chemical composition (%) of *Mentha piperita L.* essential oil

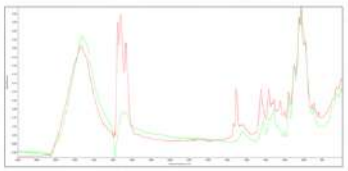

Fig 5. FTIR-ATR spectrum of fibre refined containing Mentha piperita L. essential oil (red) compared with the fibrous matrix without essential oil (Green).

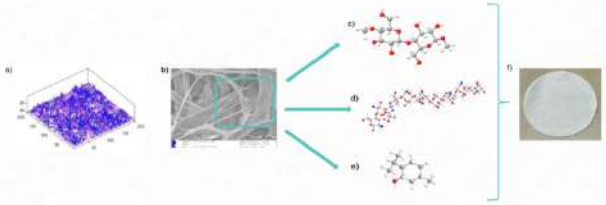

Fig 7. Visual representation of the DDS structural hierarchy. a) Structures obtained by Computational Simulation, representing fibers at the end of their deposition, b) SEM image of the fibrous matrix, c) cellulose, d) chitosan, e) menthol and f) laboratory DDS. Molecules made using ChemDraw ® Professional 16.0 by Moreira, J. Model and computational Simulation by Curto, J.

Conclusions

- The masks prototype produced present optimized properties of strength, smoothness, stability, and retention of the therapeutic molecules.
- The distribution of the pore size has an impact on the essential oil molecules retention and release kinetics.
- The optimization of the pore dimension and the 3D porous network using computational simulation was able to achieve the optimum porosity faster, saving experimental resources.
- The use of porous biocompatible and biodegradable materials using MC and NC for dermal application is a promising research topic for improving the delivery of biomolecules.
- FTIR-ATR results indicate that the peppermint essential oil is retained in the fibrous structure, due to the peak in the wavelength 2700-3000 cm -1 due to the OH groups, since the main component of the essential oil is menthol.

References

[1]Bourbon, A.I.; Pereira, R.N.; Pastrana, L.M.; Vicente, A.A.; Cerqueira, M.A.(2019) "Protein-Based Nanostructures for Food Applications", Gels, 5, 9. https://doi.org/10.3390/gels5010009
[2] Curto, J. M. R., Conceição, E. L. T., Portugal, a. T. G., & Simões, R. M. S. (2011). "Three-dimensional modelling of fibrous materials and experimental validation." Materialwissenschaft Und Werkstofftechnik, 42(5), 370–374. https://doi.org/10.1002/mawe.201100790
[3] Morais, F. P., Carta, A. M., Amaral, M. E., & Curto, J. M. (2021). "Micro/nano-fibrillated cellulose (MFC/NFC) fibers as an additive to maximize eucalyptus fibers on tissue paper production". Cellulose, 1-19.
[4] Morais, F. M., Simões R. M. S, Curto, J. M., (2020). "Biopolymeric Delivery Systems for Cosmetic Applications Using Chlorella vulgaris Algae and Tea Tree Essential Oil", Polymers, 12(11). https://doi.org/10.3390/polym12112689
[5] Morais, F.P.; Curto, J.M.R. Design and Engineering of Natural Cellulose Fiber-Based Biomaterials with Eucalyptus Essential Oil Retention to Replace Non-Biodegradable Delivery Systems. *Polymers* **2022**, *14*, 3621. https://doi.org/10.3390/polym14173621
[6] Moreira, J., Lopes, C., Lis Arias, M.J., Silva, L., Curto, J.M.R. (2021). Development of Biodegradable, Cellulose-Based, Essential Oil and Chitosan Drug Delivery Systems for Cosmetic Mask Applications . In *Proceedings of the 1st International FibEnTech Congress - New opportunities for fibrous materials in the ecological transition*, Online Conference, 9-10 December 2021, *KnE Materials Science*. https://doi.org/10.18502/5
[7] Soiridon, I., Duarte, A. P., and Curto, J. (2003)." Influence of xilanase treatment on Pinus pinaster kraft pulp". Cellulose chemistry and technology, (37 (3-4)).


Certificado
Prémio para o melhor poster
VIII Ciclo de Conferências
da Faculdade de Ciências
Escola e Universidade
FACULDADE CIÊNCIAS
A Faculdade de Ciências da Universidade da Beira Interior certifica que
Joana Moreira e Joana Cunto
obtiveram o Prémio para o melhor poster com a comunicação intitulada
"Development of dermic application systems made from micro/nano cellulose biopolymeric materials with 3D porosity simulation to optimize the retention and release of essential oils biomolecules"
no V Ciclo de Conferências da Faculdade de Ciências, subordinadas ao tema Ensino Pós-pandemia - O novo amanhã.
realizado nos dias 23 e 24 de setembro de 2022
O Presidente da Faculdade de Ciências
Paulo Jorge da Silva Almeida

FibEnTech

FACULDADE CIÊNCIAS
Departamento de Química

ENCONTRO COM A CIÊNCIA E TECNOLOGIA EM PORTUGAL
16-18 maio

Drug Delivery Systems (DDS) for oral and dermic applications using Cannabis fibres and Essential Oils

Paulo Saraiva[1], Joana Moreira[1], Catarina Lopes[1], Lúcia Silva[1], Joana Curto[1],*
[1]FibEnTech-UBI, Fiber Materials and Environmental Technologies Research Unit, Chemistry Dep., UBI
*Corresponding author: joana.curto@ubi.pt

Abstract

The purpose of this study was to develop innovative biopolymeric Drug Delivery Systems (DDS) containing a 3D nano cellulose-based matrix to retain active molecules. Two main types of DDS were investigated for oral therapy and dermic applications. For oral therapy the DDS were made using Cannabis fibres to reinforce the 3D nano/micro cellulose matrix. For dermic application the active molecules from Mentha piperita L essential oil were chosen and assembled using an oil in water emulsion. To improve the DDS cellulose-based matrix porosity and strength properties the optimization was carried out trough 3D computational simulation studies. The results showed that the drug delivery systems are able to retain the active molecules under different pH conditions.

Introduction

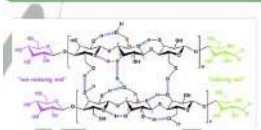

Fig 1. Schematic representation of the chemical structure and intra- and inter-molecular hydrogen bonds in crystalline cellulose (Adapted from Lin and Dufresne 2014)

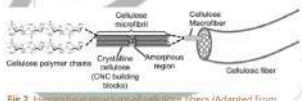

Fig 2. Hierarchical structure of cellulose fibers (Adapted from Parry, 2016)

Micro/nano Cellulose :

- Obtained from plants
- Biopolymer constituted by glucose monomers
- Sustainable
- Biodegradable
- Safe

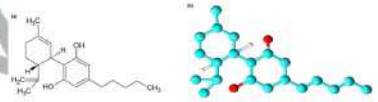

Fig 3. Molecular structure of cannabinoid CBD, in 2D (a) and in 3D (b) (elaborated in ChemSketch software)

Methodology

Enzymatic treatment

Fibrous Structure formation: nano and microfiber

SEM porosity, fiber and pore dimension and distribution

Emulsion containing sunflower oil and the bioactive molecule

Prototype Manufacturing containing biomolecule

Computational Simulation
Computational model developed and implemented in Matlab®

Results

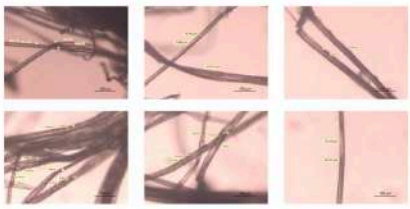

Fig 4. Microscopic images of Cannabis fibres obtained from a combination of alkaline and hydrogen peroxide delignification processes (images analysis obtained by LAS X software)

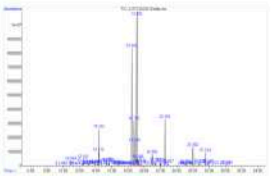

Fig. 5. Chromatogram representing the relative chemical composition of *Mentha piperita L.* essential oil molecules, obtained by GC-MS [9]

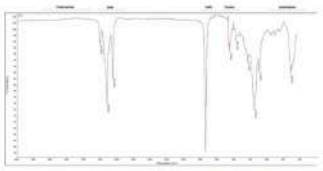

Fig. 6. FTIR-ATR spectrum of a sample of cannabis oil

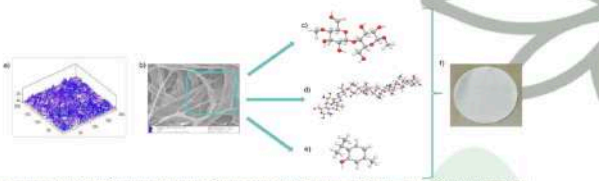

Fig. 7. Visual representation of the DDS structural hierarchy. a) Structures obtained by Computational Simulation of the 3D cellulose-based fibre matrix (7, 9) b) SEM image of the fibrous matrix, c) cellulose, d) chitosan, e) menthol and f) laboratory made DDS for dermic applications.

Conclusions

A 3D cellulose-based matrix was tailor-made for oral and dermic therapeutic applications using a combination of experimental and computational methodology.
The results indicate that after optimization the DDS for oral therapy using Cannabis fibres are able to retain the active molecules under different pH conditions and that the DDS for dermic applications are able to retain and the active molecules from Mentha piperita L essential oil, and to maintain their stability during a period of time compatible to their application.

References

[1] Morais, F.M., Simões R.M.S, Curto, J.M., (2020). "Biopolymeric Delivery Systems for Cosmetic Applications Using Chlorella vulgaris Algae and Tea Tree Essential Oil", Polymers, 12(11). https://doi.org/10.3390/polym12112689
[2] Morais, F.P., Carta, A.M.M.S., Amaral, M.E., Curto, J.M.R. (2021). Micro/nano-fibrillated cellulose (MFC/NFC) fibers as an additive to maximize eucalyptus fibers on tissue paper production. Cellulose, 28, 6587–6605. https://doi.org/10.1007/s10570-021-03912-9
[3] Morais, F.P., Carta, A.M.M.S., Amaral, M.E., Curto, J.M.R. (2021). Cellulose Fiber Enzymatic Modification to Improve the Softness, Strength, and Absorption Properties of Tissue Papers. BioResources, 16, 846-861.
[4] Spiridon, I., Duarte, A. P., Curto, J. (2003). Influence of xilanase treatment on Pinus pinaster kraft pulp. Cellulose chemistry and technology, (37 (3-4))
[5] Arias, M., López, A., Vilaseca, M., Vallès, B., Prieto, R., Simó, M., Valle, J., Valle, R., Bezerra, F., Bellalta, J. (2021). Influence of Chitosan Characteristics in the Microencapsulation of Essential Oils. Journal of Biomedical Science and Engineering, 14, 119-129. https://doi.org/10.4236/jbise.2021.143012.
[6] Mota, A.S., Rosário Martins, M., Arantes, S., Lopes, V.R., Bettencourt, E., Pombal, S., Gomes, A.C., Silva, L.A., (2015). Antimicrobial activity and chemical composition of the essential oils of Portuguese Foeniculum vulgare fruits, Natural Product Communications, 10 (4) 673-676.
[7] Curto, J.M.R., Conceição, E.L.T., Portugal, A.T.G., Simões, R.M.S. (2011). Three-dimensional modelling of fibrous materials and experimental validation. Materialwissenschaft Und Werkstofftechnik, 42(5), 370–374. https://doi.org/10.1002/mawe.201100790.
[8] Morais F.P., Carta A.M.M.S, Amaral M.E., Curto J.M.R. (2020). 3D Fiber Models to Simulate and Optimize Tissue Materials. BioResources 15, 8833-8848
[9] Moreira, J., Lopes, C., Lis Arias, M.J., Silva, L., Curto, J.M.R. (2021). Development of Biodegradable, Cellulose-Based, Essential Oil and Chitosan Drug Delivery Systems for Cosmetic Mask Applications . In *Proceedings of the 1st International FibEnTech Congress - New opportunities for fibrous materials in the ecological transition*, Online Conference, 9-10 December 2021, *KnE Materials Science*. https://doi.org/10.18502/5
[10] – Zhu, J.Y., Agarwal, U.P., Ciesielski, P.N., Himmel, M.E., Gao, R., Deng, Y., Morits, M., Österberg, M. (2021). Towards sustainable production and utilization of plant-biomass-based nanomaterials: a review and analysis of recent developments. Biotechnology for Biofuels .14, 114. https://doi.org/10.1186/s13068-021-01963-5

FibEnTech

VII Ciclo de Conferências
Escola e Universidade
24 e 25 set 2021

Development of dermic application systems made from micro/nano cellulose biopolymeric materials with 3D porosity simulation to optimize the retention and release of essential oils biomolecules

Joana Moreira [1] (joana.maria.moreira@ubi.pt)
Joana Curto [1,2] (joana.curto@ubi.pt)

1 FibEnTech, Departamento de Química, Faculdade de Ciências, Universidade da Beira Interior
2 CIEPQPF, Departamento de Engenharia Química, FCTUC, Universidade de Coimbra

FACULDADE CIÊNCIAS
Departamento de Química

Introduction

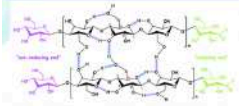

Fig 1 . Schematic representation of the chemical structure and intra- and inter-molecular hydrogen bonds in crystalline cellulose (Adapted from Lin and Dufresne 2014)

Cellulose :

- Obtained from plants
- Biopolymer constituted by glucose monomers
- Sustainable
- Biodegradable
- Safe

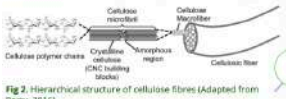

Fig 2. Hierarchical structure of cellulose fibres (Adapted from Parry, 2016)

Micro Cellulose	Nano Cellulose	
Obtained by mechanical treatment	Obtained by mechanical and enzymatic treatment	Optimized structures
High specific surface area	Retention capacity	
High strength	Control of porosity	
Biodegradability		

Characteristics/properties:

- Antibacterial;
- Antifungal;
- Anti-inflammatory;
- Antioxidant;
- Wound healing properties (or scab properties);
- Hypotensive/ antidepressant.

Results

Fig 3. SEM images of the cellulose fiber structure containing. Magnification of x500 (a) and x1000 (b).

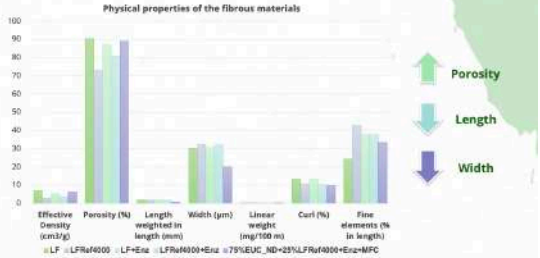

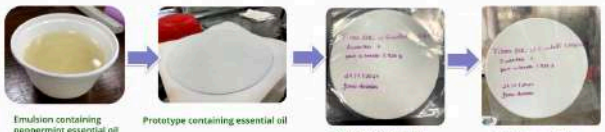

Emulsion containing peppermint essential oil and extract

Prototype containing essential oil

Prototype containing peppermint essential oil. Picture taken on Jan 21st, 2021

Prototype containing peppermint essential oil. Picture taken on Jun 22nd, 2021

Methodology

Enzymatic treatment

Fibrous Structure formation: nano and microfiber

SEM porosity, fiber and pore dimension and distribution

Emulsion containing sunflower oil and the bioactive molecule

Prototype Manufacturing containing biomolecule

Computational Simulation Computational model developed and implemented in Matlab®

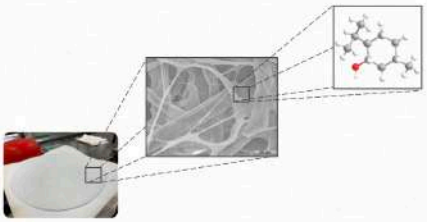

Fig 4. Facial mask structural hierarchy : Fiber and 3D molecule of ***Mentha piperita*** essential oil.

Conclusions

- The masks prototype produced present optimized properties of strength, smoothness, stability, and retention of the therapeutic molecules.
- The distribution of the pore size has an impact on the essential oil molecules retention and release kinetics.
- The optimization of the pore dimension and the 3D porous network using computational simulation was able to achieve the optimum porosity faster, saving experimental resources.
- The use of porous biocompatible and biodegradable materials using MC and NC for dermal application is a promising research topic for improving the delivery of biomolecules.

References

Bourbon, A.I.; Pereira, R.N.; Pastrana, L.M.; Vicente, A.A.; Cerqueira, M.A.(2019) "Protein-Based Nanostructures for Food Applications". Gels, 5, 9. https://doi.org/10.3390/gels5010009

Curto, J. M. R., Conceição, E. L. T., Portugal, a. T. G., & Simões, R. M. S. (2011). "Three-dimensional modelling of fibrous materials and experimental validation." Materialwissenschaft Und Werkstofftechnik, 42(5), 370–374. https://doi.org/10.1002/mawe.201100790

Morais, F. P., Carta, A. M., Amaral, M. E., & Curto, J. M. (2021). "Micro/nano-fibrillated cellulose (MFC/NFC) fibers as an additive to maximize eucalyptus fibers on tissue paper production". Cellulose, 1-19.

Morais, F. M., Simões R. M. S, Curto, J. M., (2020). "Biopolymeric Delivery Systems for Cosmetic Applications Using Chlorella vulgaris Algae and Tea Tree Essential Oil", Polymers, 12(11). https://doi.org/10.3390/polym12112689

Spiridon, I., Duarte, A. P., & Curto, J. (2003)." Influence of xilanase treatment on Pinus pinaster kraft pulp". Cellulose chemistry and technology, (37 (3-4)).

Appendix B. Data obtained regarding the different types of cellulosic structures subjected to mechanical treatments

B1. Characterization of cellulosic structures using mechanical treatment

Table B. 1 - Structure characterization of softwood fibers refined

	SW	***SW_Ref 500***	***SW_Ref 1000***	***SW_Ref 1500***	***SW_Ref 2000***	***SW_Ref 3000***	***SW_Ref 4000***	***SW_Ref 6000***
Weight (g)	0,429 ±0,088	0,416 ±0,049	0,436 ±0,042	0,424 ±0,110	0,409 ±0,049	0,682 ±0,424	0,774 ±0,517	0,699 ±0,448
Area (m^2)	0,02138 ±0	0,02138 ±0	0,02138 ±0	0,02138 ±0	0,02138 ±0	0,02138 ±0	0,02138 ±0	0,02138 ±0
Grammage (g/m^2)	20,080 ±4,098	19,459 ±2,312	20,371 ±1,976	19,842 ±5,156	19,135 ±2,272	31,910 ±19,837	36,220 ±24,191	32,716 ±20,968
Tissue Thickness (mm)	0,139 ±0,020	0,125 ±0,012	0,127 ±0,016	0,128 ±0,022	0,120 ±0,016	0,113 ±0,045	0,092 ±0,038	0,097 ±0,032
Tissue Thickness (µm)	138,854 ±19,638	124,6 ±12,276	126,867 ±16,058	128,176 ±28,058	120,083 ±15,732	113,483 ±44,523	91,710 ±38,195	96,857 ±32,230
Bulk (cm^3/g)	7,066 ±1,147	6,474 ±0,873	6,268 ±0,916	6,533 ±1,106	6,338 ±1,003	4,012 ±0,802	2,945 ±0,921	3,440 ±0,835
Structure Density (g/cm^3)	0,144 ±0,018	0,157 ±0,018	0,162 ±0,019	0,156 ±0,020	0,160 ±0,017	0,261 ±0,062	0,406 ±0,292	0,312 ±0,091
Density/1,5	0,096 ±0,012	0,105 ±0,012	0,108 ±0,013	0,104 ±0,013	0,107 ±0,012	0,174 ±0,042	0,271 ±0,195	0,208 ±0,061
Porosity	0,904 ±0,012	0,895 ±0,012	0,892 ±0,013	0,896 ±0,013	0,893±0,012	0,826 ±0,042	0,729 ±0,195	0,792 ±0,061
Porosity (%)	90,376 ±1,216	89,548±1,206	89,188 ±1,261	89,579 ±1,342	89,306±1,165	82,589 ±4,160	72,926 ±19,463	79,217 ±6,071

Values reported are the mean ± standard deviations.

B2. Structure Characterization of Assays containing mixtures of Mechanical and enzymatical treatment

Table B. 2 - Description of the assays containing the different fiber mixtures

Assay Number	Assay Description
1	75%HW+25%SW_Ref4000+Enz+Biopolymer+MFC
2	75%HW+25%SW_Ref4000+Enz+Biopolymer
3	75%HW+25%SW_Ref4000+Enz+MFC
4	75%HW+25%SW_Ref4000+Enz
5	90%HW+10%SW_Ref4000+Enz+Biopolymer+MFC
6	90%HW+10%SW_Ref4000+Enz+Biopolymer
7	90%HW+10%SW_Ref4000+Enz+MFC
8	90%HW+10%SW_Ref4000+Enz
9	SW_Ref4000+Enz
10	SW+Enz

Table B. 3 - Structure characterization results for the assays containing various fiber mixtures

	1	*2*	*3*	*4*	*5*	*6*	*7*	*9*	*10*
Weight (g)	0,507 ±0,229	0,4884 ±0,277	0,471 ±0,217	0,391 ±0,031	0,365 ±0,030	0,417 ±0,043	0,423 ±0,050	0,616 ±0,374	0,654 ±0,410
Area (m^2)	0,02138 ±0	0,02138 ±0	0,02138 ±0	0,02138 ±0	0,02138 ±0	0,02138 ±0	0,02138 ±0	0,02138 ±0	0,02138 ±0
Grammage (g/m^2)	23,692 ±10,693	22,836 ±12,978	22,022 ±10,141	18,310 ±1,455	17,091 ±1,412	19,515 ±2,024	19,772 ±2,322	28,815 ±17,476	30,583 ±19,155
Tissue Thickness (mm)	0,131 ±0,036	0,128 ±0,051	0,128 ±0,034	0,113 ±0,009	0,116 ±0,009	0,146 ±0,017	0,110 ±0,010	0,094± 0,032	0,146 ±0,065
Tissue Thickness (µm)	131,358 ±36,225	127,564 ±51,189	128,426 ±33,838	112,894 ±9,421	115,878 ±8,738	146,452 ±17,101	110,160 ±9,642	93,919± 32,000	146,462 ±64,663
Bulk (cm^3/g)	5,736 ±0,681	5,852 ±0,757	6,077 ±0,769	6,178 ±0,413	6,804 ±0,536	7,520 ±0,687	5,601 ±0,458	3,593 ±0,636	5,181 ±0,723
Structure Density (g/cm^3)	0,177 ±0,022	0,174 ±0,025	0,167 ±0,024	0,163 ±0,011	0,148 ±0,011	0,134 ±0,012	0,180 ±0,015	0,289 ±0,063	0,197 ±0,032
Density/1,5	0,118 ±0,015	0,116 ±0,017	0,112 ±0,016	0,108 ±0,007	0,099 ±0,008	0,089 ±0,008	0,120 ±0,010	0,193 ±0,042	0,132 ±0,021
Porosity	0,882 ±0,015	0,884 ±0,017	0,888 ±0,016	0,892 ±0,007	0,901 ±0,008	0,911 ±0,008	0,880 ±0,010	0,807 ±0,042	0,868 ±0,021
Porosity (%)	88,212 ±1,481	88,403 ±1,669	88,837 ±1,606	89,163 ±0,711	90,144 ±0,754	91,066 ±0,782	88,017 ±1,031	80,736 ±4,194	86,847 ±2,120

Values reported are the mean ± standard deviations.

B3. Characterization of bleached cellulosic fiber structures using mechanical treatment

Table B. 4 - Structure characterization of bleached softwood fibers refined

	SW_Ref_2500	*SW_Ref_4500*	*SW_Ref_7500*
Weight (g)	1,348±0,0084	1,353±0,012	1,343±0,0118
Area (m^2)	0,02138±3,657E-18	0,02138±3,657E-18	0,02138±3,657E-18
Grammage (g/m^2)	63,059±0,392	63,293±0,552	62,816±0,556
Tissue Thickness(mm)	0,1437±0,0060	0,1001±0,0014	0,0768±0,0023
Tissue Thickness (µm)	143,7±5,964	100,1±1,370	76,8±2,348
Bulk (cm^3/g)	2,2785±0,0846	1,581±0,0248	1,223±0,038
Structure Density (g/cm^3)	0,439±0,016	0,6324±0,0099	0,819±0,025
Density/1,5	0,293±0,0107	0,4216±0,0067	0,546±0,017
Porosity	0,707±0,0107	0,578±0,0067	0,454±0,0168
Porosity (%)	70,705±1,0745	57,840±0,666	45,428±1,680

Values reported are the mean ± standard deviations.

B4. Characterization of unbleached cellulosic fiber structures using mechanical treatment

Table B. 5 - Structure characterization of bleached softwood fibers refined

	NSW_Ref_2500	*NSW_Ref_4500*	*NSW_Ref_7500*
Weight (g)	1,353±0,0229	1,383±0,0568	1,344±0,0449
Area (m^2)	0,02138±0	0,02138±0	0,02138±0
Grammage (g/m^2)	63,265±1,070	64,682±2,656	62,839±2,099
Tissue Thickness(mm)	0,163±0,0096	0,1414±0,007	0,108±0,006
Tissue Thickness (µm)	162,6±9,617	141,4±6,995	107,8±6,033
Bulk (cm^3/g)	2,572±0,172	2,187±0,083	1,715±0,0745
Structure Density (g/cm^3)	0,390±0,0264	0,458±0,0173	0,584±0,025
Density/1,5	0,260±0,018	0,305±0,012	0,389±0,017
Porosity	0,740±0,018	0,695±0,012	0,611±0,017
Porosity (%)	73,970±1,761	69,474±1,152	61,073±1,666

Values reported are the mean ± standard deviations.

Appendix C. ISO Norms

C1. ISO 638 Standard

The sample of pulp is next sliced or torn to dimensions that are more suitable for the test, taking into consideration the goals of the investigation. When working with the pulp, one must exercise extra caution in order to prevent any changes in its moisture content. It is imperative that the cutting and weighing of samples that have been preserved in airtight containers be completed as rapidly as possible in order to limit the amount of change in humidity.

Every single one of the weights is determined with an accuracy of 0.001 grams. Put approximately 10 grams of pulp into the closed weigh-filter, which should have been dried and weighed before now. After weighing the substance, open the container, put it along with the sample and the cover in the oven, and heat it to 105 ±2°C for a sufficient amount of time so that the mass remains constant. When two successive weighings of the same specimen do not differ by more than 0.1% of the specimen's initial mass when it was in the wet state, this is taken to indicate that the mass has remained constant. The minimum amount of time that must pass for drying in between each of two successive weighings is the same as the minimum amount of time that must pass for drying initially. After the sample has been dried, the lid is placed back on the container, and it is placed back into the desiccator for a period of forty-five minutes. After the temperature difference between the interior and outside of the weight filter has been brought to the same level, the lid will immediately open and close. Perform a weight check on the filter weigher together with its contents.

C2. ISO 5263/1 Standard

Cellulosic pulp that has a dry fiber content of 20% (m/m) or above are required to be soaked in two liters of distilled water at a temperature of 20±5 degrees Celsius for the allotted amount of time. After this step, the pulps are put into a suitable disintegrator with 2 liters of water and appropriately timed revolutions. The type of pulp that is used determines the schedule for the revolutions.

After this stage, the pulps are put into an appropriate disintegrator with 2 liters of water, which in this case is the distilled water that the fiber was immersed in, and appropriately timed revolutions. The timing for the revolutions is organized according to the sort of pulp that is utilized.

C3. ISO 5269/1 Standard

Following the completion of the structures in accordance with this specification through the utilization of a structure forming, they are required to go through a pressing procedure. This method involves repeatedly stacking blotting paper with the structures that are created on a drying plate. This action is carried out multiple times. After this step, the drying plates and the structures of blotting paper that are attached to them are separated from one another and then arranged in an appropriate manner within a laboratory that has been properly conditioned. This ensures that the structures remain in contact with their respective drying plates throughout the duration of the drying process. This air-conditioned laboratory has sufficient air circulation, making it capable of preserving the same temperature (22 ºC) and humidity (50 %) across the entire space.

C4. Standard ISO 5264/2:2011 – Refining of cellulosic pulps using a PFI-mill refiner

A mechanical refining was conducted using a suitable refiner, in accordance with this ISO standard, the PFI-mill, in order to research and assess the impact of the mechanical refining process on the variation of the properties of the cellulose structures.

1. the preparation of various cellulosic pulps

The various suspensions containing cellulosic fibers were mechanically processed at three distinct revolution rates. Initial disintegration of the cellulosic pulps was performed in accordance with the ISO 5263 standard. The various disintegrating cellulosic pulps were then filtered using a Buchner funnel in accordance with the individual ISO standard, thereby obtaining an overall structure for each specific fiber.

Initial temperature adjustments for the PFI-mill and other disintegrated cellulosic pulps must not exceed 20±5 ºC. After regulating the temperature, the refiner is activated, followed by the implementation of the necessary number of revolutions.

Prior to the refining process, it is vital to consider various factors in order to carry out a correct refining, including ensuring that the Vernier screw is entirely unscrewed, and that the refiner is clean and free of cellulose pulp residues.

After achieving the necessary conditions, the various cellulosic pulps are refined by spreading the pulp uniformly over the cylinder wall so as to prevent the formation of pulp-free spaces. Then, tighten the device by screwing the Vernier screw into place.

Afterwards, simultaneously click both "Start" buttons with the correct refiner lid placement. Checking the correct placement of the lid by carefully touching it. In addition, it is required to consider the previously determined number of rotations and initiate the refining procedure. Unscrew the Vernier screw to bring the blades closer to the refiner,

bringing them into contact with the cellulose pulp inside the refiner and therefore initiating the refining process. Click the "Stop" button to lift the refiner's arm and acquire the refined cellulosic pulps after the process is complete.

The cellulose pulps are then resuspended in 2000 25 mL of demineralized water, followed by disintegration at 10,000 revolutions, as outlined in ISO 5263. After acquiring the disintegrated refined cellulosic fibers, cellulosic structures are generated according to the ISO 5269/1 standard, and their fibrous properties are further analyzed using the ISO 534 standard.

Appendix D. FTIR spectra

D1. Softwood bleached cellulose refined at 2500 rev

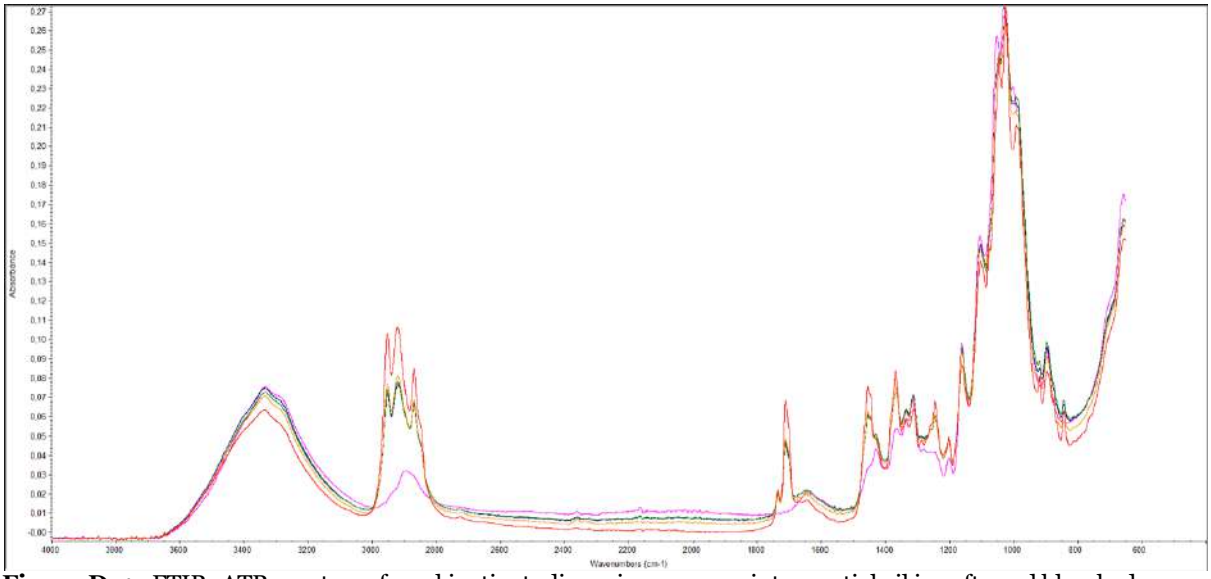

Figure D. 1 - FTIR- ATR spectrum from kinetic studies using peppermint essential oil in softwood bleached cellulose refined at 2500 rev. Pink corresponds SW without EO. The colors red (t0), blue (t1), green(t2) and yellow(t3), represent each time studied in the kinetic assay

D2. Softwood Unbleached fiber refined at 2500 revolutions:

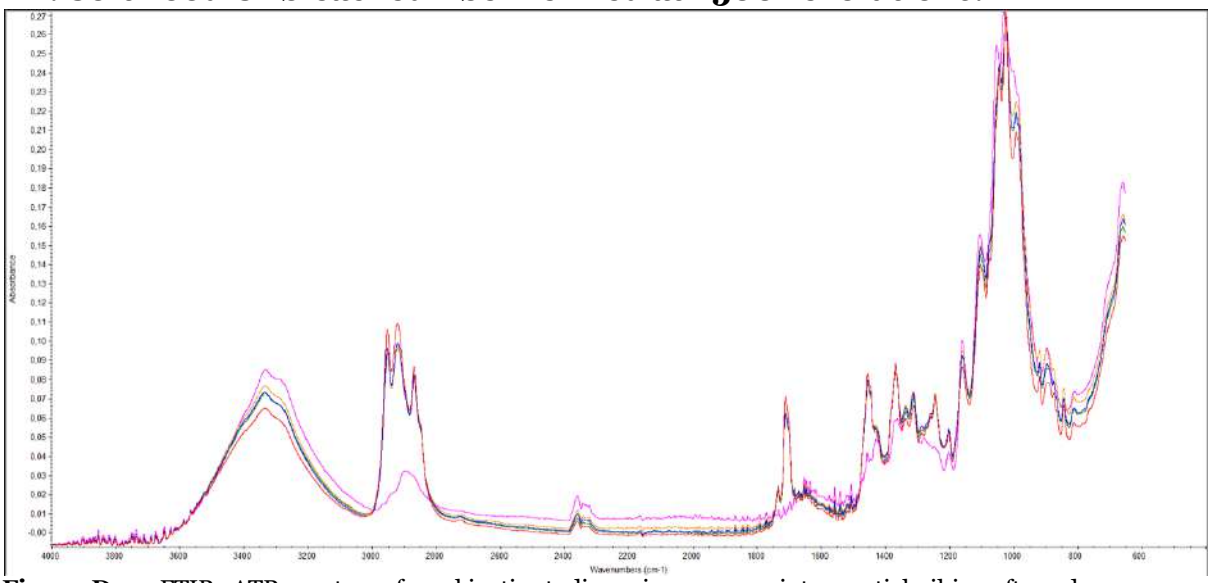

Figure D. 2 -FTIR- ATR spectrum from kinetic studies using peppermint essential oil in softwood non-bleached cellulose refined at 2500 rev. Pink- corresponds NSW without EO. Red(t0), green (t1), yellow (t2) and blue (t3), represent each time studied in the kinetic assay

Appendix E. FTIR spectra of the Carboxymethyl Cellulose Assays

E1. Softwood bleached cellulose with 800mg CMC

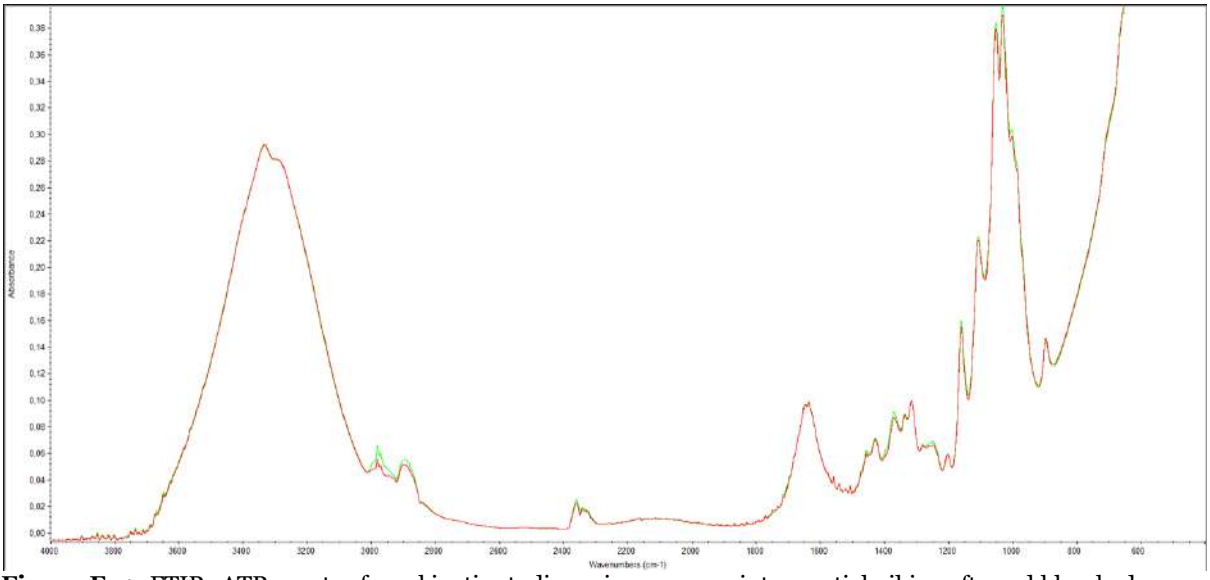

Figure E. 1 -FTIR- ATR spectra from kinetic studies using peppermint essential oil in softwood bleached cellulose, covered by carboxymethylcellulose hydrogel (800 mg). Red represents the cellulose with the CMC hydrogel and green represents cellulose with peppermint essential oil and CMC hydrogel

E2. Softwood bleached cellulose with 800mg CMC + 200mg CaCl2

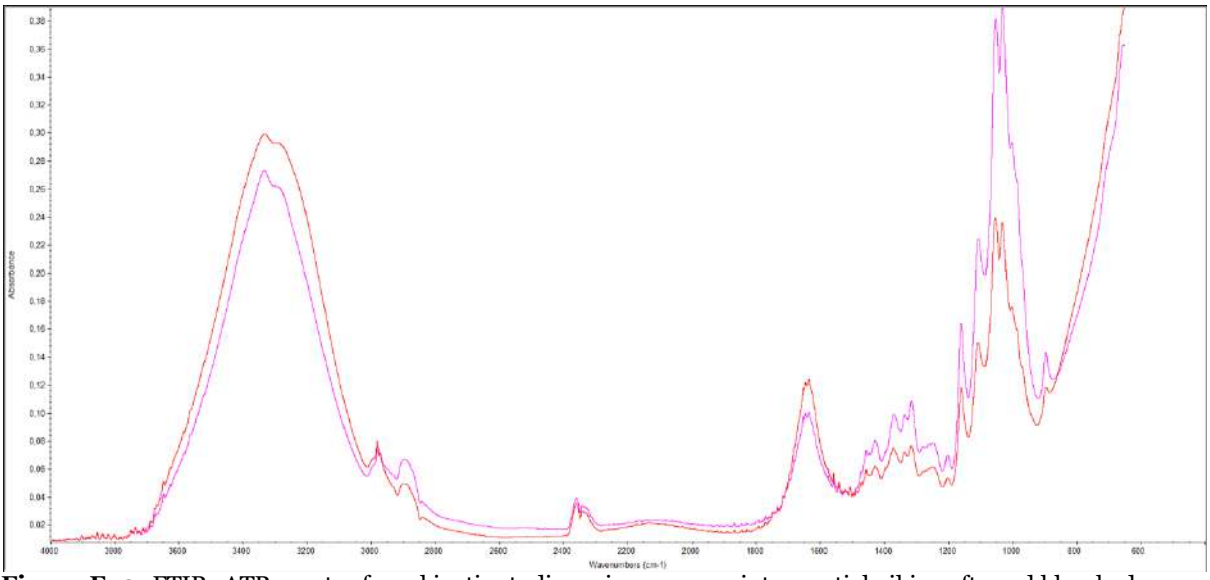

Figure E. 2 -FTIR- ATR spectra from kinetic studies using peppermint essential oil in softwood bleached cellulose, covered by carboxymethylcellulose hydrogel (800 mg). Red represents the cellulose with the CMC hydrogel and pink represents cellulose with peppermint essential oil and CMC hydrogel

E3. Softwood bleached cellulose with 1600mg CMC

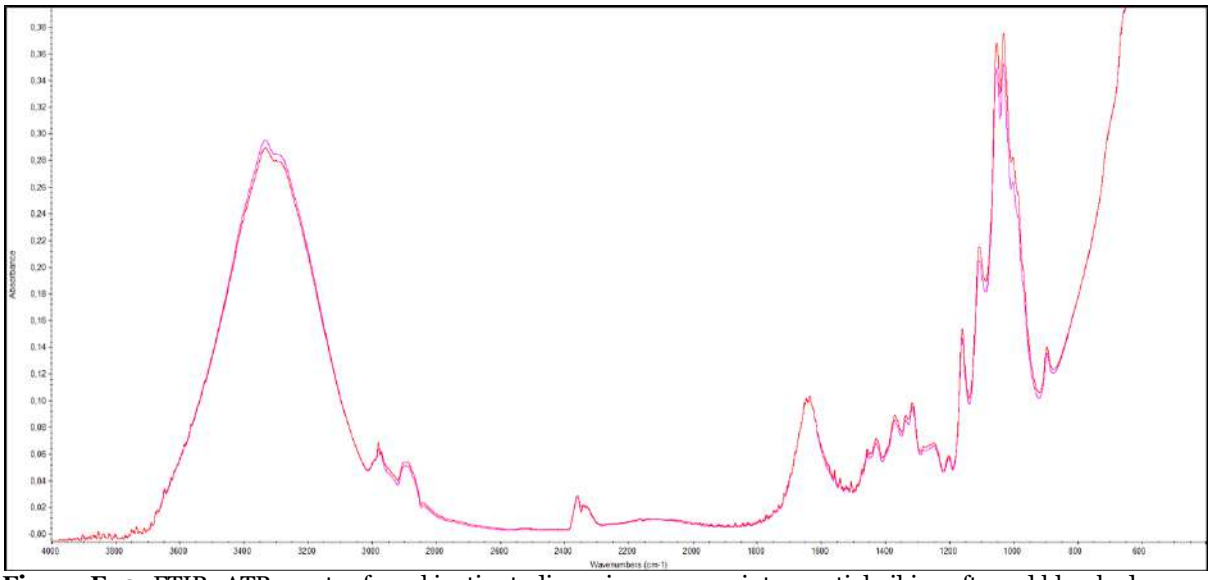

Figure E. 3 -FTIR- ATR spectra from kinetic studies using peppermint essential oil in softwood bleached cellulose, covered by carboxymethylcellulose hydrogel (1600 mg). Pink represents the cellulose with the CMC hydrogel and red represents cellulose with peppermint essential oil and CMC hydrogel

E4. Softwood non-bleached cellulose with 800mg CMC + 200mg $CaCl_2$

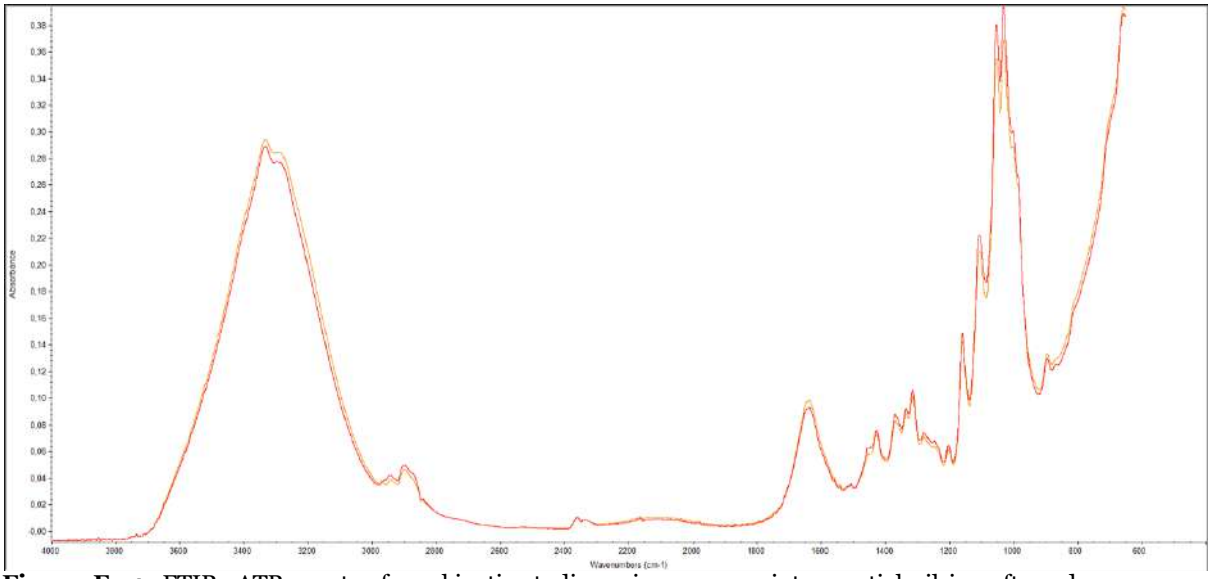

Figure E. 4 -FTIR- ATR spectra from kinetic studies using peppermint essential oil in softwood non-bleached cellulose, covered by CMC hydrogel (800 mg) and $CaCl_2$ (200mg). Yellow represents the cellulose with the CMC hydrogel and red represents cellulose with peppermint essential oil and CMC hydrogel

Appendix F. Manufaktura products composition

F1. Nourishing Bath with Lavender & Thermal Spring Salt

Figure F. 1 - Nourishing Bath with Lavender & Thermal Spring Salt

Composition:

Aqua, Paraffinum Liquidum, Sodium Laureth Sulfate, Cocamidopropyl Betaine, Cocamide DEA, Prunus Amygdalus Dulcis (Sweet Almond) Oil, Sodium Cocoyl Hydrolyzed Wheat Protein, Lavandula Angustifolia Herb Oil, Parfum, Natural Mineral Salt, Panthenol, Sodium Benzoate, Potassium Sorbate, Phenoxyethanol, Benzophenone-4, Citric Acid, Linalool, CI 17200, CI 42090, CI 73015

Ingredients:

Thermal spring salt, lavender, almond oil, corn sprouts

F2. Cooling Massage Gel with Sweet Balm & Thermal Spring Salt

Figure F. 2 - Cooling Massage Gel with Sweet Balm & Thermal Spring Salt

Composition:

Aqua, Glycerin, Polyquaternium-7, Alcohol Denat., Melissa Officinalis Leaf Extract, Rosmarinus Officinalis (Rosemary) Leaf Extract , Chamomilla Recutita (Matricaria) Flower Extract, Equisetum Arvense Extract, Salvia Officinalis Leaf Extract, Urtica Dioica Leaf Extract, Humulus Lupulus (Hops) Cone Extract, Mineral Salts (Carlsbad Natural Salt), Propylene Glycol, Menthol, Panthenol, Parfum, Acrylates/ C10-30 Alkyl Acrylate Crosspolymer, Triethanolamine, Phenoxyethanol, Ethylhexylglycerin, Limonene, Citral, Linalool, Citronellol, Geraniol

Ingredients:

Menthol, sweet balm, rosemary, chamomile, sage, hops, thermal spring salt

Appendix G. Analysis of commercial products

G1. Softwood Bleached fiber compared to lavender essential oil

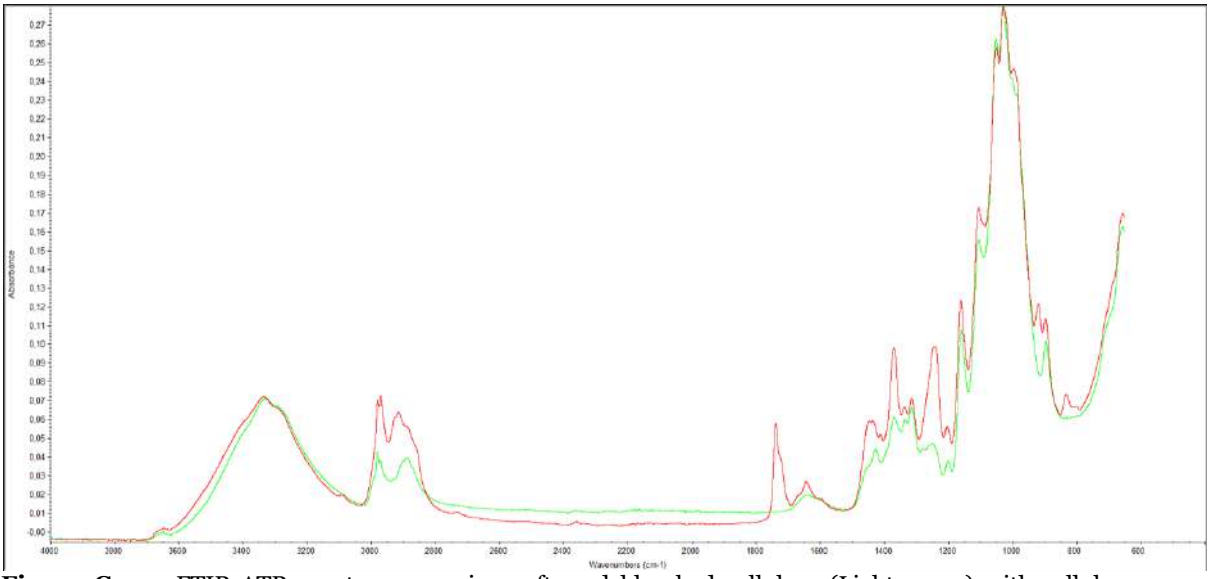

Figure G. 1 - FTIR-ATR spectra comparing softwood bleached cellulose (Light green) with cellulose containing lavender essential oil(Red).

G2. Softwood Bleached fiber compared to commercial emulsion

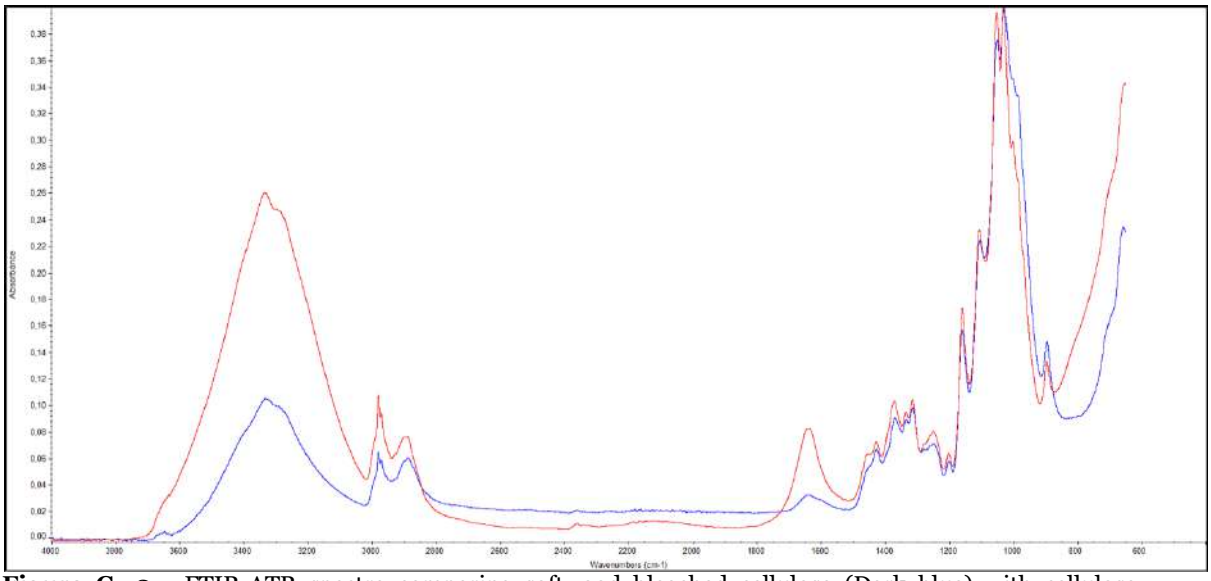

Figure G. 2 - FTIR-ATR spectra comparing softwood bleached cellulose (Dark blue) with cellulose containing commercial emulsion with lavender (Red).

G3. Softwood non-bleached cellulose with Lavender Essential Oil

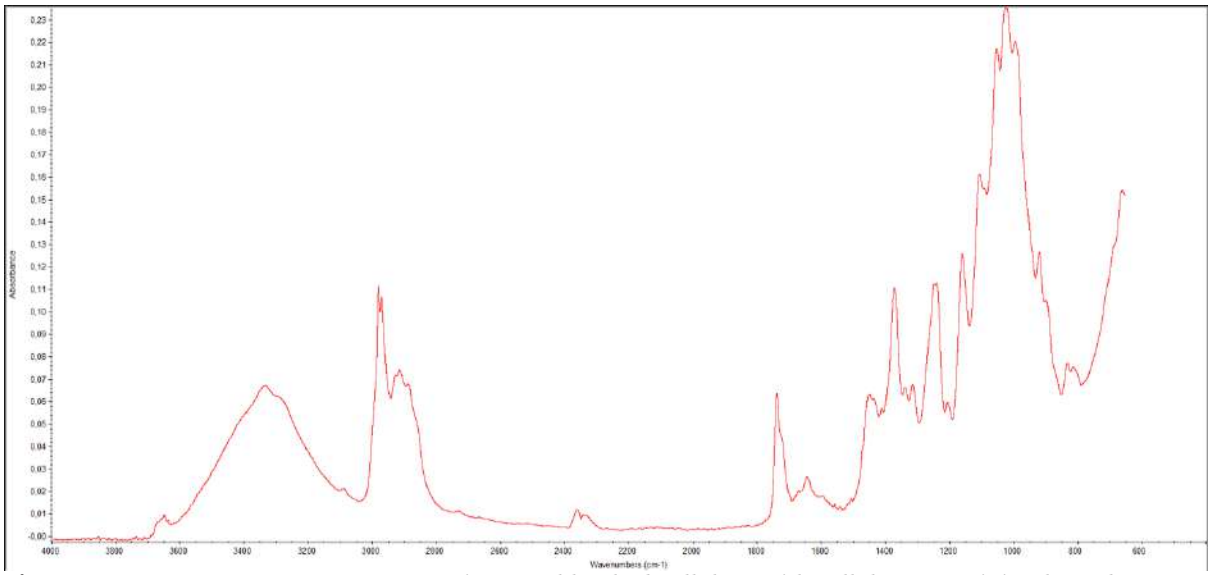

Figure G. 3 - FTIR-ATR spectra comparing non-bleached cellulose with cellulose containing lavender essential oil

G4. Softwood non-bleached cellulose with commercial emulsion

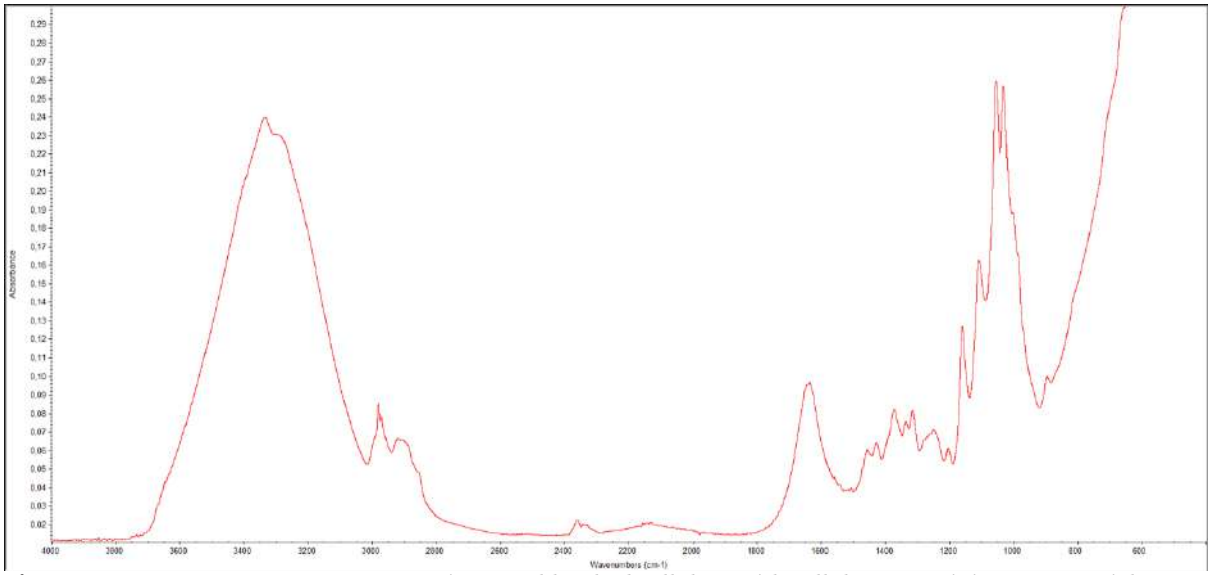

Figure G. 4 - FTIR-ATR spectra comparing non-bleached cellulose with cellulose containing commercial emulsion with lavender.